DANMARKS OG GRØNLANDS GEOLOGISKE UNDERSØGELSE RAPPORT 2009/86

Blokelv-1 core Well, GGU 511101, Upper Jurassic Hareelv Formation in Jameson Land, East Greenland - Final Well Report. Volume 3(3)

Contribution to Petroleum Geological Studies, Services and Data in East and Northeast Greenland

Morten Bjerager, Peter Alsen, Jørgen Bojesen-Koefoed, Peter Japsen, Claus Kjøller, Lotte Melchior Larsen, Hans Peter Nytoft, Mette Olivarius, Dan Olsen, Henrik Ingermann Petersen, Stefan Piasecki & Niels Schovsbo

GEOLOGICAL SURVEY OF DENMARK AND GREENLAND
MINISTRY OF ENVIRONMENT AND ENERGY

GEUS

DANMARKS OG GRØNLANDS GEOLOGISKE UNDERSØGELSE RAPPORT 2009/86

Blokelv-1 Core Well, GGU 511101, Upper Jurassic Hareelv Formation in Jameson Land, East Greenland – Final Well Report. Volume 3(3)

Contribution to Petroleum Geological Studies, Services and Data in East and Northeast Greenland

Morten Bjerager, Peter Alsen,
Jørgen Bojesen-Koefoed, Peter Japsen,
Claus Kjøller, Lotte Melchior Larsen,
Hans Peter Nytoft, Mette Olivarius,
Dan Olsen, Henrik Ingermann Petersen,
Stefan Piasecki & Niels Schovsbo

Confidential report

Copy No.

Released 01.07.2025

GEOLOGICAL SURVEY OF DENMARK AND GREENLAND
MINISTRY OF CLIMATE END ENERGY

GEUS

11.7 Appendix

Thermal History reconstruction in the Blokelv Borehole, East Greenland, based on AFTA® and VR data, GEOTRACK report #1052.

THERMAL HISTORY RECONSTRUCTION IN THE BLOKELV BOREHOLE, EAST GREENLAND, BASED ON AFTA® AND VR DATA

GEOTRACK REPORT #1052

A report prepared for the Geological Survey of Denmark and Greenland (GEUS), Copenhagen, by Geotrack International Pty Ltd

Report prepared by: P.F. Green

November 2009

Geotrack International Pty Ltd ABN 16006 1052 209
37 Melville Road, Brunswick West, Victoria 3055 Australia tel: +613 9380 1077 fax: +613 9380 1477

email: mail@geotrack.com.au website: www.geotrack.com.au

THERMAL HISTORY RECONSTRUCTION IN THE BLOKELV BOREHOLE, EAST GREENLAND, BASED ON AFTA® AND VR DATA

GEOTRACK REPORT #1052

CONTENTS

TABLES

FIGURES

Continued....\

FIGURES (continued)

THERMAL HISTORY RECONSTRUCTION IN THE BLOKELV BOREHOLE, EAST GREENLAND, BASED ON AFTA® AND VR DATA

GEOTRACK REPORT #1052

EXECUTIVE SUMMARY

Introduction and Objectives

This report describes a Thermal History Reconstruction study of **the Blokelv Borehole, East Greenland**. The study was commissioned by **the Geological Survey of Denmark and Greenland (GEUS), Copenhagen**, and is based on new Apatite Fission Track Analysis (AFTA®) data in two core samples from the borehole, together with vitrinite reflectance (VR) and other organic maturity data provided by GEUS. AFTA and VR data have been used to *identify*, *characterise* and *quantify* any episodes of heating and cooling which have affected the section intersected in this borehole. This information is then synthesised to provide a thermal history framework for the well, within which the tectonic development of the region can be understood. The report was completed in November 2009.

Summary Conclusions

1. The AFTA data generated for this study are of very high quality, reflecting the excellent apatite yields in both samples analysed.

2. No specific information is available on the quality of the vitrinite reflectance provided by GEUS for this report. But with reported VR values based on large numbers of measurements, the mean values are well defined, and are regarded as reliable.

3. In both AFTA samples, both the fission track age and track length data display a greater degree of post-depositional annealing than can be explained on the basis of the Default Thermal History, showing that the sampled units have been much hotter than present-day temperatures at some time after deposition.

4. AFTA data in sample GC1052-1 clearly require at least two paleo-thermal episodes, while the AFTA data in sample GC1052-2 appear to require three paleo-thermal episodes, although the precise timing of the earliest episode cannot be define with confidence. Thermal history solutions derived from the AFTA data in each sample are summarised in Table i.

5. As illustrated in Figure i, timing constraints derived from AFTA data in each sample show a high degree of consistency with the timing of dominant regional episodes defined from AFTA in samples from southern Jameson Land and adjacent areas in a regional study of Eastern Greenland between 60 and 67°N (Geotrack Report GC1016 for GEUS), in the intervals:

   56 to 45 Ma **"Early Eocene"**
   37 to 35 Ma **"Late Eocene"**
   ~12 Ma **"Middle Miocene"**

   On this basis, we interpret the results from sample GC1052-1 as representing the two most recent episodes (i.e. Late Eocene and Middle Miocene episodes), while all three episodes are recognised in sample GC1052-2.

6. VR data and VR_{eq} values derived from RockEval Tmax data are much higher than expected on the basis of the Default Thermal history, confirming the evidence from AFTA that the sampled units have been hotter than their present-day temperatures at some time since deposition.

7: Paleotemperature constraints from AFTA and from the measured VR values are plotted against depth in Figure ii. We interpret the paleotemperature constraints derived from AFTA and VR data in the Blokelv Borehole as representing the combined effects of deeper burial during the Cretaceous to Eocene, followed by (at least) two episodes of Late Cenozoic exhumation, combined with localised Early Eocene heating due either to contact heating or hydrothermal effects associated with intrusive activity. This interpretation is highly consistent with regional data and is regarded as reliable.

8. Figure iii illustrates the preferred thermal history reconstruction for the sedimentary units intersected in the Blokelv Borehole. Details of the reconstruction are explained in the Figure caption.

9. The conclusions of this study are regarded as reliable, and it is unlikely that further AFTA or VR analyses from the Blokelv Borehole would add much insight into the history. However, it would be useful to investigate possible diagenetic effects within the sandstone units intersected by the borehole. Extension to additional outcrop samples within the vicinity of the borehole, as well as samples from any future boreholes, would assist in defining the extent and magnitude of the key paleo-thermal episodes identified in this report.

Table i: Paleotemperature analysis summary: AFTA and VR data from The Blokelv Borehole, East Greenland (Geotrack Report #1052)

Sample number GC1052-	Mean depth (mkb)	Present temp-erature [*1] (°C)	Strati-graphic age (Ma)	Maximum paleo-temperature [*2] (°C)	Onset of cooling [*2] (Ma)	Maximum paleo-temperature [*2] (°C)	Onset of cooling [*2] (Ma)
1	**6**	**5**	**159-146**	**100-105**	**58-28**	**70-80**	**17-5**
	23.59		159-146	86			
	32.78		159-146	90			
	68.77		159-146	83			
	80.77		159-146	91			
	92.74		159-146	93			
	104.79		159-146	-			
	116.82		159-146	96			
	152.75		159-146	100			
	164.82		159-146	113			
	176.77		159-146	102			
	188.77		159-146	108			
	200.76		159-146	109			
	212.77		159-146	125			
2	**219**	**12**	**159-146**	***>110***	***60-50?***		
				100-110	**50-28**	**80-85**	**13-3**
	224.74		159-146	121			
			Combined timing (Ma):		***60-50***		**13-5**
					50-28		

[*1] Present temperature estimates based on an assumed surface temperature of 4°C, and an assumed thermal gradient of 30°C/km.

[*2] Thermal history interpretation of AFTA data is based on an assumed heating rate of 1°C/Myr and a cooling rate of 10°C/Myr (see Section 2). Quoted ranges for paleotemperature and onset of cooling correspond to ±95% confidence limits. Conditions shown in italics represent events that cannot be rigorously defined from the AFTA data.

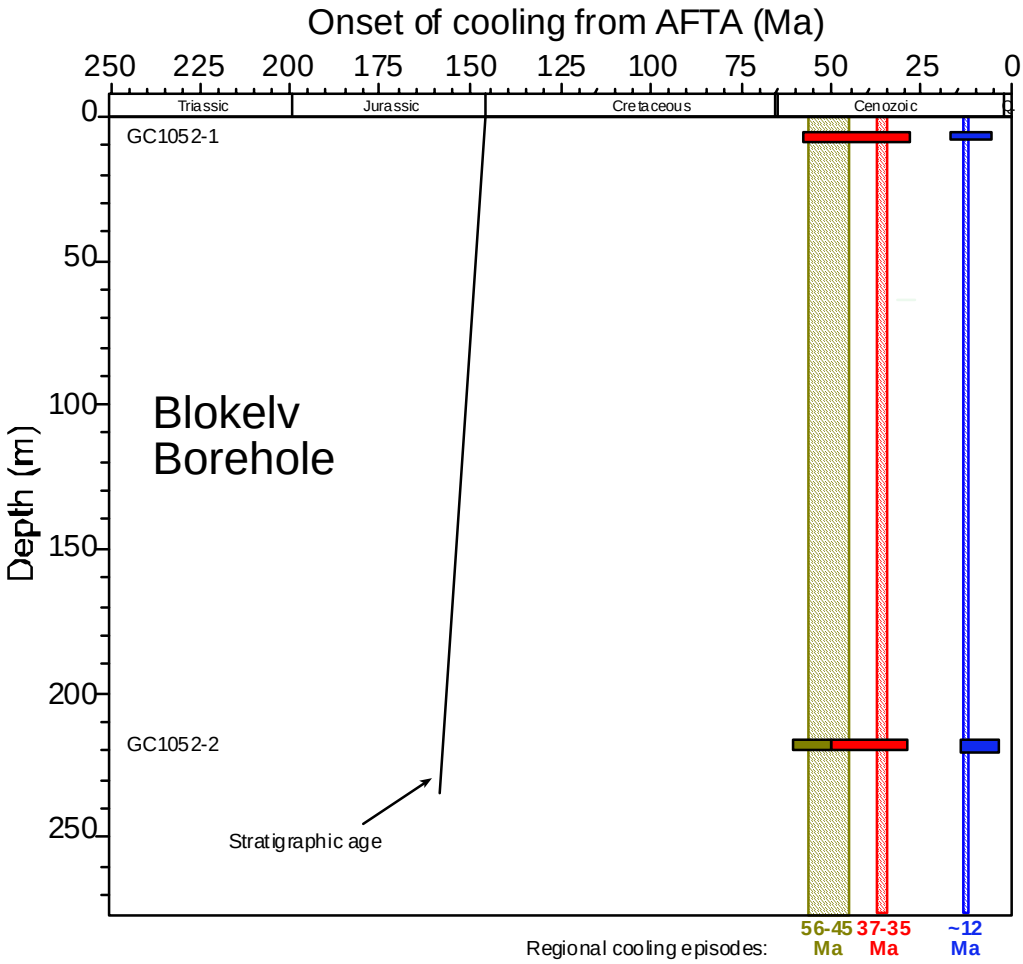

Figure i: Timing constraints on cooling episodes derived from AFTA data in two samples from **the Blokelv Borehole, Jameson Land, East Greenland**. The timing of cooling in three regional paleo-thermal episodes identified from AFTA data in a regional study of outcrop samples across Jameson Land and adjacent regions are also shown. The three episodes identified in samples from this study show good agreement with the timing of the regional episodes and the results presented in this report are interpreted on this basis, as explained in the text.

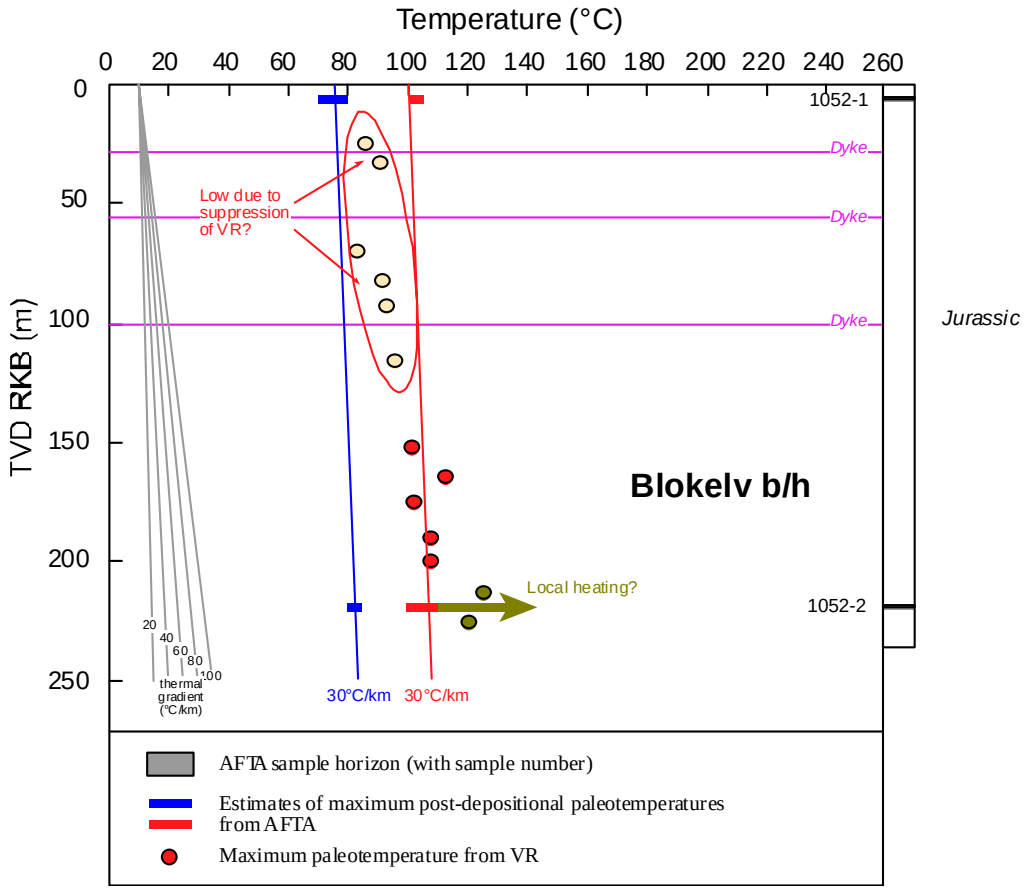

Figure ii: Interpreted paleotemperature profiles describing the paleotemperatures in three episodes derived from AFTA and VR data in **the Blokelv Borehole, Jameson Land, East Greenland**. Based on evidence from an extensive regional study of East Greenland, we interpret the maximum paleotemperature revealed by AFTA data in sample GC1052-2 as representing localised heating due to intrusive activity, possibly from the passage of hot fluids within the sand-dominated section from where this sample was collected. The end-Eocene (37-35 Ma) and Miocene (~12 Ma) paleotemperatures revealed by AFTA are interpreted as representing the effects of regional burial, with end-Eocene cooling representing the onset of regional exhumation, and Miocene cooling representing the final phase. On this basis, the VR values shallower than 120 metres are interpreted as anomalously low, most likely due to suppression of reflectance in source-rock facies organic rich mudstones. VR values deeper than 120 metres are regarded as providing reliable indications of the degree of post-depositional heating. Linear profiles representing various thermal gradients are shown, for reference, together two profiles representing with our preferred interpretation, based on regional data, involving paleogeothermal gradients of ~30°C/km for the end-Eocene and Miocene episodes.

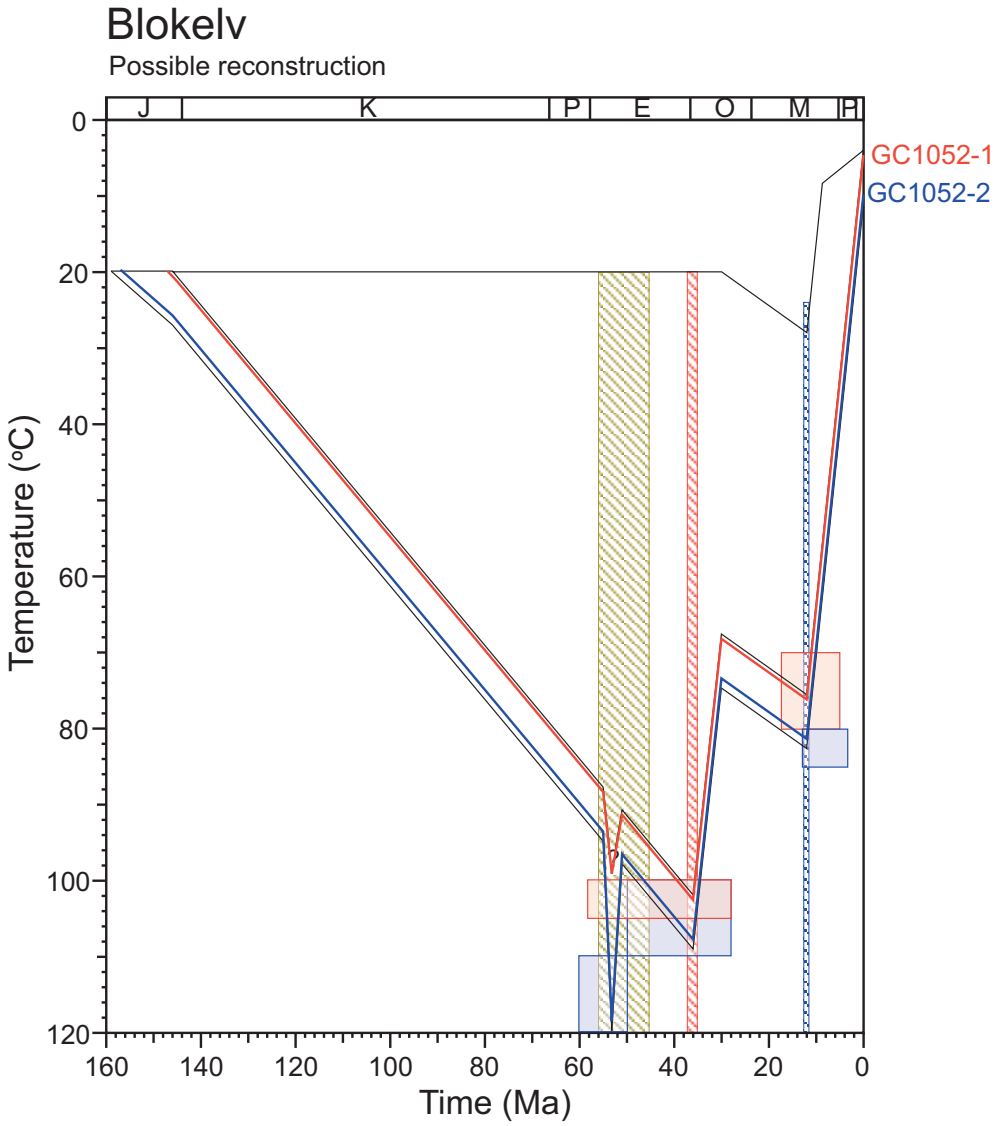

Figure iii: Schematic illustration of the preferred thermal history reconstruction for the section intersected in the **Blokelv Borehole, Jameson land, East Greenland**, based on the AFTA and VR data presented in this report, comparing paleo-thermal constraints from AFTA in selected samples with thermal histories of the corresponding sample horizons, coded by colour. The vertical columns show the preferred timing of three dominant paleo-thermal episodes identified in the region.

Key aspects of this reconstruction are:

- Surface temperature of 20°C at 30 Ma and earlier, decreasing to 10°C at 12 Ma and to the present-day value of 4°C over the last 12 Myr.
- Paleogeothermal gradient of 30°C/km, constant to the present day.
- Localised heating within the vicinity of sample GC1052-2 to a paleotemperature around 120°C, shown at ~53 Ma but any time between 56 and 45 Ma is allowed by the regional timing constraints on this episode.
- Deposition of an additional 2750 metres of section above the Late Jurassic section intersected in the borehole, between 146 and 36 Ma.
- Subsequent removal of 1150 metres of section between 36 and 30 Ma, followed by deposition of a further 600 metres of section between 30 and 12 Ma.
- Removal of the remaining 2200 metres of additional section between 12 Ma and the present day.

Note that the amount of re-burial between the two episodes of exhumation is not controlled by the data, and therefore also the exact amount of section removed in the initial episode beginning at 36 Ma is also not constrained. Note also that local Early Eocene heating in sample GC1052-2 was probably more rapid and most likely involved a higher paleotemperature than shown. These factors apart, this reconstruction is considered to provide a reliable depiction of the history of the Late Jurassic section intersected in the Blokelv Borehole.

1. Introduction

1.1 Aims and objectives

This report describes a Thermal History Reconstruction study of **the Blokelv Borehole, East Greenland** (Figure 1.1). The study was carried out for **the Geological Survey of Denmark and Greenland (GEUS), Copenhagen**, and is based on new Apatite Fission Track Analysis (AFTA®) data in two core samples from the borehole, together with vitrinite reflectance (VR) and other organic maturity data provided by GEUS. The report was completed in November 2009.

The primary aim of this study was to provide a thermal history framework for the vicinity of the borehole as a basis for understanding the history of source rock maturation and structural development in the region. Specific objectives were to investigate the magnitude and timing of possible paleo-thermal events which may have affected the samples, and to determine likely mechanisms of heating and cooling, although the borehole is too shallow to allow rigorous definition of paleogeothermal gradients and amounts of additional section that may once have been present and subsequently removed.

Details of the two core samples supplied for AFTA are summarised in Table A.1 (Appendix A). Details of VR and RockEval Tmax data provided by GEUS are summarised in Table D.2 (Appendix D).

The basic approach adopted for this study involves application of AFTA to determine the magnitude of maximum paleotemperatures in individual samples, and the time at which each sample began to cool from the paleo-thermal maximum. VR and other maturity data also provide independent estimates of maximum paleotemperatures, the timing of which can be interpreted on the basis of information provided by AFTA. This information is then synthesised to define the timing of any episodes of heating and cooling that have affected the section intersected in this well. The variation of paleotemperature with depth in individual paleo-thermal episodes is used to constrain paleogeothermal gradients, and to characterise the mechanisms of heating and cooling in each episode. Where appropriate, extrapolation of paleogeothermal gradients to assumed paleo-surface temperatures allows estimation of amounts of section removed by uplift and erosion. These results are then integrated into a coherent thermal history framework, which provides a basis for understanding tectonic and maturation histories in the region.

1.2 Report structure

The main conclusions of this report are provided in the Executive Summary. A summary of the thermal history interpretation of AFTA data in individual samples from the well is provided in Table i. Figure i provides a summary of timing constraints obtained from AFTA in this study and their attribution to regional cooling episodes, while Figure ii illustrates the paleotemperatures derived from AFTA and VR data in these regional paleo-thermal episodes. Figure ii provides a schematic illustration of the preferred thermal history interpretation of results from the Blokelv Borehole.

Introductory aspects of the report are dealt with in Section 1, including comments on data quality. Section 2 briefly explains the principles of interpretation of AFTA (also see Appendix C) and VR data, use of the resulting paleotemperatures to determine paleogeothermal gradients, and how this information can be used (with some caveats) to estimate amounts of eroded section. Section 3 presents detailed results from the Blokelv Borehole. AFTA data in individual samples are summarised in Table 3.1 and plotted against depth in Figure 3.1. Results of thermal history interpretation of AFTA data in each sample are presented in Tables 3.2 & 3.3. Paleotemperatures derived from VR and RockEval Tmax data are summarised in Table 3.4. A plot of paleotemperature constraints from AFTA and VR data against depth is presented in Figure 3.5 while an interpretation of these results is provided in Figure 3.6. Reconstructed thermal and burial histories for the units intersected in the well are then developed (and illustrated in Figures 3.7 and 3.8, respectively). Finally, Section 4 presents some recommendations for further work, which might allow further insight into the topics discussed in preceding sections.

Supporting information and data are provided in four Appendices (A, B, C and D). Details of AFTA samples from the two wells are presented in Table A.1 (Appendix A). This Table also contains information on the yields and quality of detrital apatite obtained after mineral separation. Sample preparation and analytical procedures for AFTA are described in Appendix B, followed by the presentation of all AFTA data, including raw track counts, fission track ages and the chlorine contents of dated grains. Appendix C outlines the principles employed in interpreting the AFTA data in terms of thermal history. VR and Tmax data provided by the client for this study are summarized in Appendix D, together with corresponding sample details. Appendix D also discusses the principles involved in integrating AFTA and VR data to provide coherent thermal history interpretations.

1.3 Data quality

AFTA data

Quality of the etched surfaces of the apatites analysed for this report was generally high. The resulting AFTA data are of very high quality, reflecting the excellent apatite yields in both samples analysed, as summarised in Table A.1 (Appendix A). Fission track ages were determined on 20 or more grains in each sample, and over 100 track lengths were measured in both samples (100 track length measurements is the usual "target" number, considered as desirable for an analysis of the highest quality). With high quality AFTA data in both samples, the final thermal history interpretations are regarded as highly reliable within the stated uncertainty limits.

VR data

No specific information is available on the quality of the vitrinite reflectance provided by GEUS for this report. But all reported VR values are based on large numbers of measurements, and mean values are well defined, so the values provided as indicating the mean reflectance of indigenous vitrinite are regarded as reliable.

1.4 Apatite Compositions

The annealing kinetics of fission tracks in apatite are affected by chemical composition, specifically the Cl content, as explained in more detail in Appendix C. For this study, chlorine compositions were determined for all individual apatite grains analysed for this study (i.e. all grains in which fission track ages were determined and/or lengths were measured). Knowledge of chlorine contents is essential in interpreting AFTA data, and provides both improved accuracy and precision in establishing the time and magnitude of thermal events.

The measured ranges of chlorine contents of dated grains and/or grains used for confined track length measurements are shown in histogram format in the Fission Track Age Data Sheets at the end of Appendix B. Table B.3 (Appendix B) contains single grain fission track age and track length data collected into discrete compositional groups, on the basis of the chlorine contents of the grains from which the data were derived. In addition, plots of single grain age versus weight % chlorine are shown in the Fission Track Age Data Sheets, which also list the chlorine contents of individual age grains.

2. Interpretation strategy

2.1 Thermal history interpretation of AFTA data

Basic principles

Interpretation of AFTA data in this report begins by assessing whether the fission track age and track length data in each sample could have been produced if the sample has never been hotter than its present temperature at any time since deposition. To this end, we consider a "Default Thermal History" for each sample, which forms the basis of interpretation. Default Thermal Histories throughout a well are derived from the stratigraphy of the preserved sedimentary section, combined with constant values for paleogeothermal gradient and paleo-surface temperature which are adopted from present-day values. For outcrop samples, the Default Thermal Histories simply represent long-term residence at the prevailing surface temperature.

Using this history, AFTA parameters are predicted for each sample. If the measured data show a greater degree of fission track annealing (in terms of either fission track age reduction or track length reduction) than expected on the basis of this history, the sample must have been hotter at some time in the past. In this case, the AFTA data are analysed to provide estimates of the magnitude of the maximum paleotemperature in that sample, and the timing of cooling from the thermal maximum.

Because of the possible presence of tracks inherited from sediment source terrains, it is possible that track length data might show definite evidence that the sample has been hotter in the past (since deposition) while fission track ages are still greater than predicted from the Default Thermal History (which only refers to tracks formed after deposition). Similarly in samples in which all or most fission tracks were totally annealed in a paleo-thermal episode, and which have subsequently been cooled and then reburied, fission track age data might show clear evidence of exposure to higher temperatures in the past while track length data may be dominated by the present-day thermal regime and will not directly reveal the paleo-thermal effects. In circumstances such as these, evidence from either track length or fission track age data alone is sufficient to establish that a sample has been hotter in the past.

As AFTA data provide no information on the *approach* to a thermal maximum, they cannot independently constrain the heating rate and a value must therefore be assumed in order to interpret the data. The resulting paleotemperature estimates are

therefore conditional on this assumed value. AFTA data do provide some control on the history after cooling from maximum paleotemperatures, through the lengths of tracks formed during this period.

Wherever possible, data from each sample are normally interpreted in terms of two episodes of heating and cooling, using assumed heating and cooling rates during each episode. The maximum paleotemperature is assumed to be reached during the earlier episode. The timing of the onset of cooling and the peak paleotemperatures during the two episodes are varied systematically, and by comparing predicted and measured parameters the range of conditions which are compatible with the data can be defined. One additional episode during the cooling history is the limit of resolution from typical AFTA data. Alternatively, if the data can be explained by a single episode of heating and cooling, then a heating rate is assumed and the range of values of maximum paleotemperature and the time of cooling is defined as before.

If AFTA data show a lower degree of fission track annealing (age and/or length reduction) than expected on the basis of the Default Thermal History, this either suggests present temperatures may be overestimated or temperatures have increased very recently. In such cases, the data may allow a more realistic estimate of the present temperature, or an estimate of the time over which temperatures have increased.

AFTA data are predicted using a multi-compositional kinetic model for fission track annealing in apatite developed by Geotrack, described in more detail in Appendix C.

Specific to this report

For all samples analysed for this report, chlorine content has been determined in every apatite grain analysed (i.e., for both fission track age and track length measurement), as explained in more detail in Appendix A. For rigorous thermal history interpretation the age and length data have been grouped into 0.1 wt% Cl divisions (see Table B.3, Appendix B).

In this report, AFTA data in all samples have been interpreted using heating rates of 1°C/Myr and cooling rates of 10°C/Myr. These values are assumed arbitrarily, and all paleotemperature estimates are conditional on the assumed rates. For the kinetics characterising both AFTA and VR, increasing or decreasing heating rates by an order of magnitude is equivalent to raising or lowering the required maximum paleotemperature by about 10°C.

2.2 Thermal history interpretation of VR data

Basic principles

Interpretation of VR data follows similar principles to those used in interpreting the AFTA data (Section 2.1). If a measured VR value is higher than the value predicted from the Default Thermal History (making due allowance for analytical uncertainty), the sample must have been hotter at some time in the past. In this case, VR data provide an independent estimate of maximum paleotemperature, which can be calculated using an assumed heating rate and timing information provided from AFTA data, if available (assumed, otherwise). Cooling rates do not significantly affect VR data, which are dominated by the maximum paleotemperature provided that cooling occurs immediately after reaching the thermal maximum. If both AFTA and VR data are available from the same sample or well, then an identical heating rate must be used to obtain consistent paleotemperature estimates.

If a measured VR value is lower than expected on the basis of the Default Thermal History, either present temperatures may have been overestimated or temperatures have increased very recently. In such cases, the measured VR value may allow an estimate of the true present-day temperature. Alternatively the measured VR value may underestimate the true maturity for some other reason, e.g., suppression of reflectance in certain organic macerals, misidentification of true "in-situ" vitrinite, presence of caved material etc. Comparison of AFTA and VR data usually allows such factors to be identified, and where applicable they are discussed in the relevant section of text.

Vitrinite reflectance data (specifically $R_o$max values) are predicted using the distributed activation energy model describing the evolution of VR, with temperature and time developed by Burnham and Sweeney (1989) (see also Sweeney and Burnham, 1990).

Values of VR less than ~0.3% and greater than 4% cannot be assigned to a specific maximum paleotemperature with confidence, and such values are given maximum and minimum limits, respectively, appropriate to the particular heating rate used (see Appendix D). Further discussion of the methodology employed in interpreting VR data are given in Appendix D, which also briefly discusses the benefits of integrating AFTA and VR data.

Specific to this report

For this report, VR data in all samples have been interpreted using heating and cooling rates of 1 and 10°C/Myr (respectively), for consistency with interpretation of the AFTA data, as specified in Section 2.1.

Maximum paleotemperatures determined for the VR samples are attributed to one of the paleo-thermal episodes identified by AFTA on the basis of comparison of the VR-derived maximum paleotemperature with observed paleo-heating of a similar style in adjacent AFTA samples.

2.3 Comparison of paleotemperature estimates from AFTA and VR

Maximum paleotemperatures derived from AFTA and VR ($R_o$max) using the strategies outlined above are usually highly consistent. Estimates of maximum paleotemperature from AFTA (Table i) are often quoted in terms of a range of paleotemperatures, as the data can often be explained by a variety of scenarios. Paleotemperature estimates from VR (Table i) are usually quoted to the nearest degree Celsius, as the value which predicts the exact measured reflectance. This is not meant to imply VR data can be used to estimate paleotemperatures to this degree of precision. VR data from individual samples typically show a scatter equivalent to a range of between ±5 and ±10°C. Estimates from a series of samples are normally used to define a paleotemperature profile in samples from a well, or a regional trend in paleotemperatures from outcrop samples.

2.4 Estimates of paleogeothermal gradients and mechanisms of heating and cooling

Basic principles

A series of paleotemperature estimates from AFTA and/or VR over a range of depths can be used to reconstruct a paleotemperature profile through the preserved section. The slope of this profile defines the paleogeothermal gradient. As explained by Bray et al. (1992), and as illustrated in Figure 2.1, the shape of the paleotemperature profile and the magnitude of the paleogeothermal gradient provides unique insights into the origin and nature of the heating and cooling episodes expressed in the observed paleotemperatures.

Linear paleotemperature profiles with paleogeothermal gradients close to the present-day geothermal gradient provide strong evidence that heating was caused by greater depth of burial with no significant increase in basal heat flow, implying in turn that cooling was due to uplift and erosion. Paleogeothermal gradients significantly higher than the present-day geothermal gradient suggest that heating was due, at least in part, to increased basal heat flow, while a component of deeper burial may also be important as discussed in the next section. Paleogeothermal gradients significantly lower than the present-day geothermal gradient suggest that a simple conductive model is inappropriate, and more complex mechanisms must be sought for the observed heating. One common cause of low paleogeothermal gradients is transport of hot fluids shallow in the section. However the presence of large thicknesses of sediment with uniform lithology dominated by high thermal conductivities can produce similar paleotemperature profiles and each case has to be considered individually.

A paleotemperature profile can only be characterised by a single value of paleogeothermal gradient when the profile is linear. Departures from linearity may occur where strong contrasts in thermal conductivities occur within the section, or where hot fluid movement or intrusive bodies have produced localised heating effects. In such cases a single value of paleogeothermal gradient cannot be calculated, and different values (possibly negative) may apply through different parts of the section. However it is important to recognise that the validity of the paleotemperatures determined from AFTA and/or VR are independent of these considerations, and can still be used to control possible thermal history models.

Estimation of paleogeothermal gradients in this report

As samples have been analysed only over a very narrow range of depths, paleogeothermal gradients have not been estimated.

2.5 Determination of removed section

Basic principles

Subject to a number of important assumptions, extrapolation of a linear paleotemperature profile to a paleo-surface temperature allows estimation of the amount of eroded section represented by an unconformity, as explained in more detail in Section C.9 (Appendix C).

Specifically, this analysis assumes:

- The paleotemperature profile through the preserved section is linear
- The paleogeothermal gradient through the preserved section can be extrapolated linearly through the missing section.
- The paleo-surface temperature is known.
- The heating rate used to estimate the paleotemperatures defining the paleogeothermal gradient is correct

It is important to realise that any method of determining the amount of eroded section based on thermal methods is subject to these and/or additional assumptions. For example methods based on heat-flow modelling must assume values of thermal conductivities in the eroded section, which can never be known with confidence. Such models also require some initial assumption of the amount of eroded section to allow for the effect of compaction on thermal conductivity. Methods based on geothermal gradients, as used in this study, are unaffected by this consideration, and can therefore provide independent estimates of the amount of eroded section. But these estimates are always subject to the assumptions set out above, and should be considered with this in mind.

The analysis used to estimate paleogeothermal gradients is easily extended to provide maximum likelihood values of eroded section for an assumed paleo-surface temperature, together with ±95% confidence limits. These parameters are quoted for each well in which the paleotemperature profile suggests that heating may have been due, at least in part, to deeper burial.

Estimates of paleogeothermal gradient and eroded section derived from fitting linear profiles to paleotemperature data as a function of depth are highly correlated, since the profile is constrained to pass through the main body of the data. Thus, higher paleo-gradients within the allowed range correspond to lower amounts of section removed, while lower paleo-gradients correspond to higher amounts of removed section. In plots of paleogeothermal gradient against removed section, paired values of each parameter which are consistent with the paleotemperature data can be defined, thus allowing the range of allowed values at various levels of statistical significance to be contoured. In general, the greater the depth intervals over which paleotemperature constraints are available, the tighter the resulting constraints on both the paleogeothermal gradient and the amount of removed section.

However, it is emphasised that reconstructed burial histories produced in this way do not produce unique solutions, and alternative interpretations are always possible. For instance, where the eroded section was dominated by units with high thermal conductivities the paleogeothermal gradient through the missing section may have been much higher than in the preserved section, and extrapolation of a linear gradient will lead to overestimation of the eroded section.

Specific to this report

Because samples have been analysed only over a very narrow range of depths, paleogeothermal gradients have not been estimated, and therefore no rigorous determination of amounts of removed section is possible.

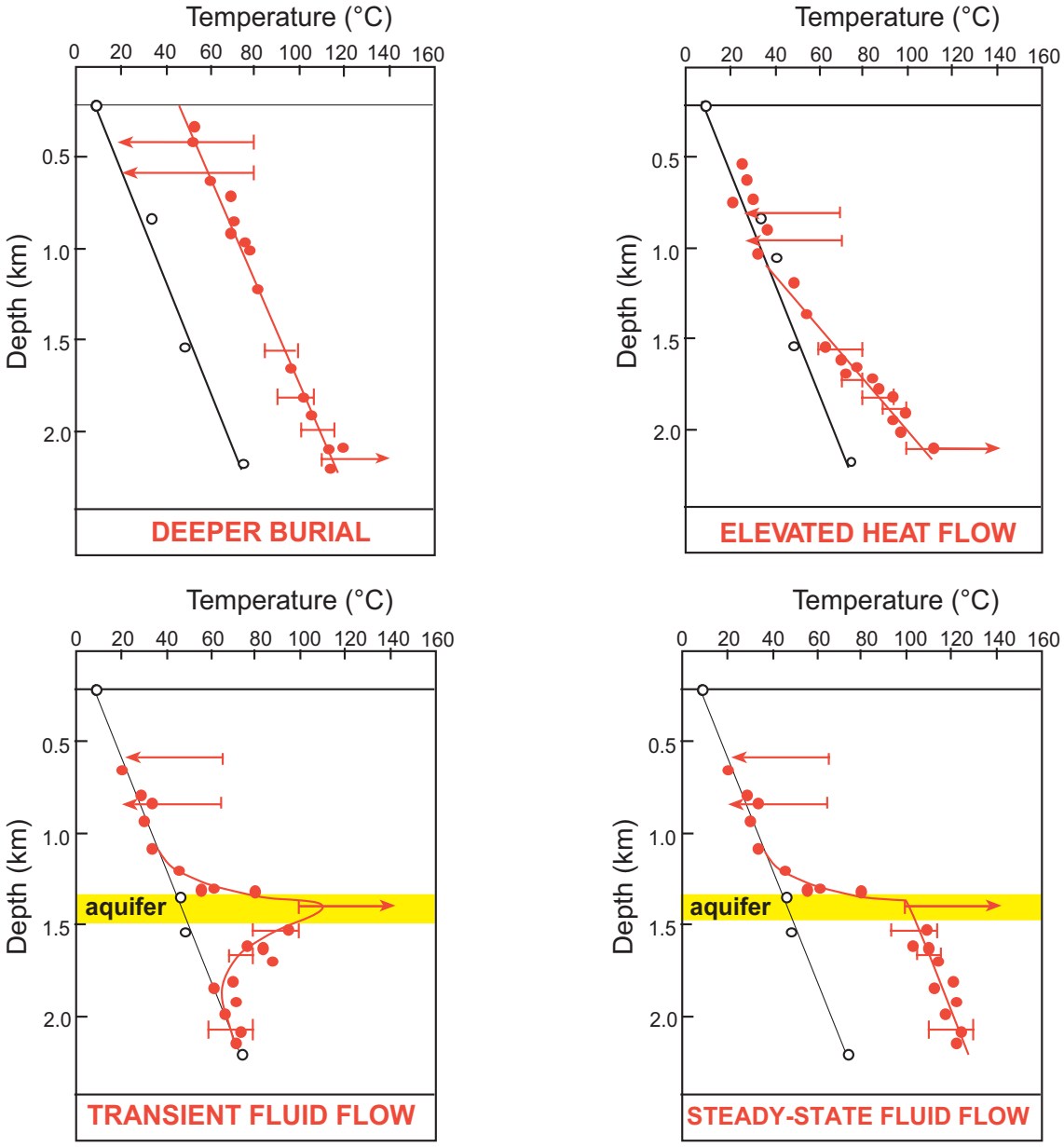

Figure 2.1: The way in which paleotemperatures characterising a particular paleo-thermal episode vary with depth, or the "paleotemperature profile", provides key information on the mechanisms of heating and cooling. Deeper burial followed by exhumation, with little or no change in basal heat flow, typically results in paleotemperatures defining a linear profile sub-parallel to the present-day thermal profile but offset to higher temperatures. Elevated heat flow results in a linear paleotemperature profile with a higher slope compared to the present-day profile. In contrast, transient hot fluid flow through a localised aquifer results in a markedly non linear profile with a maximum centred on the aquifer, while prolonged fluid flow can result in a linear profile below the aquifer as the deeper section reaches a "steady-state" situation. Combinations of these four simple cases are possible.

3. Thermal history reconstruction in the Blokelv Borehole, East Greenland

3.1 Introduction

The Blokelv Borehole was drilled in the Jameson Land Basin, East Greenland, and intersected a ~239 m section of Late Jurassic sedimentary units, with dolerite intrusions noted at depths of ~27, ~56 and ~101 metres. The stratigraphic succession in this well is summarised in Table A.2. A present-day geothermal gradient of 30°C/km has been assumed for the section intersected in the borehole, although given the shallow depths involved, the thermal history solutions extracted from the AFTA data are not at all sensitive to this parameter.

3.2 Thermal history interpretation of AFTA data

Introduction

Two samples of core were processed for AFTA from this borehole. Excellent apatite yields were obtained from each sample, and the normal "target" numbers of 20 single grain fission track ages and 100 track lengths were obtained in both samples. AFTA data from both samples provide highly reliable thermal history constraints, as explained below.

Fission track ages and mean track lengths measured in samples analysed from this well are summarised in Table 3.1 and plotted as a function of depth and present temperature in Figure 3.1, where the fission track age data are contrasted with the variation of stratigraphic age through the section. The variation of fission track age and length vs depth predicted from the Default Thermal History (see Section 2.1) for this well are also shown in Figure 3.1, for selected apatite chlorine contents.

Measured fission track ages in both samples in Figure 3.1 are significantly less than predicted from the Default Thermal History, showing immediately that the sampled units have been much hotter than present-day temperatures at some time after deposition. AFTA data in each sample and the resulting thermal history interpretations are discussed in detail in the following Sections.

Evidence for elevated paleotemperatures from AFTA

Qualitative interpretation of the AFTA data in each sample, in terms of evidence that the samples may have been hotter in the past, is summarised in Table 3.2. As noted

above, in both samples the AFTA data provide clear evidence that the host units must have been hotter than present-day values at some time after deposition. This evidence comes from both the fission track age and track length data, which both display a greater degree of post-depositional annealing than can be explained on the basis of the Default Thermal History alone.

Magnitude of paleotemperatures and timing of cooling from AFTA

Following the strategy outlined in Section 2.1, quantitative interpretation of the AFTA data in each sample is summarised in Table 3.3. AFTA data in sample GC1052-1 clearly require at least two paleo-thermal episodes, while the AFTA data in sample GC1052-2 appear to require three paleo-thermal episodes, although the precise timing of the earliest episode cannot be defined with confidence.

Thermal history solutions derived from the AFTA data in each sample are summarised in Table i.

Definition of paleo-thermal episodes

Timing constraints derived from AFTA data in each sample (from Table 3.3) are compared in Figure 3.2, where they are compared with the timing of three regional cooling episodes defined from AFTA in samples from southern Jameson Land and adjacent areas in a regional study of Eastern Greenland between 60 and 67°N (Geotrack Report GC1016 for GEUS). Cooling in these three episodes began in the intervals:

56 to 45 Ma ("Early Eocene")

37 to 35 Ma ("Late Eocene")

~12 Ma ("Middle Miocene")

Figure 3.2 illustrates a high degree of consistency between the timing of cooling identified in this study and the dominant regional episodes. On this basis, we interpret the results from sample GC1052-1 as representing the two most recent episodes (i.e. Late Eocene and Middle Miocene episodes), while all three episodes are recognised in sample GC1052-2. Possible reasons why the earliest of these three episodes might only be identified in sample GC1052-2 are discussed in Section 3.4.

Equivalent maturity values from AFTA

Estimates of maximum allowed paleotemperature from AFTA data in each sample have been converted to equivalent vitrinite reflectance values (using the Burnham

and Sweeney, 1989, algorithm) which are summarised in Table 3.3. These values increase from between 0.61% and 0.63% in sample GC1052-1 to >0.66% in sample GC1052-2. Comparison of these equivalent VR values with measured VR data, is discussed further in Section 3.4, where detailed integration of results from AFTA and VR is discussed.

3.3 Thermal history interpretation of VR data

Introduction

Results of vitrinite reflectance analyses provided by GEUS for this report are summarised in Table D.2. Rock Eval Tmax values provided by GEUS, together with equivalent VR (VR_{eq}) values derived from these values using the correlation shown in Appendix D (Table D.1c and Figure D.1) are also listed in Table D.2.

Mean VR and VR_{eq} values are plotted against depth (with respect to ground surface) in Figure 3.3, together with the range of equivalent VR values derived from AFTA data in samples GC1052-1 and 2. Also shown in Figure 3.3 is the VR profile predicted on the basis of the Default Thermal History - i.e. the thermal history predicted for samples from this well if they have never been hotter than their present temperatures at any time in the past, as defined in Section 2.1. The Default Thermal History used in producing Figure 3.3 is based on the burial history derived from the units intersected in the well (shown in Figure 3.4), combined with an assumed present-day thermal gradient of 30°C/km, and a mean annual surface temperature of 4°C.

Evidence that samples have been hotter in the past

Both VR and VR_{eq} data plot well above the profile predicted by the Default Thermal History in Figure 3.2, confirming the evidence from AFTA that the sampled units have been hotter than their present-day temperatures at some time since deposition.

In detail, the VR values tend to be slightly lower than the VR_{eq} values derived from the Tmax data throughout the section. In general, Tmax values tend to be sensitive to a range of factors and are not used quantitatively to provide estimates of maximum paleotemperature in the same way that VR data are. But overall, the agreement between VR and VR_{eq} values from Tmax in Figure 3.3 is sufficient to confirm general trend of maturity with depth, with the two datasets defining an arcuate trend with depth, first decreasing to depths around 30 m and then increasing at greater

depths. Note that VR_{eq} values from Tmax data define local contact effects due to the three recognised intrusions, which the VR values do not show. Comparison between the VR values and ranges of equivalent VR derived from AFTA data in samples GC1052-1 and -2 is discussed in Section 3.4.

Magnitude of paleotemperatures from VR

Maximum paleotemperatures derived from the VR values in this borehole, using the strategy outlined in Section 2.2, are summarised in Table 3.4. Values show a general increase from 86 to 125°C through the section intersected in the borehole. The significance of these paleotemperatures and the underlying heating mechanisms are discussed in Section 3.4.

3.4 Integration of AFTA and VR data, paleotemperature profiles and mechanisms of heating and cooling

Paleotemperature constraints from AFTA and from the measured VR values are plotted against depth in Figure 3.5. Comparison of maximum paleotemperatures indicated by AFTA and VR data reveals some consistencies and some differences.

The range of maximum paleotemperatures indicated by AFTA data in sample GC1052-1 (100 to 105°C) is higher than the corresponding values indicated by the shallowest VR values, which come from slightly greater depth. In contrast, the two techniques provide more consistent results around the depth interval from which AFTA sample GC1052-2 was collected.

Comparing paleotemperatures from AFTA and VR data in the uppermost 50 m of the section in Figure 3.5, the decrease from AFTA in sample GC1052-1 to the VR data at slightly greater depth echoes the variation of VR and VR_{eq} with depth in Figure 3.3, as part of the arcuate trend. But on the basis of regional AFTA data from our regional AFTA database (Geotrack Report GC1016), we regard the Late Eocene event as pervasive in this region, and therefore we would expect measured VR values at shallow depth to be similar to the range of equivalent values defined from AFTA data in sample GC1052-1. The consistent expression of the Late Eocene episode in both AFTA samples supports this expectation. We therefore regard the measured VR values at shallow depths in this well as being slightly suppressed, as is often observed in late Jurassic organic-rich mudstones of the North Atlantic region. On this basis, we interpret the paleotemperatures defined from AFTA and VR data in the borehole as shown in Figure 3.6. Paleotemperatures from VR data at depths between

~150 and 200 m, together with Late Eocene paleotemperatures derived from AFTA in samples GC1052-1 and -2 define a linear profile characterised by a paleogeothermal gradient around 30°C/km, and Middle Miocene paleotemperatures defined from AFTA in the two samples are interpreted in similar fashion.

The Early Eocene paleotemperature revealed by AFTA data in sample GC1052-2 is then interpreted as representing localised heating restricted to the vicinity of this sample, and most likely represented by the VR data in adjacent samples, as illustrated in Figure 3.6. This interpretation is highly consistent with the explanation of regional paleo-thermal data from southern Jameson Land and adjacent regions in Geotrack Report GC1016, in which the Middle Miocene and Late Eocene cooling episodes were regarded as representing successive episodes of exhumation, while Early Eocene effects were interpreted as due to local effects associated with igneous intrusions, either in terms of contact heating or hydrothermal effects. This would explain why the effects of the Early Eocene episode are not recognised in AFTA data from sample GC1052-1.

3.5 Thermal history synthesis

On the basis of the discussion presented above, we interpret the paleotemperature constraints derived from AFTA and VR data in the Blokelv Borehole as representing the combined effects of deeper burial followed by (at least) two episodes of exhumation, combined with localised heating due either to contact heating or hydrothermal effects associated with intrusive activity. The results provided here are highly consistent with regional data and the interpretation presented here is regarded as reliable.

3.6 Thermal history reconstruction

Introduction

In this Section, we present reconstructed thermal and burial-uplift histories for the section intersected in the **Blokelv Borehole**, based on the results presented in previous Sections. It should be emphasised that while the preferred reconstruction illustrated here provides a satisfactory explanation of the AFTA and VR data from this well, the reconstruction is not unique, and a range of alternative scenarios can be invoked for each well. Therefore, in considering these reconstructions, it is

important to appreciate those aspects of the histories that are constrained by the data, and those that are not.

Factors that can be confidently defined in this study (within the limits of analytical uncertainty) include:

- Magnitude of heating at the paleo-thermal maximum and the subsequent paleo-thermal peaks
- Timing of the onset of cooling in each episode

Factors that can be defined when samples are available over a sufficiently large range of depths or elevations (within the limits of analytical uncertainty), but cannot be constrained in this study include:

- Paleogeothermal gradients during each episode (subject to the reliability of the constraints employed)
- Additional burial during each episode for a specified values of paleogeothermal gradient, assuming a linear paleotemperature profile (heterogeneous section).

Aspects which cannot be uniquely defined in any situation include:

- Thermal history prior to the paleo-thermal maximum and/or the subsequent paleo-thermal peak
- amounts of re-burial between multiple episodes within a single unconformity
- Detailed style of cooling history from each episode

Any reconstruction that matches the constraints on the magnitude of paleo-thermal effects in individual samples and the onset of cooling can be considered as reliable, and integration with regional geological trends will be required to further restrict the range of realistic scenarios.

Blokelv Borehole

Figure 3.7 illustrates a possible thermal history reconstruction for the sedimentary units intersected in the **Blokelv Borehole**, based on the synthesis developed in preceding Sections. The corresponding burial history reconstruction is illustrated in Figure 3.8. Key aspects of this reconstruction are:

- Surface temperature of 20°C at 30 Ma and earlier, decreasing to 10°C at 12 Ma and to the present-day value of 4°C over the last 12 Myr.
- Paleogeothermal gradient of 30°C/km, constant to the present day.

- Localised heating within the vicinity of sample GC1052-2 to a paleotemperature around 120°C, shown at ~53 Ma but any time between 56 and 45 Ma is allowed by the regional timing constraints on this episode.
- Deposition of an additional 2750 metres of section above the Late Jurassic section intersected in the borehole, between 146 and 36 Ma.
- Subsequent removal of 1150 metres of section between 36 and 30 Ma, followed by deposition of a further 600 metres of section between 30 and 12 Ma.
- Removal of the remaining 2200 metres of additional section between 12 Ma and the present day.

Note that the amount of re-burial between the two episodes of exhumation is not controlled by the data, and therefore also the exact amount of section removed in the initial episode beginning at 36 Ma is also not constrained.

In this reconstruction, for the purposes of illustration the localised heating around sample GC1052-2 at ~53 Ma is shown as taking place over a duration of 2 Myr, as is the subsequent cooling. In reality, heating most likely occurred over a much shorter timescale, as it was related to either contact or hydrothermal effects associated with igneous activity. This implies, in turn, that the paleotemperatures required to explain the AFTA and VR data must have been higher that those listed in Tables 3.3 and 3.4, which are predicated on heating rates of 1°C/Myr and cooling rates of 10°C/Myr. As a rough "rule of thumb", an increase of an order of magnitude in heating rate requires an increase in the corresponding paleotemperature by ~10°C, for both AFTA and VR.

With the above caveats in terms of timescales of heating and cooling, this reconstruction is considered to provide a reliable depiction of the history of the Late Jurassic section intersected in the Blokelv Borehole.

Table 3.1: Summary of apatite fission track data in samples from the Bloklev Borehole, Jameson Land, East Greenland (Geotrack Report #1052)

Sample number	Average depth (m)	Present temperature[*1] (°C)	Stratigraphic age (Ma)	Mean track length (µm)	Predicted mean track length[*2] (µm)	Fission track age (Ma)	Predicted fission track age[*2] (Ma)
GC1052-1	6	5	159-146	12.25±0.22	14.9	50.4±6.2	148
GC1052-2	219	12	159-146	11.71±0.23	14.7	38.5±4.0	155

[*1] Se-e Appendix A for discussion of present temperature data.

[*2] Values predicted from the Default Thermal History (Section 2.1); i.e. assuming that each sample is now at its maximum temperature since deposition. The values refer only to tracks formed after deposition. Samples may contain tracks inherited from sediment provenance areas. Calculations refer to apatites within the measured compositional range for each sample, as discussed in Appendix A. For this reason, predicted ages may not vary smoothly with depth.

Note: all depths quoted are TVD with respect to kb elevation.

Table 3.2: Summary of thermal history interpretation of AFTA data in samples from the Bloklev Borehole, Jameson Land, East Greenland (Geotrack Report #1052)

Sample No. Depth Present temp Strat. age	Do AFTA data require any revision of present temperature?	Evidence of higher temperatures in the past from length data?	Evidence of higher temperatures in the past from fission track age data?	Conclusion
GC1052-1 6 m 5°C 159-146 Ma	No	Yes [Mean track length is ~2.6 µm shorter than expected on the basis of the Default Thermal History. Modelling the AFTA parameters through likely thermal history scenarios shows that measured lengths can be explained *only* by higher paleotemperatures after deposition and not by inheritance of short tracks from the sediment source terrain.]	Yes [Central fission track age and most of the single grain ages are significantly younger than expected on the basis of the Default Thermal History.]	AFTA data clearly show that this sample has been hotter than present temperature at some time since deposition.
GC1052-2 219 m 12°C 159-146 Ma	No	Yes [Mean track length is ~3 µm shorter than expected on the basis of the Default Thermal History. Modelling the AFTA parameters through likely thermal history scenarios shows that measured lengths can be explained *only* by higher paleotemperatures after deposition and not by inheritance of short tracks from the sediment source terrain.]	Yes [Central fission track age and most of the single grain ages are significantly younger than expected on the basis of the Default Thermal History.]	AFTA data clearly show that this sample has been hotter than present temperature at some time since deposition.

Note: Interpretation of AFTA data is based on comparison of measured AFTA parameters with values predicted from "Default Thermal History" (Section 2.1); i.e., assuming that each sample is now at its maximum temperature since deposition. The predicted values for each sample are summarised in Table 3.1, and refer only to tracks formed after deposition. Samples may also contain tracks inherited from sediment provenance areas, which must be allowed for in interpreting the data. Calculations refer to apatites with the compositional range appropriate to each sample, as explained in Appendix A.

Table 3.3: Estimates of timing and magnitude of elevated paleotemperatures from AFTA data in samples from the Bloklev Borehole, Jameson Land, East Greenland (Geotrack Report #1052)

Sample Details	**Paleo-thermal constraints**			**Comments**
Sample No. Depth Present temp Strat. age	Event	Maximum paleo-temperature (°C)	Onset Of Cooling (Ma)	
GC1052-1 6 m 5°C 159-146 Ma	1: 2:	100-105 70-80	58-28 17-5	Excellent quality AFTA data (20 ages, 103 lengths) clearly require at least two discrete paleo-thermal events, as shown left. Cooling from a maximum paleotemperature between 100 and 105°C beginning some time between 58 and 28 Ma is required in order to explain the degree of fission track age reduction and the shorter tracks in the length distribution, while subsequent cooling from a peak paleotemperature in the range 70 to 80°C which began between 17 and 5 Ma is required to explain the reduction in the length of tracks forming the main mode in the length distribution. **Equivalent $R_o$max: 0.61-0.63%.** Measured VR values between 0.50 and 0.56% from slightly deeper in the borehole (Table D.2), equivalent to maximum paleotemperatures of 86 to 93°C (Table 3.4), are slightly lower than the range derived from the AFTA solution, and are interpreted as being slightly suppressed, as commonly observed in organic-rich source rock facies.
GC1052-2 219 m 12°C 159-146 Ma	1: 2: 3:	*>110* 100-110 80-85	*60-50?* 50-28 13-3	Excellent quality AFTA data (20 ages, 103 lengths) clearly require at least two discrete paleo-thermal events, and probably also require a third, as shown left. Cooling from a maximum paleotemperature between 100 and 110°C beginning some time between 50 and 28 Ma is required in order to explain the degree of fission track age reduction and the shorter tracks in the length distribution, while subsequent cooling from a peak paleotemperature in the range 80 to 85°C which began between 13 and 3 Ma is required to explain the reduction in the length of tracks forming the main mode in the length distribution. But this two event solution does not provide a good match to the detail of the length distribution, or to the variation of fission track age with wt% Cl, and all aspects of the data can only be brought into a consistent solution by including a third, earlier episode of cooling from >110°C at some time around 60 to 50 Ma, although the precise timing of this episode cannot be defined with high precision. **Equivalent $R_o$max: >0.66% (assuming the three-event solution).** Measured VR values between 0.66 and 0.74% from slightly deeper in the borehole (Table D.2), equivalent to maximum paleotemperatures of 109 to 121°C (Table 3.4), are highly consistent with the range of equivalent VR values derived from the AFTA solution in this sample.

All thermal history constraints are based on assumed heating rates of 1°C/Myr and cooling rates of 10°C/Myr.

Events shown in italics are not required by the AFTA data, though they are allowed within the limits shown.

Table 3.4: Maximum paleotemperatures from VR data in samples from the Blokelv Borehole, East Greenland (Geotrack Report #1052)

Sample number	Average depth (m)	Stratigraphic age (Ma)	Supplied VR $R_o$max[*1] (%)	Number of readings (%)	Maximum paleotemperature[*2] (°C)
16822	23.59	159-146	0.52	43	86
16823	32.78	159-146	0.54	84	90
16826	68.77	159-146	0.50	39	83
16827	80.77	159-146	0.55	82	91
16828	92.74	159-146	0.56	97	93
16829	104.79	159-146	-	-	-
16830	116.82	159-146	0.56	101	96
16833	152.75	159-146	0.61	47	100
16834	164.82	159-146	0.68	150	113
16835	176.77	159-146	0.62	86	102
16836	188.77	159-146	0.65	77	108
16837	200.76	159-146	0.66	107	109
16838	212.77	159-146	0.78	98	125
16839	224.74	159-146	0.74	48	121

[*1] Numbers in brackets denote the number of fields measured. A target of 25 fields is usually considered to characterise an analysis of the highest quality.

[*2] All estimates of maximum paleotemperature were determined using assumed heating rates of 1°C/Myr and cooling rates of 10°C/Myr. See Section 2.2 for further details.

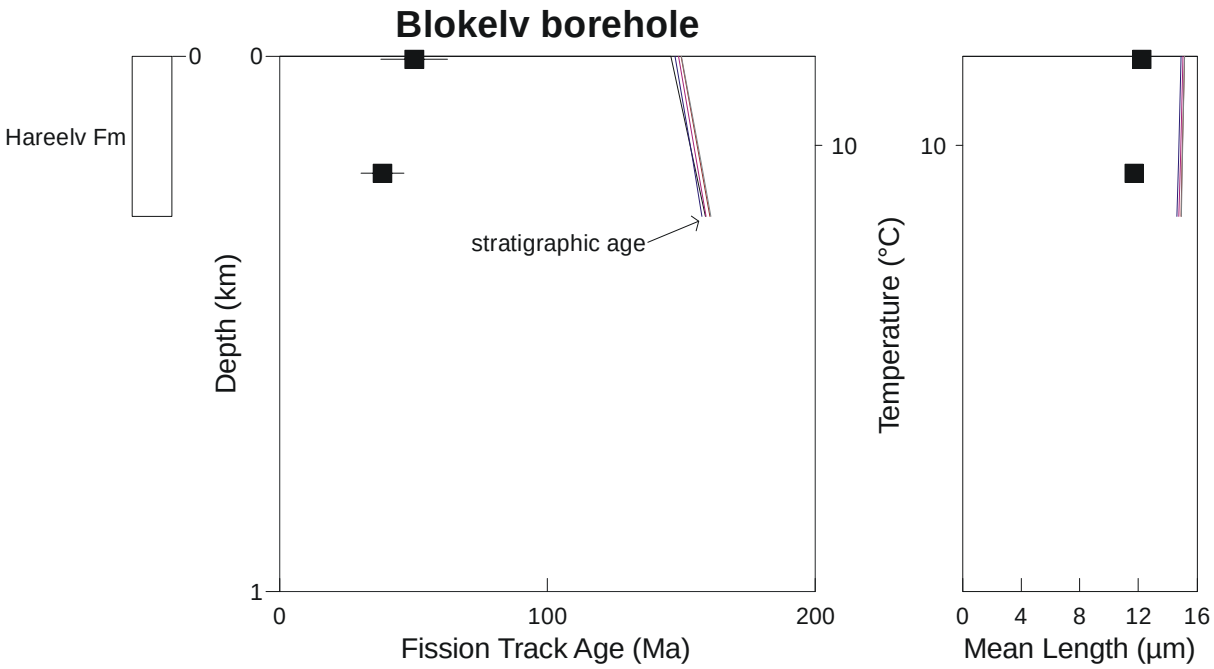

Figure 3.1: AFTA parameters plotted against sample depth and present temperature for samples from **the Blokelv Borehole, Jameson Land, East Greenland**. The variation of stratigraphic age with depth is also shown, as the solid line in the central panel. Present-day temperatures shown here are based on a surface temperature of 4°C and an assumed present-day thermal gradient of 30°C/km. Coloured lines show the pattern of fission track age and mean track length predicted (for apatites containing 0.0-0.1, 0.4-0.5, 0.9-1.0 and 1.5-1.6 wt% Cl) from the Default Thermal History (see Section 2.1) based on the thermal structure reported above, combined with the burial history shown in Figure 3.4.

Measured fission track ages in the two samples are significantly less than the respective depositional ages and the values predicted from the Default thermal History, and mean track lengths are much shorter than predicted from the Default Thermal History. This shows clearly that the sampled units have been hotter in the past. See text for further details.

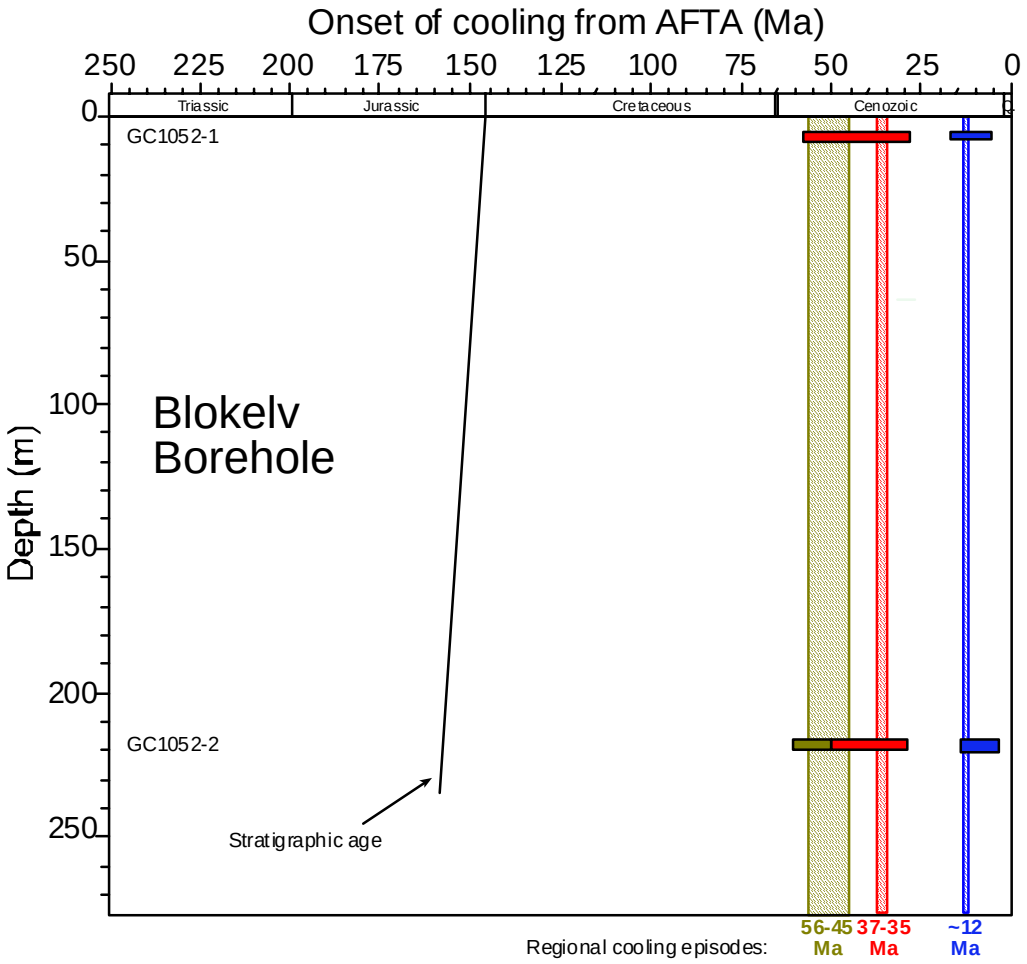

Figure 3.2: Timing constraints on cooling episodes derived from AFTA data in two samples from **the Blokelv Borehole, Jameson Land, East Greenland**. The timing of cooling in three regional paleo-thermal episodes identified from AFTA data in a regional study of outcrop samples across Jameson Land and adjacent regions are also shown. The three episodes identified in samples from this study show good agreement with the timing of the regional episodes and the results presented in this report are interpreted on this basis, as explained in the text.

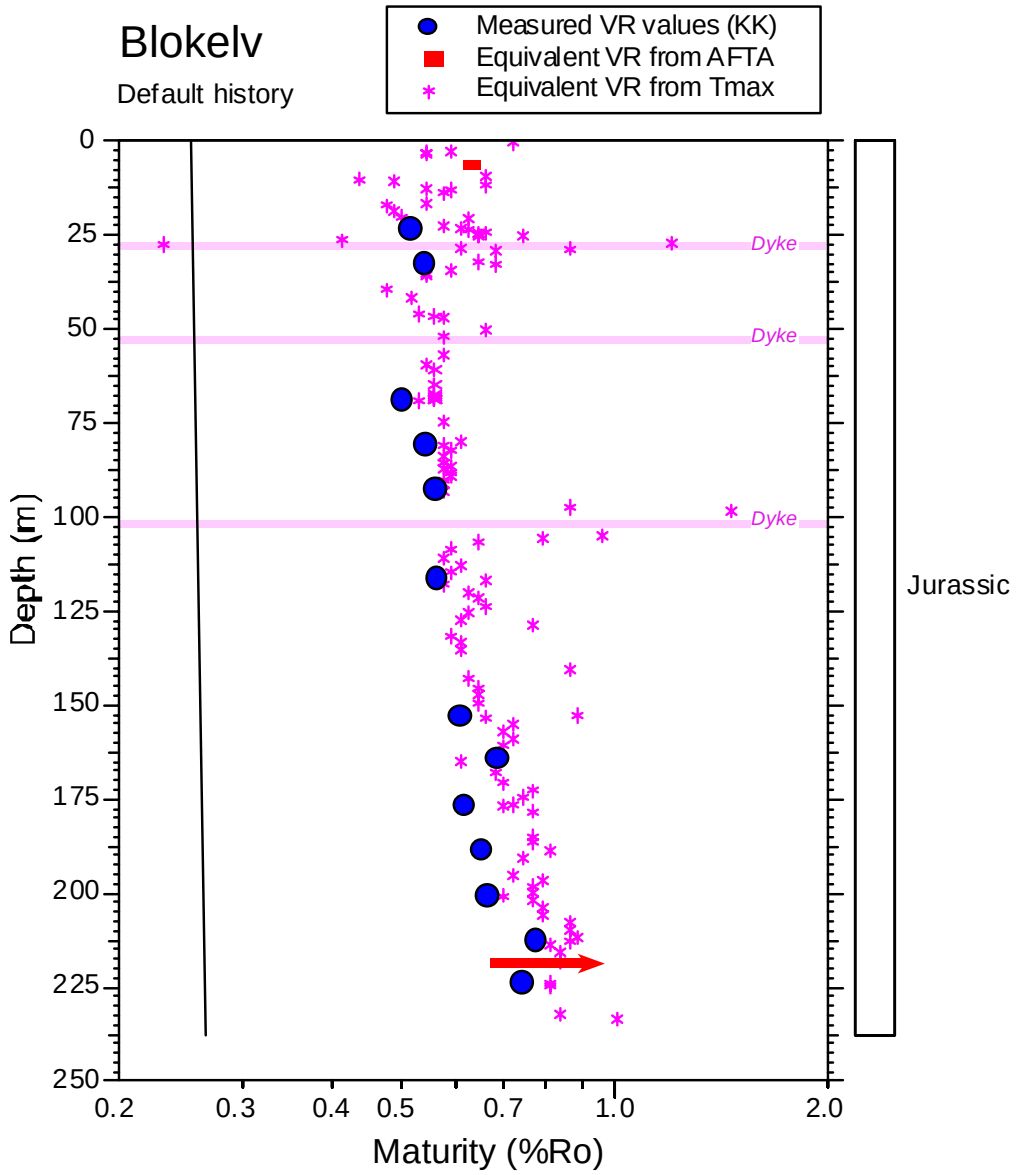

Figure 3.3: Vitrinite reflectance values in samples from **the Blokelv Borehole, Jameson Land, East Greenland** (summarised in Table D.2), plotted against depth (TVD rkb), together with equivalent VR values (VR_{eq}) derived from RockEval Tmax data as explained in Appendix D, and equivalent ranges of VR defined from the AFTA data (Table 3.3). The solid line shows the profile predicted from the "Default Thermal History", i.e., the history calculated from the assumption that all units throughout the well are currently at their maximum temperatures since deposition (see Section 2.1). The Default Thermal History was constructed using the burial history derived from the section intersected in the well (shown in Figure 3.4), combined with an assumed mean present-day thermal gradient of 30°C/km and an assumed surface temperature of 4°C.

All VR and VR_{eq} values are consistently higher than predicted from the Default Thermal History, showing that the sampled units must have been hotter in the past. Excursions in the Tmax data above the background trend define contact heating effects associated with minor intrusions intersected by the borehole. Comparison of paleotemperatures derived from AFTA and VR values is discussed in the text.

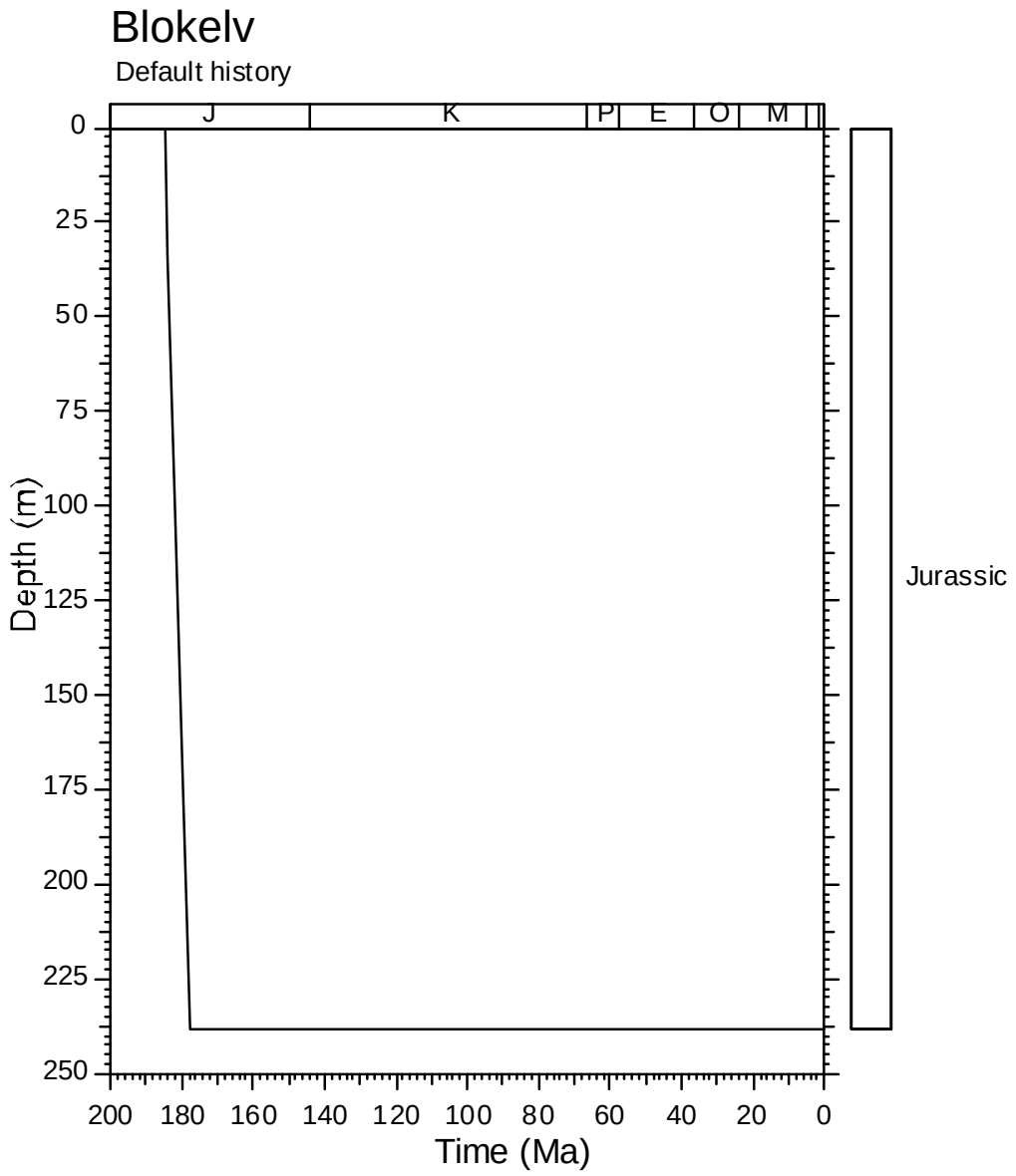

Figure 3.4: Burial History derived from the preserved section in **the Blokelv Borehole, Jameson Land, East Greenland**, used together with an assumed present-day thermal gradient of 30°C/km and an assumed surface temperature of 4°C (Appendix A) to predict the Default Thermal Histories for individual AFTA samples and the maturity-depth profile shown in Figure 3.2.

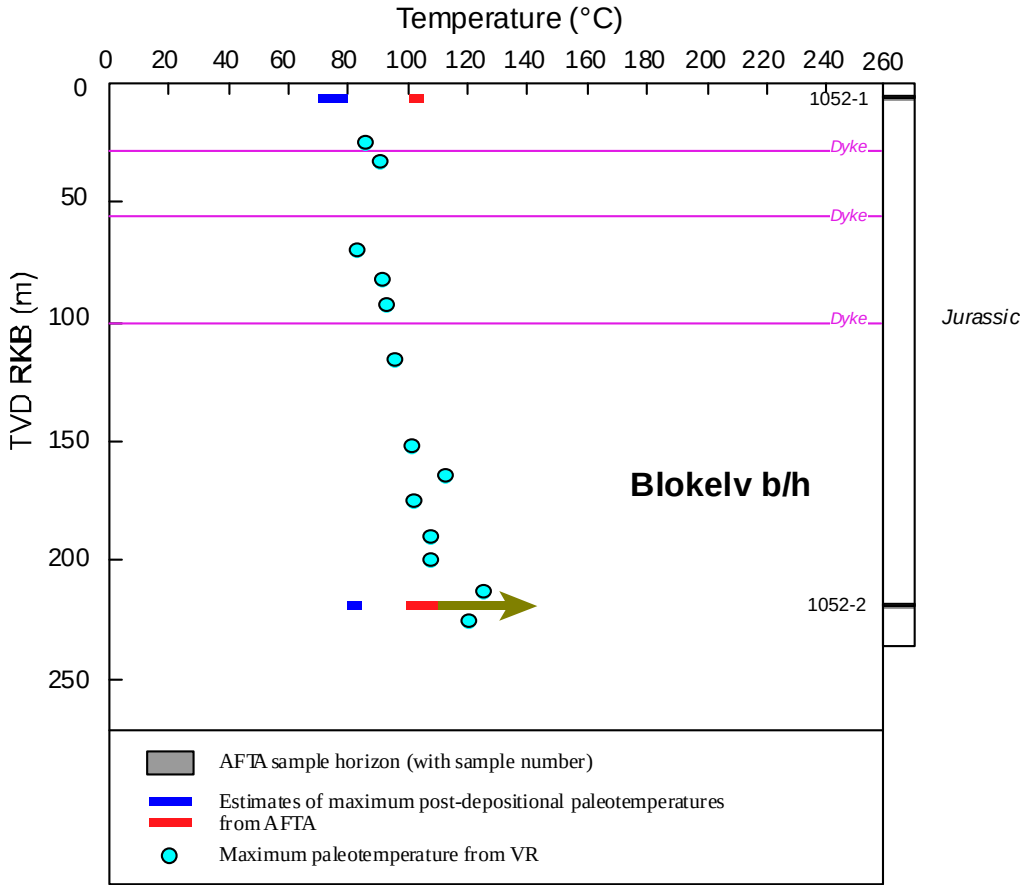

Figure 3.5: Paleotemperature constraints derived from AFTA and VR data in **the Blokelv Borehole, Jameson Land, East Greenland**, plotted against depth (rkb). AFTA data in the deeper sample, GC1052-2, define three discrete paleo-thermal episodes, while only two episodes can be resolved in AFTA data from the shallower sample, GC1052-1. Paleotemperature constraints are colour-coded to the appropriate paleo-thermal episode as in Figure 3.2.

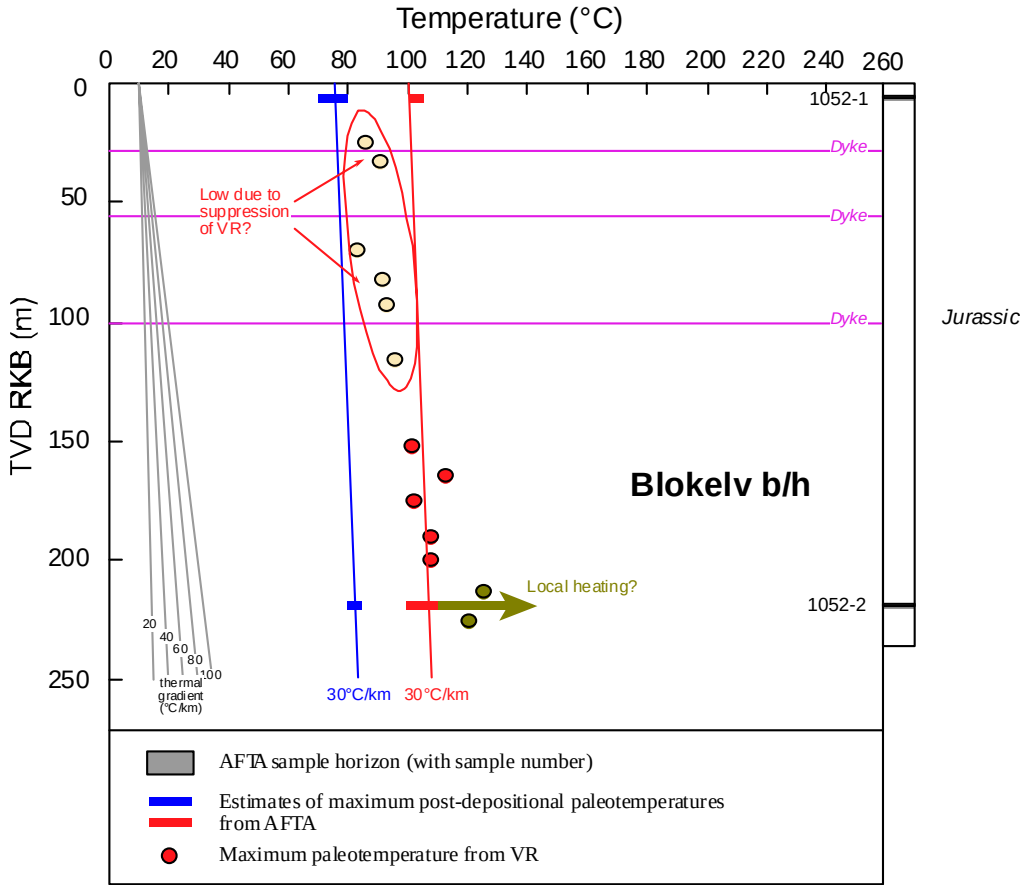

Figure 3.6: Interpreted paleotemperature profiles describing the paleotemperatures in three episodes derived from AFTA and VR data in **the Blokelv Borehole, Jameson Land, East Greenland**, from Figure 3.5. Based on evidence from an extensive regional study of East Greenland, we interpret the maximum paleotemperature revealed by AFTA data in sample GC1052-2 as representing localised heating due to intrusive activity, possibly from the passage of hot fluids within the sand-dominated section from where this sample was collected. The end-Eocene (37-35 Ma) and Miocene (~12 Ma) paleotemperatures revealed by AFTA are interpreted as representing the effects of regional burial, with end-Eocene cooling representing the onset of regional exhumation, and Miocene cooling representing the final phase. On this basis, the VR values shallower than 120 metres are interpreted as anomalously low, most likely due to suppression of reflectance in source-rock facies organic-rich mudstones. VR values deeper than 120 metres are regarded as providing reliable indications of the degree of post-depositional heating. Linear profiles representing various thermal gradients are shown, for reference, together two profiles representing with our preferred interpretation, based on regional data, involving paleogeothermal gradients of ~30°C/km for the end-Eocene and Miocene episodes.

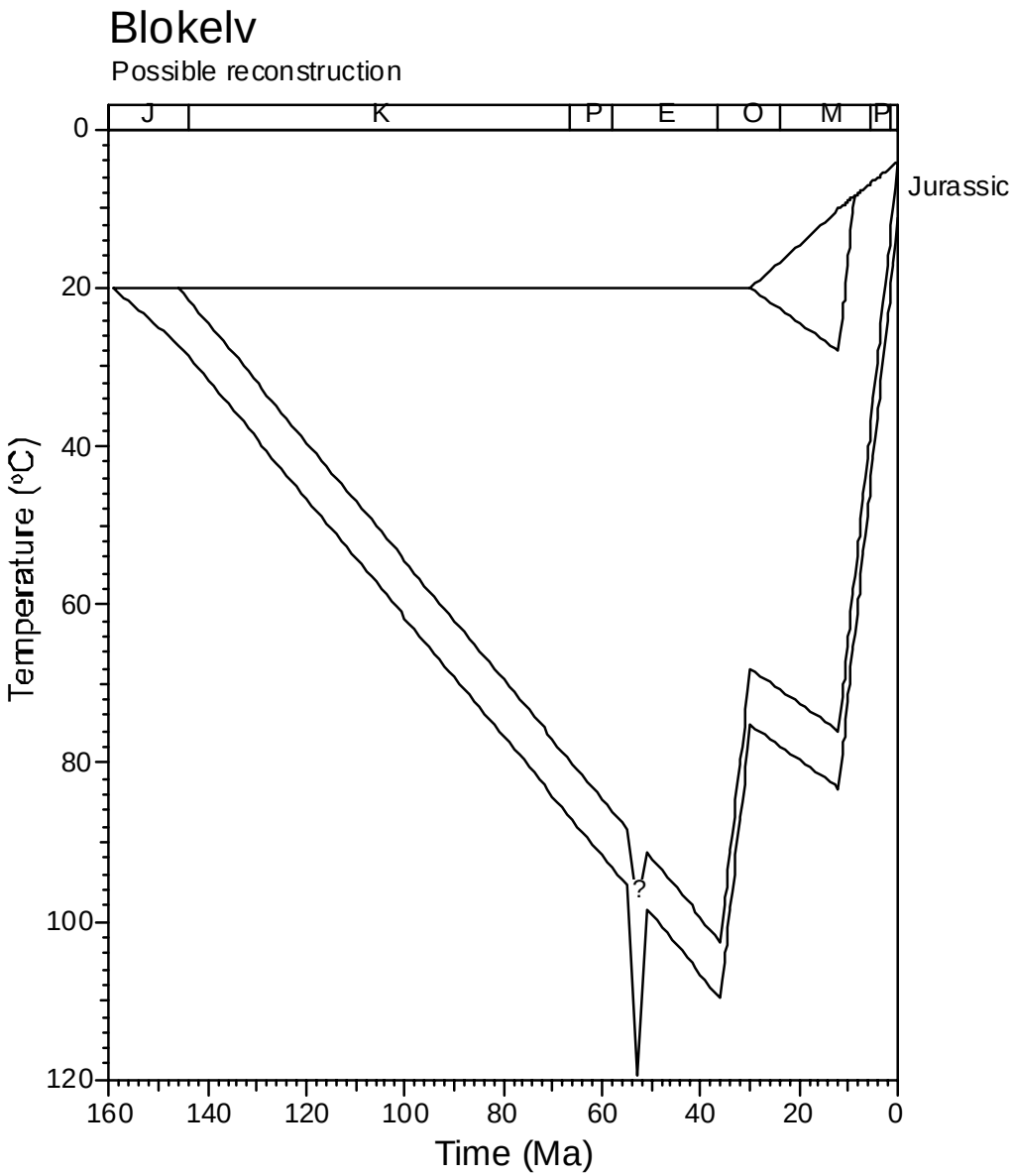

Figure 3.7: Schematic illustration of a possible thermal history reconstruction for **the Blokelv Borehole, Jameson Land, East Greenland**. Note that the earliest heating event is likely to be localised within the deeper part of the section intersected in the borehole, and the magnitude of any heating at this time shallower in the section is uncertain. See text for further details.

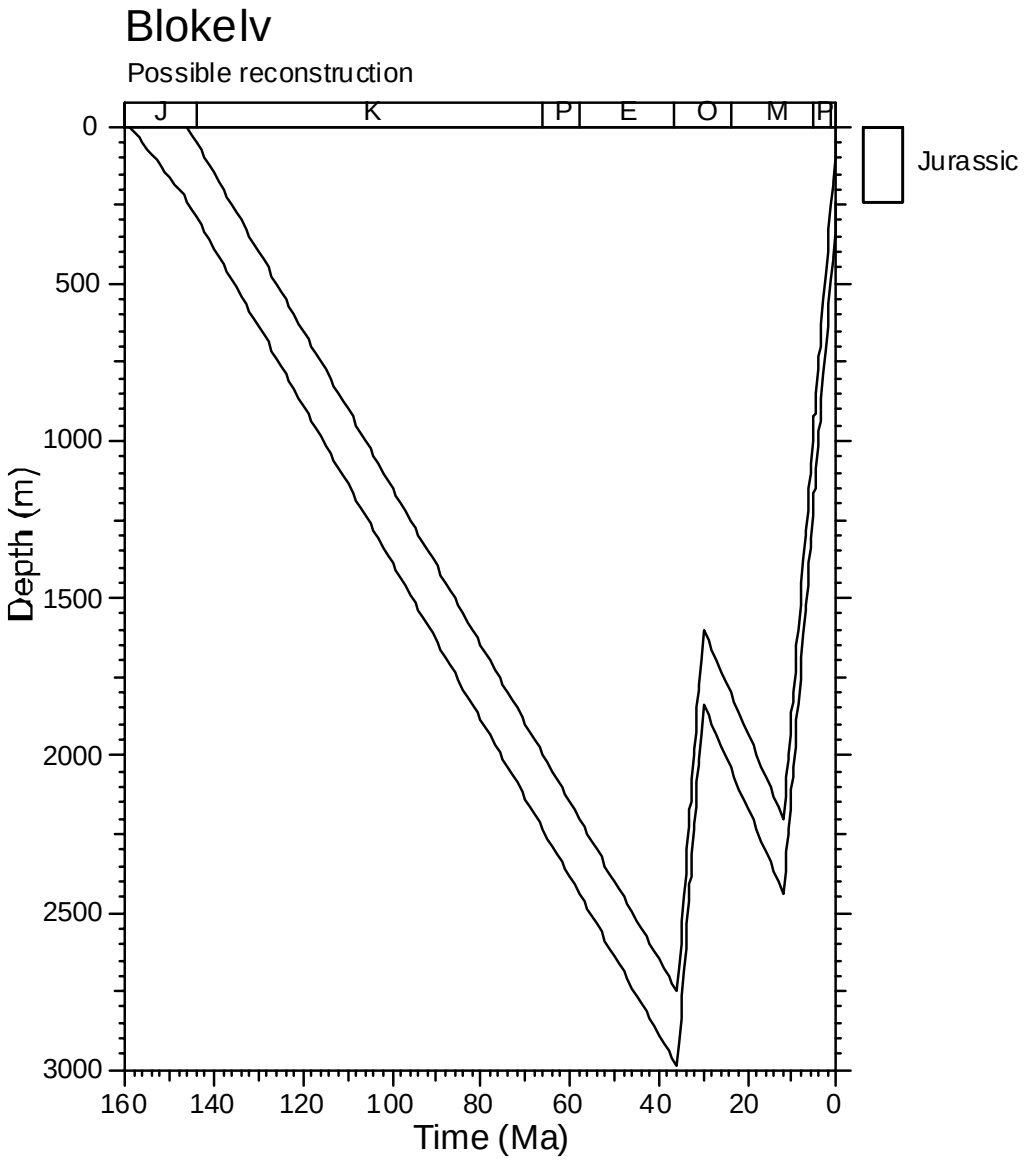

Figure 3.8: Burial history reconstruction derived from AFTA and VR data in **the Blokelv Borehole, Jameson Land, East Greenland**. This reconstruction is based on burial of the preserved Upper Jurassic section by an additional 2.75 km of Late Jurassic to Eocene section, which is removed in two episodes of exhumation in the latest Eocene and Miocene. The exact magnitude of any reburial between these two episodes is unknown, and the reconstruction illustrated is just one of many possibilities.

4. Recommendations for further work

The overall conclusions of this study concerning the thermal history interpretation of AFTA and VR data from the Blokelv Borehole are regarded as reliable, and it is unlikely that further AFTA or VR analyses from this borehole would add much insight into the history.

However, it would be useful to investigate possible diagenetic effects within the sandstone units intersected by the borehole, in terms of the history cementation and fluid inclusion measurements, to assess the extent of hydrothermal circulation inferred in sample GC1052-2.

Extension to additional outcrop samples within the vicinity of the borehole, as well as analysis of samples from any future boreholes, would assist in defining the extent and variation in magnitude of the key paleo-thermal episodes identified in this report.

References

Bray, R.J., Green, P.F. and Duddy, I.R., (1992). Thermal History Reconstruction using apatite fission track analysis and vitrinite reflectance: a case study from the UK East Midlands and the Southern North Sea. In: Hardman, R.F.P. (ed.), Exploration Britain: Into the next decade. *Geological Society Special Publication*, 67, 3-25.

Burnham, A.K. and Sweeney, J.J., (1989). A chemical kinetic model of vitrinite reflectance maturation. *Geochimica et Cosmochimica Acta.*, 53, 2649-2657.

Sweeney, J.J. and Burnham, A.K., (1990). Evaluation of a simple model of vitrinite reflectance based on chemical kinetics. *AAPG Bulletin*, 74, 1559-1570.

APPENDIX A

Sample Details, Geological Data and Apatite Compositions

A.1 Sample details

Samples of core from two depth intervals in **the Blokelv Borehole, Jameson Land, West Greenland,** were submitted for AFTA by **the Geological Survey of Denmark and Greenland (GEUS), Copenhagen**. Details of these samples, including sample depths, stratigraphic ages and estimates of present temperature for each sample, are summarised in Table A.1. (Details of present temperature estimation for each well are presented in Section A.3, below). Yields of apatite obtained from each AFTA sample are also listed in Table A.1. These yields are summarised and discussed in Section 1.3, together with discussion of overall AFTA data quality.

No new VR analyses were undertaken for this report. A set of existing VR data was provided by GEUS, with details summarised in Table D.2

A.2 Stratigraphic details

Details of the stratigraphic breakdown of the preserved section in the well were provided by the client. The chronostratic (relative succession) assignment of each sample was converted to a chronometric (numerical) scale using Gradstein et al. (2004), with results summarised in Table A.2. The stratigraphic age of each AFTA sample, derived from this information, is summarised in Table A.1. Similar information for VR samples is summarised in Tables D.2.

Any slight errors in the estimated chronometric ages of each sample are not expected to affect the thermal history interpretation of either the AFTA or VR data to any significant degree.

A.3 Present temperatures

In application of any technique involving estimation of paleotemperatures, it is critical to control the present temperature profile, since estimation of maximum

paleotemperatures proceeds from assessing how much of the observed effect could be explained by the magnitude of present temperatures.

For this report, a present-day thermal gradient of 30°C/km was assumed, together with a mean annual surface temperature of 4°C. Because of the shallow depth of both samples analysed, the final interpretation is insensitive to the precise value of present-day temperature in each sample.

A.4 Grain morphologies

The apatite grains in samples analysed for this study showed a variety of morphologies, with euhedral, sub-euhedral to sub-rounded and rounded grains present in each sample. No clear trends were evident which could be interpreted in terms of systematic variation in sedimentary provenance between different samples.

A.5 Apatite compositions

The annealing kinetics of fission tracks in apatite are affected by chemical composition, specifically the Cl content, as explained in more detail in Appendix C. In all samples analysed for this report, Cl contents were measured in all apatite grains analysed (i.e. for both fission track age determination and track length measurement), and the measured compositions in individual grains have been employed in interpreting the AFTA data, using methods outlined in Appendix C.

Chlorine contents were measured using a fully automated Jeol JXA-5A electron microprobe equipped with a computer controlled X-Y-Z stage and three computer controlled wavelength dispersive crystal spectrometers, with an accelerating voltage of 15kV and beam current of 25nA. The beam was defocussed to 20 µm diameter to avoid problems associated with apatite decomposition, which occur under a fully focussed 1 - 2 µm beam. The X-Y co-ordinates of dated grains within the grain mount were transferred from the Autoscan Fission Track Stage to a file suitable for direct input into the electron microprobe. The identification of each grain was verified optically prior to analysis. Cl count rates from the analysed grains were converted to wt% Cl by reference to those from a Durango apatite standard (Melbourne University Standard APT151), analysed at regular intervals. This approach implicitly takes into account atomic number absorption and fluorescence matrix effects, which are normally calculated explicitly when analysing for all elements. A value of 0.43 wt% Cl was used

for the Durango standard, based on repeated measurements on the same single fragment using pure rock salt (NaCl) as a standard for chlorine. This approach gives essentially identical results to Cl contents determined from full compositional measurements, but has the advantage of reducing analytical time by a factor of ten or more.

Chlorine contents in individual grains are listed in the fission track age summary data sheet for each sample in Appendix B. Table B.3 contains fission track age and length data grouped into 0.1 wt% Cl intervals on the basis of chlorine contents of the grains from which the data are derived. A plot of fission track age against Cl content is also shown in the data sheet for each sample, together with a histogram of Cl contents in all individual apatite grains analysed from each sample (i.e. grains analysed for both age and length measurements).

Lower limits of detection for chlorine content have been calculated for typical analytical conditions (beam current, counting time, etc.) and are listed in Table A.4. Errors in wt% composition are given as a percentage and quoted at 1σ for chlorine determinations. A generalised summary of errors for various wt% chlorine values is presented in Table A.5.

Apatite compositions in this study

In both samples analysed for this study, the histograms of Cl content show a similar pattern, typical of the distribution of Cl contents found in detrital apatites from common quartzo-feldspathic sandstone samples from around the world. The majority of grains have Cl contents between 0 and 0.1 wt%, while a smaller number of grains give values up to ~0.5 wt% (close to the value found in the Durango apatite on which our original kinetic model of fission track behaviour was based, see Appendix C). Some samples of this rock type may contain a few grains with between 0.5 and 1.0 wt% Cl, but in these two samples, no grains contain above 0.5 wt% Cl.

In all samples analysed for this report, the measured distribution of compositions has been employed in interpreting the AFTA data, using methods outlined in Appendix C.

References

Gradstein, F.M., Ogg, J.G. and Smith, A.G. (2004). *A geologic time scale 2004*, Cambridge University Press.

Table A.1: Details of fission track samples and apatite yields - samples from East Greenland (Geotrack Report #1052)

Sample number	Depth (m)	Sample type	Stratigraphic Subdivision	Stratigraphic age (Ma)	Present temperature *1 (°C)	Raw weight (g)	Washed weight (g)	Apatite yield *2
Blokelv borehole								
GC1052-1	6	borehole	Hareelv Fm	159-146	5	1060	560	excellent
GC1052-2	219	borehole	Hareelv Fm	159-146	12	1020	450	excellent

*1 See Appendix A for discussion of present temperature data.

*2 Yield based on quantity of mineral suitable for age determination. Excellent: >20 grains; Good: 15-19 grains; Fair: 10-14 grains; Poor: 5-9 grains; Very Poor: <5 grains.

Table A.2: Summary of stratigraphy - East Greenland (Geotrack Report #1052)

	KB elevation (mAMSL)	Ground level (m)	Stratigraphic Interval	Depth of Top TVD rKB (m)	Age of Top (Ma)
Blokelv borehole					
	181	181	*Unconformity*	0	0
			Hareelv Fm	0	146
			TD	300	159

All depths quoted are with respect to KB, except where otherwise stated.

Table A.3: Lower Limits of Detection for Apatite Analyses (Geotrack Report #1052)

Element	LLD (95% c.l.)		LLD (99% c.l.)	
	(wt%)	(ppm)	(wt%)	(ppm)
Cl	0.01	126	0.02	182

Table A.4: Per cent errors in chlorine content (Geotrack Report #1052)

Chlorine content (wt%)	Error (%)
0.01	9.3
0.02	8.7
0.05	7.3
0.10	6.1
0.20	4.7
0.50	3.2
1.00	2.3
1.50	1.9
2.00	1.7
2.50	1.5
3.00	1.4

Errors quoted are at 1σ. See Appendix A for more details.

APPENDIX B

Sample Preparation, Analytical Details and Data Presentation

B.1 Sample Preparation

Core and outcrop samples are crushed in a jaw crusher and then ground to sand grade in a rotary disc mill. Cuttings samples are washed and dried before grinding to sand grade. The ground material is then washed to remove dust, dried and processed by conventional heavy liquid and magnetic separation techniques to recover heavy minerals. Apatite grains are mounted in epoxy resin on glass slides, polished and etched for 20 sec in 5M HNO_3 at 20°C to reveal the fossil fission tracks.

After etching, all mounts are cut down to 1.5 x 1 cm, and cleaned in detergent, alcohol and distilled water. The mounts are then sealed in intimate contact with low-uranium muscovite detectors within heat-shrink plastic film. Each batch of mounts is stacked between two pieces of uranium standard glass, which has been prepared in similar fashion. The stack is then inserted into an aluminium can for irradiation.

After irradiation, the mica detectors are removed from the grain mounts and standard glasses and etched in hydrofluoric acid to reveal the fission tracks produced by induced fission of ^{235}U in the apatite and standard glass.

B.2 Analytical Details

Fission track ages

Fission track ages are calculated using the standard fission track age equation using the zeta calibration method (equation five of Hurford and Green, 1983), viz:

$$\text{F.T. AGE} = \frac{1}{\lambda_D} \ln \left[1 + \left(\frac{\zeta \lambda_D \rho_s g \rho_D}{\rho_i} \right) \right] \qquad \text{B.1}$$

where:
- λ_D = Total decay constant of ^{238}U (= 1.55125 x 10^{-10})
- ζ = Zeta calibration factor
- ρ_s = Spontaneous track density
- ρ_i = Induced track density
- ρ_D = Track density from uranium standard glass
- g = A geometry factor (= 0.5)

Fission track ages are determined by the external detector method or EDM (Gleadow, 1981). The EDM has the advantage of allowing fission track ages to be determined on single grains. In apatite, tracks are counted in 20 grains from each mount wherever possible. In those samples where the desired number is not present, all available grains are counted, the actual number depending on the availability of suitably etched and oriented grains. Only grains oriented with surfaces parallel to the crystallographic c-axis are analysed. Such grains can be identified on the basis of the etching characteristics, as well as from morphological evidence in euhedral grains. The grain mount is scanned sequentially, and the first 20 suitably oriented grains identified are analysed.

Tracks are counted within an eyepiece graticule divided into 100 grid squares. In each grain, the number of spontaneous tracks (N_s) within a certain number of grid squares (N_a) is recorded. The number of induced tracks (N_i) in the corresponding location within the mica external detector is then counted. Spontaneous and induced track densities (ρ_s and ρ_i, respectively) are calculated by dividing the track counts by the total area counted, given by the product of Na and the area or each grid square (determined by calibration against a ruled stage graticule or diffraction grating). Fission track ages may be calculated by substituting track counts (N_s and N_i) for track densities (ρ_s and ρ_i) in equation B.1, since the areas cancel in the ratio.

Translation between apatite grains in the grain mount and external detector locations corresponding to each grain is carried out using Autoscan™ microcomputer-controlled automatic stages (Smith and Leigh Jones, 1985). This system allows repeated movement between grain and detector, and all grain locations are stored for later reference if required.

Neutron irradiations are carried out in a well-thermalised flux (X-7 facility; Cd ratio for Au ~98) in the Australian Atomic Energy Commission's HIFAR research reactor. Total neutron fluence is monitored by counting tracks in mica external detectors attached to two pieces of Corning Glass Works standard glass CN5 (containing ~11 ppm Uranium) included in the irradiation canister at each end of the sample stack. In determining track densities in external detectors irradiated adjacent to uranium standard glasses, 25 fields are normally counted in each detector. The total track count (N_D) is divided by the total area counted to obtain the track density (ρ_D). The positions of the counted fields are arranged in a 5 x 5 grid covering the whole area of the detector. For typical track densities of between ~5×10^5 and 5×10^6, this is a convenient arrangement to sample across the detector while gathering sufficient counts to achieve a precision of ~±2% in a reasonable time.

A small flux gradient is often present in the irradiation facility over the length of the sample package. If a detectable gradient is present, the track count in the external detector adjacent to each standard glass is converted to a track density (ρ_D) and a value for each mount in the stack is calculated by linear interpolation. When no detectable gradient is present, the track counts in the two external detectors are pooled to give a single value of ρ_D, which is used to calculate fission track ages for each sample.

A Zeta calibration factor (ζ) has been determined empirically for each observer by analysing a set of carefully chosen age standards with independently known K-Ar ages, following the methods outlined by Hurford and Green (1983) and Green (1985).

All track counting is carried out using Zeiss(R) Axioplan microscopes, with an overall linear magnification of 1068 x using dry objectives.

For further details and background information on practical aspects of fission track age determination, see e.g. Fleischer, Price and Walker (1975), Naeser (1979) and Hurford (1986).

Track length measurements

For track length studies in apatite, the full lengths of "confined" fission tracks are measured. Confined tracks are those which do not intersect the polished surface but have been etched from other tracks or fractures, so that the whole length of the track is etched. Confined track lengths are measured using a digitising tablet connected to a microcomputer, superimposed on the microscope field of view via a projection tube. With this system, calibrated against a stage graticule ruled in 2 μm divisions, individual tracks can be measured to a precision of ± 0.2 μm. Tracks are measured only in prismatic grains, characterised by sharp polishing scratches with well-etched tracks of narrow cone angle in all orientations, because of the anisotropy of annealing of fission tracks in apatite (as discussed by Green et al. 1986). Tracks are also measured following the recommendations of Laslett et al. (1982), the most important of which is that only horizontal tracks should be measured. One hundred tracks are measured whenever possible. In apatite samples with low track density, or in those samples in which only a small number of apatite grains are obtained, fewer confined tracks may be available. In such cases, the whole mount is scanned to measure as many confined tracks as possible.

Integrated fission track age and length measurement

Fission track age determination and length measurement are now made in a single pass of the grain mount, in an integrated approach. The location of each grain in which

tracks are either counted or measured is recorded for future reference. Thus, track length measurements can be tied to age determination in individual grains. As a routine procedure we do not measure the age of every grain in which lengths are determined, as this would be much too time-consuming. Likewise we do not only measure ages in grain in which lengths are measured, as this would bias the age data against low track density grains. Nevertheless, the ability to determine the fission track age of certain grains from which length data originate can be a particularly useful aid to interpretation in some cases. Grain location data are not provided in this report, but are available on request.

B.3 Data Presentation

Fission track age data

Data sheets summarising the apatite fission track age data, including full details of fission track age data for individual apatite grains in each sample, together with the primary counting results and statistical data, are given in the following pages. Individual grain fission track ages are calculated from the ratio of spontaneous to induced fission track counts for each grain using equation B.1, and errors in the single grain ages are calculated using Poissonian statistics, as explained in more detail by Galbraith (1981) and Green (1981). All errors are quoted as $\pm 1\sigma$ throughout this report, unless otherwise stated.

The variability of fission track ages between individual apatite grains within each sample can be assessed using a chi-squared (χ^2) statistic (Galbraith, 1981), the results of which are summarised for each sample in the data sheets. If all the grains counted belong to a single age population, the probability of obtaining the observed χ^2 value, for ν degrees of freedom (where ν = number of crystals -1), is listed in the data sheets as $P(\chi^2)$ or P(chi squared).

A $P(\chi^2)$ value greater than 5% can be taken as evidence that all grains are consistent with a single population of fission track age. In this case, the best estimate of the fission track age of the sample is given by the "pooled age", calculated from the ratio of the total spontaneous and induced track counts in all grains analysed. Errors for the pooled age are calculated using the "conventional" technique outlined by Green (1981), based on the total number of tracks counted for each track density measurement (see also Galbraith, 1981).

A $P(\chi^2)$ value of less than 5% denotes a significant spread of single grain ages, suggesting real differences exist between the fission track ages of individual apatite

grains. A significant spread in grain ages can result either from inheritance of detrital grains from mixed source areas (in sedimentary rocks), or from differential annealing in apatite grains of different composition, within a narrow range of temperature.

Calculation of the pooled age inherently assumes that only a single population of ages is present, and is thus not appropriate to samples containing a significant spread of fission track ages. In such cases Galbraith, has recently devised a means of estimating the modal age of a distribution of single grain fission track ages which is referred to as the "central age". Calculation of the central age assumes that all single grain ages belong to a Normal distribution of ages, with a standard deviation (σ) known as the "age dispersion". An iterative algorithm (Galbraith and Laslett, 1993) is used to provide estimates of the central age with its associated error, and the age dispersion, which are all quoted in the data sheets. Note that this treatment replaces use of the "mean age", which has used been in the past for those samples in which $P(\chi^2)<5\%$. For samples in which $P(\chi^2)>5\%$, the central age and the pooled age should be equal, and the age dispersion should be less than ~10%.

Table B.1 summarises the fission track age data in apatite from each sample analysed.

Construction of radial plots of single grain age data

Single grain age data are best represented in the form of radial plot diagrams (Galbraith, 1988, 1990). As illustrated in Figure B.1, these plots display the variation of individual grain ages in a plot of y against x, where:

$$y = (z_j - z_o) / \sigma_i \qquad x = 1/\sigma_j \qquad \text{B.2}$$

and; z_j = Fission track age of grain j
z_o = A reference age
σ_j = Error in age for grain j

In this plot, all points on a straight line from the origin define a single value of fission track age, and, at any point, the value of x is a measure of the precision of each individual grain age. Therefore, precise individual grain ages fall to the right of the plot (small error, high x), which is useful, for example, in enabling precise, young grains to be identified. The age scale is shown radially around the perimeter of the plot (in Ma). If all grains belong to a single age population, all data should scatter between y = +2 and y = -2, equivalent to scatter within $\pm 2\sigma$. Scatter outside these boundaries shows a significant spread of individual grain ages, as also reflected in the values of $P(\chi^2)$ and age dispersion.

In detail, rather than using the fission track age for each grain as in equation B.2, we use:

$$z_j = \frac{N_{sj}}{N_{ij}} \qquad \sigma_j = \{1/N_{sj} + 1/N_{ij}\} \qquad \text{B.3}$$

as we are interested in displaying the scatter within the data from each sample in comparison with that allowed by the Poissonian uncertainty in track counts, without the additional terms which are involved in determination of the fission track age (ρ_D, ζ, etc).

Zero ages cannot be displayed in such a plot. This can be achieved using a modified plot, (Galbraith, 1990) with:

$$z_j = \text{arc sin}\sqrt{\left\{\frac{N_{sj}+3/8}{N_{sj} + N_{ij} + 3/4}\right\}} \qquad \sigma_j = \frac{1}{2}\sqrt{\left\{\frac{1}{N_{sj} + N_{ij}}\right\}} \qquad \text{B.4}$$

Note that the numerical terms in the equation for z_j are standard terms, introduced for statistical reasons. Using this arc-sin transformation, zero ages plot on a diagonal line which slopes from upper left to lower right. Note that this line does not go through the origin. Figure B.2 illustrates this difference between conventional and arc-sin radial plots, and also provides a simple guide to the structure of radial plots.

Use of arc-sin radial plots is particularly useful in assessing the relative importance of zero ages. For instance, grains with $N_s = 0$, $N_i = 1$ are compatible with ages up to ~900 Ma (at the 95% confidence level), whereas grains with $N_s = 0$, $N_i = 50$ are only compatible with ages up to ~14 Ma. The two data would readily be distinguishable on the radial plot as the 0,50 datum would plot well to the right (high x) compared to the 0,1 datum.

In this report the value of z corresponding to the stratigraphic age of each sample (or the midpoint of the range where appropriate) is adopted as the reference value, z_o. This allows rapid assessment of the fission track age of individual grains in relation to the stratigraphic age, which is a key component in the interpretation of AFTA data, as explained in more detail in Appendix C.

Note that the x axis of the radial plot is normally not labelled, as this would obscure the age scale around the plot. In general labelling is not considered necessary, as we are concerned only with relative variation within the data, rather than absolute values of precision.

Radial plots of the single grain age data in apatite from each sample analysed in this report are shown on the fission track age data summary sheets at the end of this Appendix. Use of radial plots to provide thermal history information is explained in Appendix C and Figure C.7.

Track length data

Distributions of confined track lengths in apatite from each sample are shown as simple histograms on the fission track age data summary sheets at the end of this Appendix. For every track length measurement, the length is recorded to the nearest 0.1 µm, but the measurements have been grouped into 1 µm intervals for construction of these histograms. Each distribution has been normalised to 100 tracks for each sample to facilitate comparison. A summary of the length distribution in each sample is presented in Table B.2, which also shows the mean track length in each sample and its associated error, the standard deviation of each distribution and the number of tracks (N) measured in each sample. The angle which each confined track makes with the crystallographic c-axis is also routinely recorded, as is the width of each fracture within which tracks are revealed. These data are not provided in this report, but can be supplied on request.

Breakdown of data into compositional groups

In Table B.3, AFTA data are grouped into compositional intervals of 0.1 wt% Cl width. Parameters for each interval represent the data from all grains with Cl contents within each interval. Also shown are the parameters for each compositional interval predicted from the Default Thermal History (see Section 2.1). These data form the basis of interpretation of the AFTA data, which takes full account of the influence of Cl content on annealing kinetics, as described in Appendix C. Distributions of Cl contents in all apatites analysed from each sample (i.e. for both age and length determinations) are shown on the fission track age data summary sheets at the end of this Appendix.

Plots of fission track age against Cl content for individual apatite grains

Fission track ages of single apatite grains within individual samples are plotted against the Cl content of each grain on the fission track age data summary sheets at the end of this Appendix. These plots are useful in assessing the degree of annealing, as expressed by the fission track age data. For example, if grains with a range of Cl contents from zero to some upper limit all give similar fission track ages which are significantly less than the stratigraphic age, then grains with these compositions must have been totally annealed. Alternatively, if fission track age falls rapidly with decreasing Cl content, the sample displays a high degree of partial annealing.

B.4 A note on terminology

Note that throughout this report, the term "fission track age" is understood to denote the parameter calculated from the fission track age equation, using the observed spontaneous and induced track counts (either pooled for all grains or for individual grains). The resulting number (with units of Ma) should not be taken as possessing any significance in terms of events taking place at the time indicated by the measured fission track age, but should rather be regarded as a measure of the integrated thermal history of the sample, and should be interpreted in that light using the principles outlined in Appendix C. Use of the term "apparent age" is not considered to be useful in this regard, as almost every fission track age should be regarded as an apparent age, in the classic sense, and repeated use becomes cumbersome.

References

Fleischer, R. L., Price, P. B., and Walker, R. M. (1975) Nuclear tracks in solids, University of California Press, Berkeley.

Galbraith, R. F. (1981) On statistical models for fission-track counts. *Mathematical Geology*, 13, 471-488.

Galbraith, R. F. (1988) Graphical display of estimates having differing standard errors. *Technometrics*, 30, 271-281.

Galbraith, R. F. (1990) The radial plot: graphical assessment of spread in ages. *Nuclear Tracks*, 17, 207-214.

Galbraith R.F. & Laslett G.M. (1993) Statistical methods for mixed fission track ages. *Nuclear Tracks* 21, 459-470.

Gleadow, A. J. W. (1981) Fission track dating methods; what are the real alternatives? *Nuclear Tracks*, 5, 3-14.

Green, P. F. (1981) A new look at statistics in fission track dating. *Nuclear Tracks* 5, 77-86.

Green, P. F. (1985) A comparison of zeta calibration baselines in zircon, sphene and apatite. *Chem. Geol. (Isot. Geol. Sect.)*, 58, 1-22.

Green, P. F., Duddy, I. R., Gleadow, A. J. W., Tingate, P. R. and Laslett, G. M. (1986) Thermal annealing of fission tracks in apatite 1. A qualitative description. *Chem. Geol. (Isot. Geosci. Sect.)*, 59, 237-253.

Hurford, A. J. (1986) Application of the fission track dating method to young sediments: Principles, methodology and Examples. *In:* Hurford, A. J., Jäger, E. and Ten Cate, J. A. M. (*eds*), Dating young sediments, CCOP Technical Publication 16, CCOP Technical Secretariat, Bangkok, Thailand.

Hurford, A. J. and Green, P. F. (1982) A user's guide to fission track dating calibration. *Earth. Planet. Sci Lett.* 59, 343-354.

Hurford, A. J. and Green, P. F. (1983) The zeta age calibration of fission track dating. *Isotope Geoscience* 1, 285-317.

Laslett, G. M., Kendall, W. S., Gleadow, A. J. W. and Duddy, I. R. (1982) Bias in measurement of fission track length distributions. *Nuclear Tracks*, 6, 79-85.

Naeser, C. W. (1979) Fission track dating and geologic annealing of fission tracks. *In:* Jäger, E. and Hunziker, J. C. (*eds*), Lectures in Isotope Geology, Springer Verlag, Berlin.

Smith, M. J. and Leigh-Jones, P. (1985) An automated microscope scanning stage for fission-track dating. *Nuclear Tracks*, 10, 395-400.

Table B.1: Apatite fission track analytical results - samples from East Greenland (Geotrack Report #1052)

Sample number	Number of grains	ρ_D (N_D) x10^6/cm²	ρ_s (Ns) x10^6/cm²	ρ_i (Ni) x10^6/cm²	Uranium content (ppm)	P(χ^2) (%)	Age dispersion (%)	Fission track age (Ma)
Blokelv borehole								
GC1052-1	20	1.424	0.431	2.427	19	<1	39	49.5 ± 3.6
		(2241)	(269)	(1515)				*50.4 ± 6.2**
GC1052-2	20	1.429	0.413	2.936	23	3	27	39.3 ± 3.1
		(2241)	(215)	(1530)				*38.5 ± 4.0**

ρ_s = spontaneous track density; ρ_i = induced track density; ρ_D = track density in glass standard external detector. Brackets show number of tracks counted. ρ_D and ρ_i measured in mica external detectors; ρ_s measured in internal surfaces.
*Central age, used where sample contains a significant spread of single grain ages (P(χ^2)<5%). Errors quoted at 1σ.
Ages calculated using dosimeter glass CN5, with a zeta of 392.9 ± 7.4 (Analyst: M. Moore) for samples; 1 - 2

Table B.2: Length distribution summary data - samples from East Greenland (Geotrack Report #1052)

Sample number	Mean track length (µm)	Standard deviation (µm)	Number of tracks (N)	Number of tracks in Length Intervals (µm)																			
				1	2	3	4	5	6	7	8	9	10	11	12	13	14	15	16	17	18	19	20
Blokelv borehole																							
GC1052-1	12.25 ± 0.22	2.28	103	-	-	-	-	1	2	1	1	3	6	5	27	20	15	14	3	3	2	-	-
GC1052-2	11.71 ± 0.23	2.36	103	-	-	-	2	-	1	1	1	3	11	13	27	19	6	9	8	2	-	-	-

Track length measurements by: M. Moore for samples; 1 - 2

Table B.3: AFTA Data in Compositional Groups - (Geotrack Report #1052)

Cl Wt %	Default fission track age* (Ma)	Measured fission track age (Ma)	Error in age (Ma)	P (χ^2)	Number of grains	Default fission track length* (µm)	Mean Track length (µm)	Error in length (µm)	Std deviation (µm)	Number of lengths	Number of grains	Number of tracks in length interval (µm) 1	2	3	4	5	6	7	8	9	10	11	12	13	14	15	16	17	18	19	20
Blokelv borehole																															
1052-1†	**148**	**50.4**	**6.2**	**0.0**	**20**	**14.9**	**12.2**	**0.2**	**2.3**	**103**	**40**	**0**	**0**	**0**	**0**	**1**	**2**	**1**	**1**	**3**	**6**	**5**	**27**	**20**	**15**	**14**	**3**	**3**	**2**	**0**	**0**
0.0 - 0.1	148	50.5	7.0	0.0	17	14.9	12.3	0.2	2.3	91	33	0	0	0	0	1	2	1	0	3	5	5	24	17	12	13	3	3	2	0	0
0.1 - 0.2	148	42.8	6.4	15.1	2	14.9	12.2	0.6	1.9	11	6	0	0	0	0	0	0	0	1	0	1	0	2	3	3	1	0	0	0	0	0
0.2 - 0.3	148	74.8	17.0	100.0	1	15.0	11.9	0.0	0.0	1	1	0	0	0	0	0	0	0	0	0	0	0	1	0	0	0	0	0	0	0	0
1052-2†	**155**	**38.5**	**4.0**	**3.1**	**20**	**14.7**	**11.7**	**0.2**	**2.4**	**103**	**45**	**0**	**0**	**0**	**2**	**0**	**1**	**1**	**1**	**3**	**11**	**13**	**27**	**19**	**6**	**9**	**8**	**2**	**0**	**0**	**0**
0.0 - 0.1	155	37.4	4.5	1.1	16	14.7	11.6	0.3	2.4	89	39	0	0	0	2	0	1	1	1	3	10	10	26	15	5	7	7	1	0	0	0
0.1 - 0.2	155	38.4	11.0	22.7	2	14.7	11.9	1.0	2.2	5	2	0	0	0	0	0	0	0	0	0	1	1	1	1	0	0	1	0	0	0	0
0.2 - 0.3	156	48.6	11.9	85.5	2	14.8	12.1	0.6	1.2	4	2	0	0	0	0	0	0	0	0	0	0	1	0	2	1	0	0	0	0	0	0
0.3 - 0.4	-	-	-	-		-	-	-	-	-	-	-	-	-	-	-	-	-	-	-	-	-	-	-	-	-	-	-	-	-	-
0.4 - 0.5	157	0.0	0.0	0.0	0	14.8	13.7	0.9	2.1	5	2	0	0	0	0	0	0	0	0	0	0	1	0	1	0	2	0	1	0	0	0

*Fission Track Age and Mean Track Length predicted from the Default Thermal History (i.e. if the sample has not been hotter in the past)
†Combined data for all compositional groups

Estimates	z_i
Standard errors	σ_i
Reference value	z_o
Standardised estimates	$y_i = (z_i - z_o) / \sigma_i$
Precision	$x_i = 1 / \sigma_i$

PLOT y_i against x_i

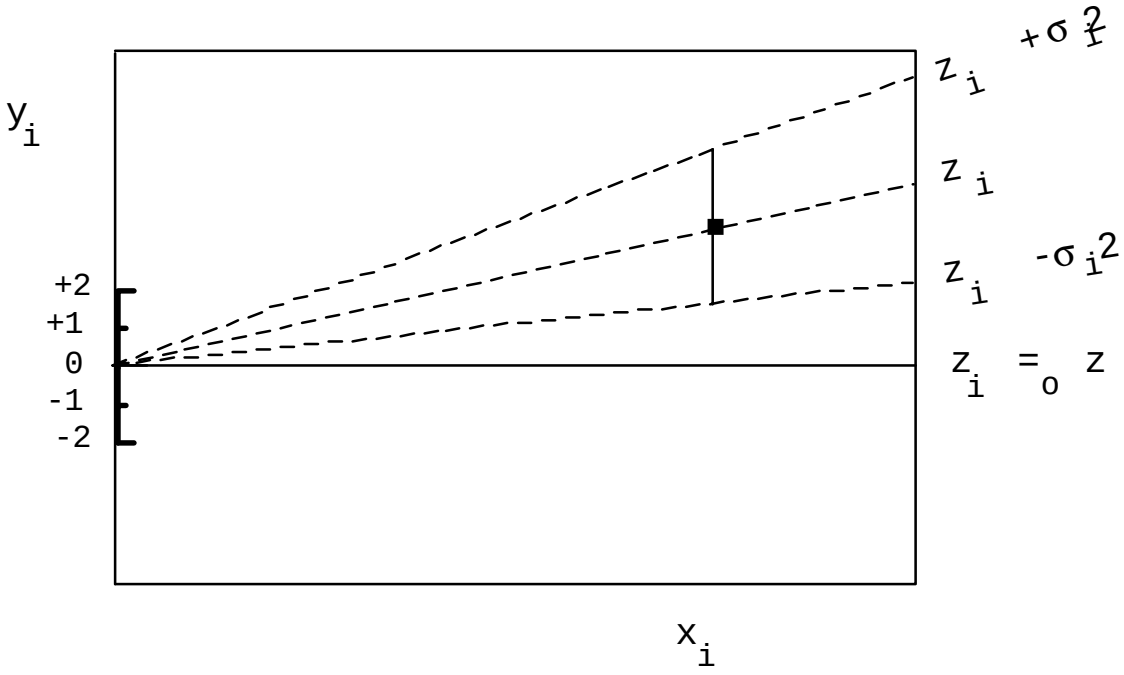

Slope of line from origin through data point $= y_i / x_i$

$= \{(z_i - z_o)/\sigma_i\} / \{1/\sigma_i\}$

$= z_i - z_o$

Key Points:

Radial lines emanating from the origin correspond to fixed values of z

Data points with higher values of x_i have greater precision.

Error bars on all points are the same size in this plot.

Figure B.1 Basic construction of a radial plot. In AFTA, the estimates z_i correspond to the fission track age values for individual apatite grains. Any convenient value of age can be chosen as the reference value corresponding to the horizontal in the radial plot. Radial lines emanating from the origin with positive slopes correspond to fission track ages greater than the reference value. Lines with negative slopes correspond to fission track ages less than the reference value.

Normal radial plot (equations B.2 and B.3)

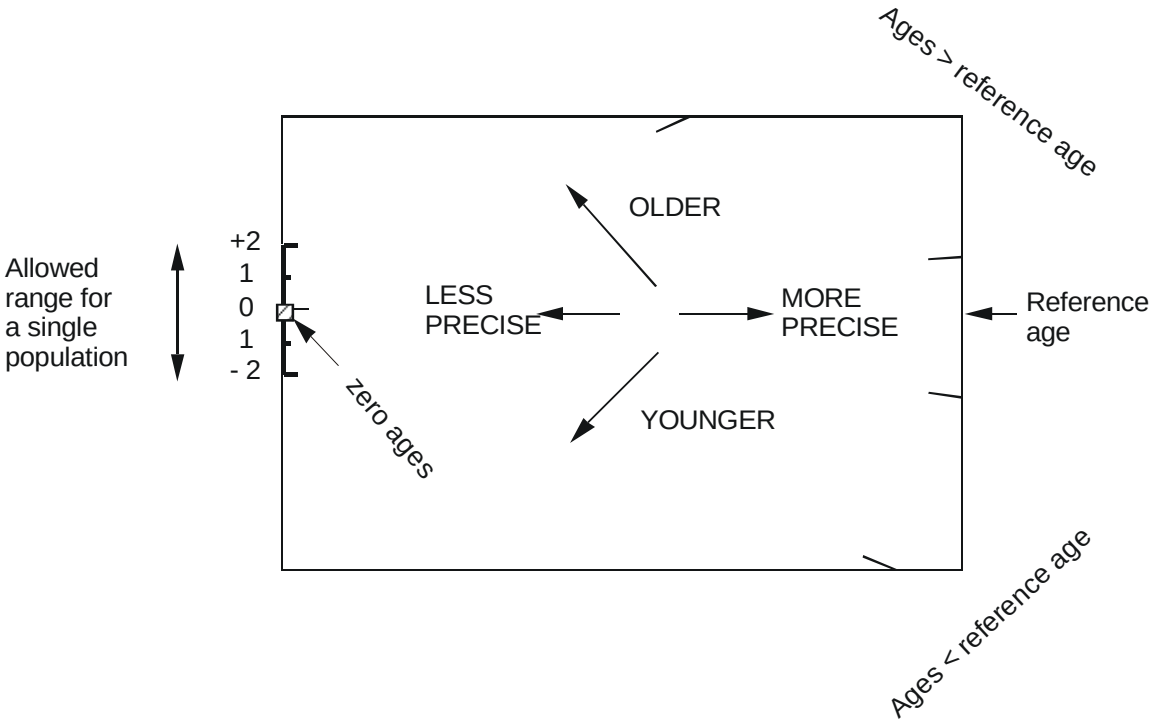

Arc-sin radial plot (equations B.2 and B.4)

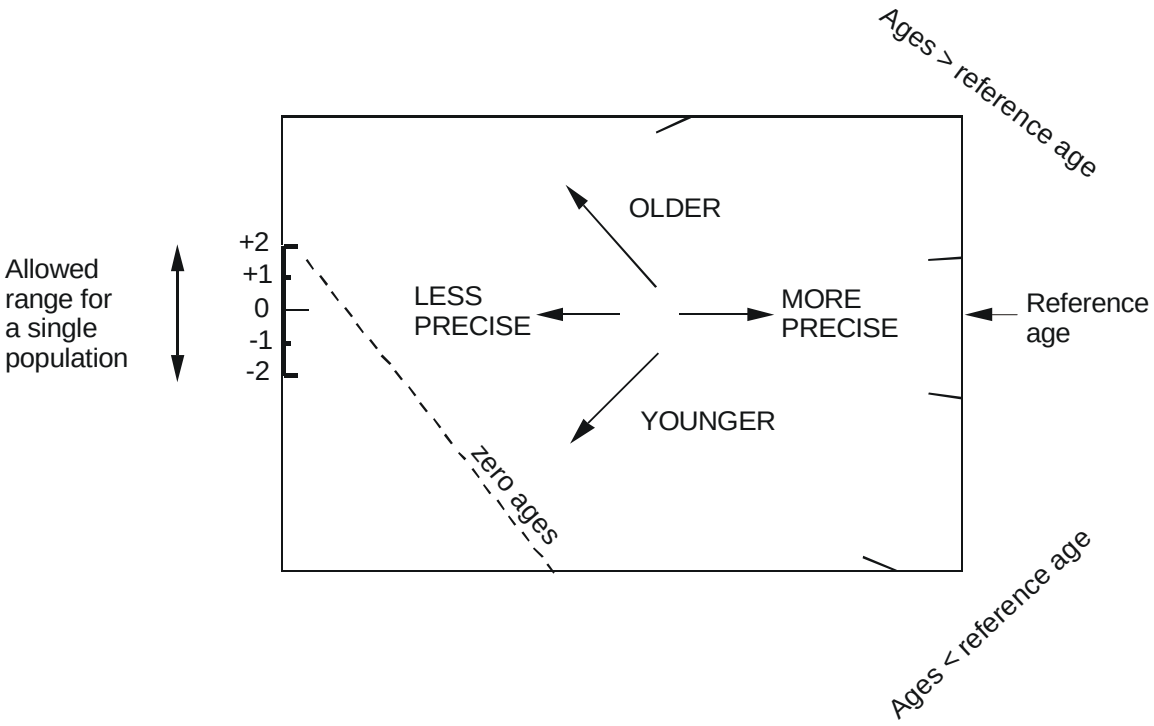

Figure B.2 Simplified structure of Normal and Arc-sin radial plots.

Fission Track Age Data Sheets - Glossary

N_s	=	Number of spontaneous tracks in N_a grid squares
N_i	=	Number of induced tracks in N_a grid squares
N_a	=	Number of grid squares counted in each grain
RATIO	=	N_S/N_i
U (ppm)	=	Uranium content of each grain (= U content of standard glass * ρ_i/ρ_D)
Cl (wt%)	=	Weight percent chlorine content of each grain
ρ_s	=	Spontaneous track density (ρ_s) = N_s/ (N_a*area of basic unit)
ρ_i	=	Induced track density (ρ_i) = N_i/(N_a*area of basic unit)
F.T. AGE	=	Fission track age, calculated using equation B.1
Area of basic unit	=	Area of one grid square
Chi squared	=	χ^2 parameter, used to assess variation of single grain ages within the sample
P(chi squared)	=	Probability of obtaining observed χ^2 value for the relevant number of degrees of freedom, if all grains belong to a single population
Age Dispersion	=	% variation in single grain ages - see discussion in text re "Central age"
N_s/N_i	=	Pooled ratio, total spontaneous tracks divided by total induced tracks for all grains
Mean ratio	=	Mean of (N_s/N_i) for individual grains
Zeta	=	Calibration constant, determined empirically for each observer
ρ_D	=	Track density (ρ_D) from uranium standard glass (interpolated from values at each end of stack)
ND	=	Total number of tracks counted for determining ρ_D
POOLED AGE	=	Fission track age calculated from pooled ratio N_s/N_i. Valid only when P(χ2) > 5%
CENTRAL AGE	=	Alternative to pooled age when P(χ2)< 5%

Key to Figures:

A: Radial plot of single grain ages *(See Figures B.1 and B.2 for details of radial plot construction)*	B: Distribution of Cl contents in apatite grains
C: Single grain age vs weight % Cl for individual apatite grains.	D: Distribution of confined track lengths

GC1052-1 Apatite 5111101-6
Counted by: MEM

Slide ref	Current grain no	N_s	N_i	N_a	ρ_s	ρ_i	RATIO	U (ppm)	Cl (wt%)	F.T. AGE (Ma)
G1124-9	3	1	23	36	4.414E+04	1.015E+06	0.043	8.1	0.04	12.2 ± 12.4
G1124-9	6	14	51	24	9.270E+05	3.377E+06	0.275	27.0	0.03	76.4 ± 23.1
G1124-9	7	0	13	49	0.000E+00	4.216E+05	0.000	3.4	0.14	0.0 ± 36.1
G1124-9	10	29	129	30	1.536E+06	6.833E+06	0.225	54.7	0.01	62.6 ± 13.0
G1124-9	11	18	48	24	1.192E+06	3.178E+06	0.375	25.4	0.06	104.1 ± 28.9
G1124-9	12	6	35	60	1.589E+05	9.270E+05	0.171	7.4	0.05	47.8 ± 21.2
G1124-9	13	27	96	60	7.151E+05	2.543E+06	0.281	20.3	0.02	78.2 ± 17.2
G1124-9	14	6	53	42	2.270E+05	2.005E+06	0.113	16.0	0.03	31.6 ± 13.6
G1124-9	15	54	339	20	4.290E+06	2.693E+07	0.159	215.6	0.11	44.4 ± 6.6
G1124-9	16	4	33	35	1.816E+05	1.498E+06	0.121	12.0	0.00	33.8 ± 17.9
G1124-9	17	1	13	60	2.648E+04	3.443E+05	0.077	2.8	0.08	21.5 ± 22.3
G1124-9	18	9	110	42	3.405E+05	4.162E+06	0.082	33.3	0.03	22.9 ± 8.0
G1124-9	19	5	18	30	2.648E+05	9.534E+05	0.278	7.6	0.02	77.3 ± 39.1
G1124-9	20	19	49	80	3.774E+05	9.733E+05	0.388	7.8	0.02	107.6 ± 29.2
G1124-9	21	4	32	70	9.080E+04	7.264E+05	0.125	5.8	0.02	34.9 ± 18.5
G1124-9	22	31	234	80	6.158E+05	4.648E+06	0.132	37.2	0.03	37.0 ± 7.1
G1124-9	23	11	113	50	3.496E+05	3.591E+06	0.097	28.7	0.03	27.2 ± 8.6
G1124-9	25	4	27	50	1.271E+05	8.581E+05	0.148	6.9	0.02	41.3 ± 22.2
G1124-9	28	1	6	100	1.589E+04	9.534E+04	0.167	0.8	0.07	46.5 ± 50.2
G1124-9	32	25	93	50	7.945E+05	2.956E+06	0.269	23.7	0.21	74.8 ± 17.0
		269	1515		4.309E+05	2.427E+06		19.4		

Area of basic unit = 6.293E-07 cm^{-2}
χ^2 = 47.992 with 19 degrees of freedom
P(χ^2) = 0.0%
Age Dispersion = 38.770%

Ns / Ni = 0.178 ± 0.012
Mean Ratio = 0.176 ± 0.024

Ages calculated using a zeta of 392.9 ± 7.4 for CN5 glass
ρ_D = 1.424E+06cm^{-2} ND = 2241
ρ_D interpolated between top of can; ρ_D = 1.388E+06cm^{-2} ND = 1092
bottom of can; ρ_D = 1.461E+06cm^{-2} ND = 1149

POOLED AGE = 49.5 ± 3.6 Ma
CENTRAL AGE = 50.4 ± 6.2 Ma

A:

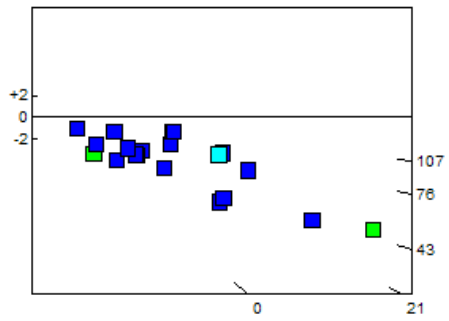

B:

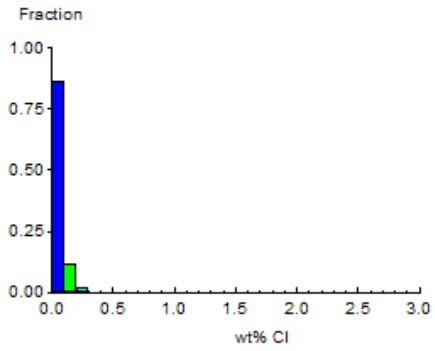

C:

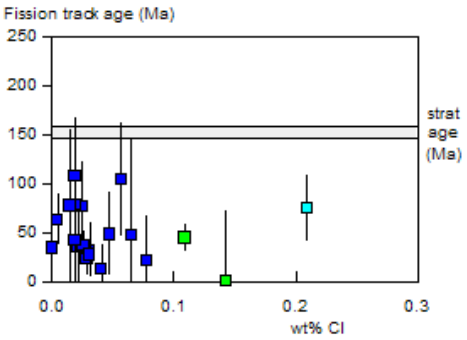

D:

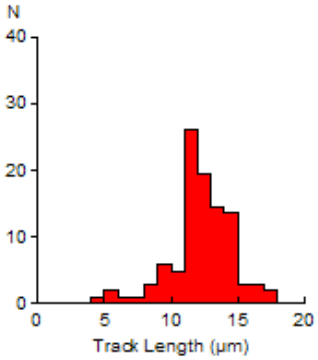

Mean track length 12.25 ± 0.22 µm Std. Dev. 2.28 µm 103 tracks

GC1052-2 Apatite 5111101-219
Counted by: MEM

Slide ref	Current grain no	N_s	N_i	N_a	ρ_s	ρ_i	RATIO	U (ppm)	Cl (wt%)	F.T. AGE (Ma)
G1124-10	3	15	84	50	4.767E+05	2.670E+06	0.179	21.3	0.23	49.9 ± 14.1
G1124-10	4	5	31	70	1.135E+05	7.037E+05	0.161	5.6	0.20	45.1 ± 21.8
G1124-10	10	7	56	50	2.225E+05	1.780E+06	0.125	14.2	0.01	35.0 ± 14.1
G1124-10	11	9	126	30	4.767E+05	6.674E+06	0.071	53.2	0.01	20.0 ± 6.9
G1124-10	12	3	63	28	1.703E+05	3.575E+06	0.048	28.5	0.02	13.4 ± 7.9
G1124-10	14	41	198	35	1.861E+06	8.990E+06	0.207	71.7	0.08	57.9 ± 10.1
G1124-10	15	14	94	36	6.180E+05	4.149E+06	0.149	33.1	0.01	41.7 ± 12.0
G1124-10	16	1	12	28	5.675E+04	6.810E+05	0.083	5.4	0.02	23.4 ± 24.3
G1124-10	17	9	48	48	2.980E+05	1.589E+06	0.188	12.7	0.10	52.4 ± 19.1
G1124-10	19	5	54	30	2.648E+05	2.860E+06	0.093	22.8	0.03	25.9 ± 12.1
G1124-10	21	16	152	40	6.356E+05	6.038E+06	0.105	48.2	0.04	29.5 ± 7.8
G1124-10	22	7	35	40	2.781E+05	1.390E+06	0.200	11.1	0.02	55.9 ± 23.2
G1124-10	23	5	54	40	1.986E+05	2.145E+06	0.093	17.1	0.14	25.9 ± 12.1
G1124-10	24	15	86	35	6.810E+05	3.905E+06	0.174	31.1	0.00	48.8 ± 13.7
G1124-10	25	10	57	42	3.783E+05	2.157E+06	0.175	17.2	0.00	49.1 ± 16.9
G1124-10	26	8	93	36	3.531E+05	4.105E+06	0.086	32.7	0.02	24.1 ± 8.9
G1124-10	29	7	101	70	1.589E+05	2.293E+06	0.069	18.3	0.00	19.4 ± 7.6
G1124-10	30	21	84	40	8.343E+05	3.337E+06	0.250	26.6	0.01	69.8 ± 17.1
G1124-10	33	0	7	40	0.000E+00	2.781E+05	0.000	2.2	0.02	0.0 ± 74.1
G1124-10	34	17	95	40	6.754E+05	3.774E+06	0.179	30.1	0.04	50.0 ± 13.3
		215	1530		4.126E+05	2.936E+06		23.4		

Area of basic unit = 6.293E-07 cm^{-2}
χ^2 = 32.061 with 19 degrees of freedom
P(χ^2) =3.1%
Age Dispersion =27.489%

Ns / Ni = 0.141 ± 0.010
Mean Ratio = 0.132 ± 0.014

Ages calculated using a zeta of 392.9 ± 7.4 for CN5 glass
ρ_D = 1.429E+06cm^{-2} ND =2241
ρ_D interpolated between top of can; ρ_D = 1.388E+06cm^{-2} ND =1092
bottom of can; ρ_D = 1.461E+06cm^{-2} ND =1149

POOLED AGE = 39.3 ± 3.1 Ma
CENTRAL AGE = 38.5 ± 4.0 Ma

A:

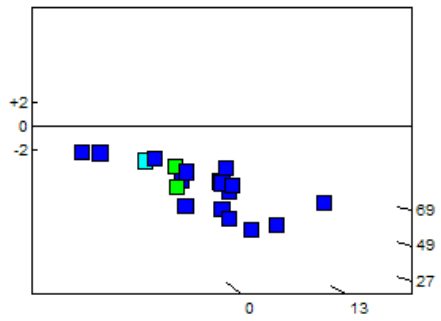

B:

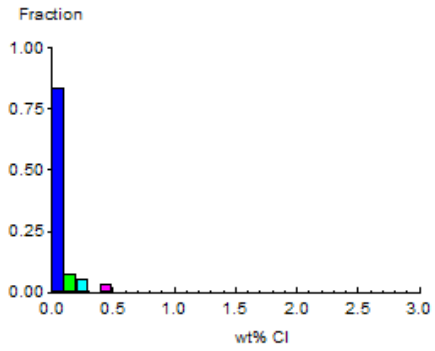

C:

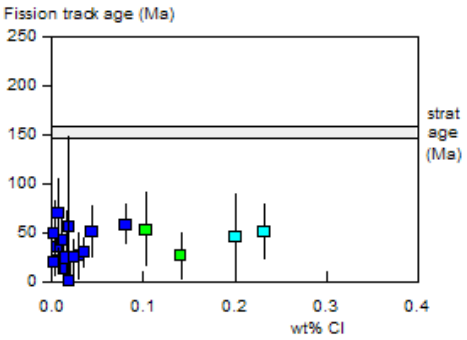

D:

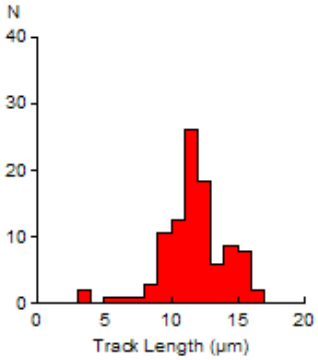

Mean track length 11.71 ± 0.23 µm Std. Dev. 2.36 µm 103 tracks

APPENDIX C

Principles of Interpretation of AFTA Data in Sedimentary Basins

C.1 Introduction

Detrital apatite grains are incorporated into sedimentary rocks from three dominant sources - crystalline basement rocks, older sediments and contemporaneous volcanism. Apatites derived from the first two sources will, in general, contain fission tracks when they are deposited, with AFTA parameters characteristic of the source regions. However, apatites derived from contemporaneous volcanism, or from rapidly uplifted basement, will contain no tracks when they are deposited. For now, we will restrict discussion to this situation, and generalise at a later point to cover the case of apatites which contain tracks that have been inherited from source regions.

C.2 Basic principles of Apatite Fission Track Analysis

Fission tracks are trails of radiation damage, which are produced within apatite grains at a more or less constant rate through geological time, as a result of the spontaneous fission of ^{238}U impurity atoms. Therefore, the number of fission events which occur within an apatite grain during a fixed time interval depends on the magnitude of the time interval and the uranium content of the grain. Each fission event leads to the formation of a single fission track, and the proportion of tracks which can intersect a polished surface of an apatite grain depends on the length of the tracks. Therefore, the number of tracks which are etched in unit area of the surface of an apatite grain (the "spontaneous track density") depends on three factors - (i) The time over which tracks have been accumulating; (ii) The uranium content of the apatite grain; and, (iii) The distribution of track lengths in the grain. In sedimentary rocks which have not been subjected to temperatures greater than ~50°C since deposition, spontaneous fission tracks have a characteristic distribution of confined track lengths, with a mean length in the range 14-15 µm and a standard deviation of ~1 µm. In such samples, by measuring the spontaneous track density and the uranium content of a collection of apatite grains, a "fission track age" can be calculated which will be equal to the time over which tracks have been accumulating. The technique is calibrated against other isotopic systems using age standards which also have this type of length distribution (see Appendix B).

In samples which have been subjected to temperatures greater than ~50°C after deposition, fission tracks are shortened because of the gradual repair of the radiation damage which constitutes the unetched tracks. In effect, the tracks shrink from each end, in a process which is known as fission track "annealing". The final length of each individual track is essentially determined by the maximum temperature which that track has experienced. A time difference of an order of magnitude produces a change in fission track parameters which is equivalent to a temperature change of only ~10°C, so temperature is by far the dominant factor in determining the final fission track parameters. As temperature increases, all existing tracks shorten to a length determined by the prevailing temperature, regardless of when they were formed. After the temperature has subsequently decreased, all tracks formed prior to the thermal maximum are "frozen" at the degree of length reduction they attained at that time. Thus, the length of each track can be thought of as a maximum-reading thermometer, recording the maximum temperature to which it has been subjected.

Therefore, in samples for which the present temperature is maximum, all tracks have much the same length, resulting in a narrow, symmetric distribution. The degree of shortening will depend on the temperature, with the mean track length falling progressively from ~14 µm at 50°C, to zero at around 110°-120°C - the precise temperature depending on the timescale of heating and the composition of the apatites present in the sample (see below). Values quoted here relate to times of the order of 10^7 years (heating rates around 1 to 10°C/Ma) and average apatite composition. If the effective timescale of heating is shorter than 10^7 years, the temperature responsible for a given degree of track shortening will be higher, depending in detail on the kinetics of the annealing process (Green et al., 1986; Laslett et al., 1987; Duddy et al., 1988; Green et al., 1989b). Shortening of tracks produces an accompanying reduction in the fission track age, because of the reduced proportion of tracks which can intersect the polished surface. Therefore, the fission track age is also highly temperature dependent, falling to zero at around 120°C due to total erasure of all tracks.

Samples which have been heated to a maximum paleotemperature less than ~120°C at some time in the past and subsequently cooled will contain two populations of tracks, and will show a more complex distribution of lengths and ages. If the maximum paleotemperature was less than ~50°C then the two components will not be resolvable, but for maximum paleotemperatures between ~50° and 120°C the presence of two components can readily be identified. Tracks formed prior to the thermal maximum will all be shortened to approximately the same degree (the precise value depending on the maximum paleotemperature), while those formed during and after cooling will be longer, due to the lower prevailing temperatures. The length distribution in such

samples will be broader than in the simple case, consisting of a shorter and a longer component, and the fission track age will reflect the amount of length reduction shown by the shorter component (determined by the maximum paleotemperature).

If the maximum paleotemperature was sufficient to shorten tracks to between 9 and 11 µm, and cooling to temperatures of ~50°C or less was sufficiently rapid, tracks formed after cooling will have lengths of 14-15 µm and the resulting track length distribution will show a characteristic bimodal form. If the maximum paleotemperature was greater than ~110 to 120°C, all pre-existing tracks will be erased, and all tracks now present will have formed after the onset of cooling. The fission track age in such samples relates directly to the time of cooling.

In thermal history scenarios in which a heating episode is followed by cooling and then temperature increases again, the tracks formed during the second heating phase will undergo progressive shortening. The tracks formed prior to the initial cooling, which were shortened in the first heating episode, will not undergo further shortening until the temperature exceeds the maximum temperature reached in the earlier heating episode. (In practice, differences in timescale of heating can complicate this simple description. In detail, it is the integrated time-temperature effect of the two heating episodes which should be considered.) If the maximum and peak paleotemperatures in the two episodes are sufficiently different (>~10°C), and the later peak paleotemperature is less than the earlier maximum value, then the AFTA parameters allow determination of both episodes. As the peak paleotemperature in the later episode approaches the earlier maximum, the two generations of tracks become increasingly more difficult to resolve, and when the two paleotemperatures are the same, both components are shortened to an identical degree and all information on the earlier heating phase will be lost.

No information is preserved on the approach to maximum paleotemperature because the great majority of tracks formed up to that time have the same mean track length. Only those tracks formed in the last few per cent of the history prior to the onset of cooling are not shortened to the same degree (because temperature dominates over time in the annealing kinetics). These form a very small proportion of the total number of tracks and therefore cannot be resolved within the length distribution because of the inherent spread of several µm in the length distribution.

To summarise, AFTA allows determination of the magnitude of the maximum temperature and the time at which cooling from that maximum began. In some circumstances, determination of a subsequent peak paleotemperature and the time of cooling is also possible.

C.3 Quantitative understanding of fission track annealing in apatite

Annealing kinetics and modelling the development of AFTA parameters

Our understanding of the behaviour of fission tracks in apatite during geological thermal histories is based on study of the response of fission tracks to elevated temperatures in the laboratory (Green et al., 1986; Laslett et al., 1987; Duddy et al., 1988; Green et al., 1989b), in geological situations (Green et al., 1989a), observations of the lengths of spontaneous tracks in apatites from a wide variety of geological environments (Gleadow et al., 1986), and the relationship between track length reduction and reduction in fission track age observed in controlled laboratory experiments (Green, 1988).

These studies resulted in the capability to simulate the development of AFTA parameters resulting from geological thermal histories for an apatite of average composition (Durango apatite, ~0.43 wt% Cl). Full details of this modelling procedure have been explained in Green et al. (1989b). The following discussion presents a brief explanation of the approach.

Geological thermal histories involving temperatures varying through time are broken down into a series of isothermal steps. The progressive shortening of track length through sequential intervals is calculated using the extrapolated predictions of an empirical kinetic model fitted to laboratory annealing data. Contributions from tracks generated throughout the history (remembering that new tracks are continuously generated through time as new fissions occur) are summed to produce the final distribution of track lengths expected to result from the input history. In summing these components, care is taken to allow for various biases which affect revelation of confined tracks (Laslett et al., 1982). The final length reduction of each component of tracks is converted to a contribution of fission track age, using the relationship between track length and density reduction determined by Green (1988). These age contributions are summed to generate the final predicted fission track age.

This approach depends critically on the assumption that extrapolation of the laboratory-based kinetic model to geological timescales, over many orders of magnitude in time, is valid. This was assessed critically by Green et al. (1989b), who showed that predictions from this approach agree well with observed AFTA parameters in apatites of the appropriate composition in samples from a series of reference wells in the Otway Basin of south-east Australia (Gleadow and Duddy, 1981; Gleadow et al., 1983; Green et al., 1989a). This point is illustrated in Figure C.1. Green et al. (1989b) also quantitatively assessed the errors associated with extrapolation of the Laslett et al. (1987) model from

laboratory to geological timescales (i.e. precision, as opposed to accuracy). Typical levels of precision are ~0.5 µm for mean lengths <~10 µm, and ~0.3 µm for lengths >~10 µm. These figures are equivalent to an uncertainty in estimates of maximum paleotemperature derived using this approach of ~10°C. Precision is largely independent of thermal history for any reasonable geological history. Accuracy of prediction from this model is limited principally by the effect of apatite composition on annealing kinetics, as explained in the next section.

Compositional effects

Natural apatites essentially have the composition $Ca_5(PO_4)_3(F,OH,Cl)$. Most common detrital and accessory apatites are predominantly Fluor-apatites, but may contain appreciable amounts of chlorine. The amount of chlorine in the apatite lattice exerts a subtle compositional control on the degree of annealing, with apatites richer in fluorine being more easily annealed than those richer in chlorine. The result of this effect is that in a single sample, individual apatite grains may show a spread in the degree of annealing (i.e. length reduction and fission track age reduction). This effect becomes most pronounced in the temperature range 90 - 120°C (assuming a heating timescale of ~10 Ma), and can be useful in identifying samples exposed to paleotemperatures in this range. At temperatures below ~80°C, the difference in annealing sensitivity is less marked, and compositional effects can largely be ignored.

Our original quantitative understanding of the kinetics of fission track annealing, as described above, relates to a single apatite (Durango apatite) with ~0.43 wt% Cl, on which most of our original experimental studies were carried out. Recently, we have extended this quantitative understanding to apatites with Cl contents up to ~3 wt%. This new, multi-compositional kinetic model is based both on new laboratory annealing studies on a range of apatites with different F-Cl compositions (Figure C.2), and on observations of geological annealing in apatites from a series of samples from exploration wells in which the section is currently at maximum temperature since deposition. A composite model for Durango apatite composition was first created by fitting a common model to the old laboratory data (from Green et al., 1986) and the new geological data for a similar composition. This was then extended to other compositions on the basis of the multi-compositional laboratory and geological data sets. Details of the multi-compositional model are contained in a Technical Note, available from Geotrack in Melbourne.

The multi-compositional model allows prediction of AFTA parameters for any Cl content between 0 and 3 wt%, using a similar approach to that used in our original single composition modelling, as outlined above. Then, for an assumed or measured distribution of Cl contents within a sample, the composite parameters for the sample can be predicted. The range of Cl contents from 0 to 3 wt% spans the range of compositions commonly encountered, as discussed in the next section.

Predictions of the new multi-compositional model are in good agreement with the geological constraints on annealing rates provided by the Otway Basin reference wells, as shown in Figure C.3. However, note that the AFTA data from these Otway Basin wells were among those used in construction of the new model, so this should not be viewed as independent verification, but rather as a demonstration of the overall consistency of the model.

Distributions of Cl content in common AFTA samples

Figure C.4a shows a histogram of Cl contents, measured by electron microprobe, in apatite grains from more than 100 samples of various types. Most grains have Cl contents less than ~0.5 wt%. The majority of grains with Cl contents greater than this come from volcanic sources and basic intrusives, and contain up to ~2 wt% Cl. Figure C.4b shows the distribution of Cl contents measured in randomly selected apatite grains from 61 samples of "typical" quartzo-feldspathic sandstone. This distribution is similar to that in Figure C.4a, except for a more rapid fall-off as Cl content increases. Apatites from most common sandstones give distributions of Cl content which are very similar to that in Figure C.4b. Volcanogenic sandstones typically contain apatites with higher Cl contents, with a much flatter distribution for Cl contents up to ~1.5%, falling to zero at ~2.5 to 3 wt%, as shown in Figure C.4c. Cl contents in granitic basement samples and high-level intrusives are typically much more dominated by compositions close to end-member Fluorapatite, although many exceptions occur to this general rule.

Information about the spread of Cl contents in samples analysed in this report can be found in Appendix A.

Alternative kinetic models

Recently, both Carlson (1990) and Crowley et al. (1991) have published alternative kinetic models for fission track annealing in apatite. Carlson's model is based on our laboratory annealing data for Durango apatite (Green et al., 1986) and other (unpublished) data. In his abstract, Carlson claims that because his model is "based on explicit physical mechanisms, extrapolations of annealing rates to the lower temperatures and longer timescales required for the interpretation of natural fission track

length distributions can be made with greater confidence than is the case for purely empirical relationships fitted to the experimental annealing data". As explained in detail by Green et al. (1993), all aspects of Carlson's model are in fact purely empirical, and his model is inherently no "better" for the interpretation of data than any other. In fact, detailed inspection shows that Carlson's model does not fit the laboratory data set at all well. Therefore, we recommend against use of this model to interpret AFTA data.

The approach taken by Crowley et al. (1991) is very similar to that taken by Laslett et al., (1987). They have fitted models to new annealing data in two apatites of different composition - one close to end-member Fluorapatite (B-5) and one having a relatively high Sr content (113855). The model developed by Crowley et al. (1991) from their own annealing data for the B-5 apatite gives predictions in geological conditions which are consistently higher than measured values, as shown in Figure C.5. Corrigan (1992) reported a similar observation in volcanogenic apatites in samples from a series of West Texas wells. Since the B-5 apatite is close to end-member Fluor-apatite, while the Otway Group apatites contain apatites with Cl contents from zero up to ~3 wt% (and the West Texas apatites have up to 1 wt%), the fluorapatites should have mean lengths rather less than the measured values, which should represent a mean over the range of Cl contents present. Therefore, the predictions of the Crowley et al. (1991) B-5 model appear to be consistently high.

We attribute this to the rather restricted temperature-time conditions covered by the experiments of Crowley et al. (1991), with annealing times between one and 1000 hours, in contrast to times between 20 minutes and 500 days in the experiments of Green et al. (1986). In addition, few of the measured length values in Crowley et al.'s study fall below 11 µm (in only five out of 60 runs in which lengths were measured in apatite B-5) and their model is particularly poorly defined in this region.

Crowley et al. (1991) also fitted a new model to the annealing data for Durango apatite published by Green et al. (1986). Predictions of their fit to our data are not very much different to those from the Laslett et al. (1987) model (Figure C.6). We have not pursued the differences between their model and ours in detail because the advent of our multi-compositional model has rendered the single compositional approach obsolete.

C.4 Evidence for elevated paleotemperatures from AFTA

The basic principle involved in the interpretation of AFTA data in sedimentary basins is to determine whether the degree of annealing shown by tracks in apatite from a particular sample could have been produced if the sample has never been hotter than its present temperature at any time since deposition. To do this, the burial history derived

from the stratigraphy of the preserved sedimentary section is used to calculate a thermal history for each sample using the present geothermal gradient and surface temperature (i.e. assuming these have not changed through time). This is termed the "Default Thermal History". For each sample, the AFTA parameters predicted as a result of the Default Thermal History are then compared to the measured data. If the data show a greater degree of annealing than calculated on the basis of this history, the sample must have been hotter at some time in the past. In this case, the AFTA data are analysed to provide estimates of the magnitude of the maximum paleotemperature in that sample, and the time at which cooling commenced from the thermal maximum.

The degree of annealing is assessed in two ways - from fission track age and track length data. The stratigraphic age provides a basic reference point for the interpretation of fission track age, because reduction of the fission track age below the stratigraphic age unequivocally reveals that appreciable annealing has taken place after deposition of the host sediment. Large degrees of fission track age reduction, with the pooled or central fission track age very much less than the stratigraphic age, indicate severe annealing, which requires paleotemperatures of at least ~100°C for any reasonable geological time-scale of heating (>~1 Ma). Note that this applies even when apatites contain tracks inherited from source areas. More moderate degrees of annealing can be detected by inspection of the single grain age data, as the most sensitive (fluorine-rich) grains will begin to give fission track ages significantly less than the stratigraphic age before the central or pooled age has been reduced sufficiently to give a noticeable signal. Note that this aspect of the single grain age data can also be used for apatites which have tracks inherited from source areas. If signs of moderate annealing (from single grain age reduction) or severe annealing (from the reduction in pooled or central age) are seen in samples in which the Default Thermal History predicts little or no effect, the sample must have been subjected to elevated paleotemperatures at some time in the past. Figure C.7 shows how increasing degrees of annealing are observable in radial plots of the single grain fission track age data.

Similarly, the present temperature from which a sample is taken, and the way in which this has been approached (as inferred from the preserved sedimentary section), forms a basic point of reference for track length data. The observed mean track length is compared with the mean length predicted from the Default Thermal History. If the observed degree of track shortening in a sample is greater than that expected from the Default Thermal History (i.e. the mean length is significantly less than the predicted value), either the sample must have been subjected to higher paleotemperatures at some time after deposition, or the sample contains shorter tracks which were inherited from sediment source areas at the time the sediment was deposited. If shorter tracks were

inherited from source areas, the sample should still contain a component of longer tracks corresponding to the tracks formed after deposition. In general, the fission track age should be greater than the stratigraphic age. This can be assessed quantitatively using the computer models for the development of AFTA parameters described in an earlier section. If the presence of shorter tracks cannot be explained by their inheritance from source areas, the sample must have been hotter in the past.

C.5 Quantitative determination of the magnitude of maximum paleotemperature and the timing of cooling using AFTA

Values of maximum paleotemperature and timing of cooling in each sample are determined using a forward modelling approach based on the quantitative description of fission track annealing described in earlier sections. The Default Thermal History described above is used as the basis for this forward modelling, but with the addition of episodes of elevated paleotemperatures as required to explain the data. AFTA parameters are modelled iteratively through successive thermal history scenarios in order to identify thermal histories that can account for observed parameters. The range of values of maximum paleotemperature and timing of cooling which can account for the measured AFTA parameters (fission track age and track length distribution) are defined using a maximum likelihood-based approach. In this way, best estimates ("maximum likelihood values") can be defined together with ±95% confidence limits.

In samples in which all tracks have been totally annealed at some time in the past, only a minimum estimate of maximum paleotemperature is possible. In such cases, AFTA data provide most control on the time at which the sample cooled to temperatures at which tracks could be retained. The time at which cooling began could be earlier than this time, and therefore the timing also constitutes a minimum estimate.

Comparison of the AFTA parameters predicted by the multi-compositional model with measured values in samples which are currently at their maximum temperatures since deposition shows a good degree of consistency, suggesting the uncertainty in application of the model should be less than ±10°C. This constitutes a significant improvement over earlier approaches, since the kinetic models used are constrained in both laboratory and geological conditions. It should be appreciated that relative differences in maximum paleotemperature can be identified with greater precision than absolute paleotemperatures, and it is only the estimation of absolute paleotemperature values to which the ±10°C uncertainty relates.

Cooling history

If the data are of high quality and provided that cooling from maximum paleotemperatures began sufficiently long ago (so that the history after this time is represented by a significant proportion of the total tracks in the sample), determination of the magnitude of a subsequent peak paleotemperature and the timing of cooling from that peak may also be possible (as explained in Section C.2). A similar approach to that outlined above provides best estimates and corresponding ±95% confidence limits for this episode. Such estimates may simply represent part of a protracted cooling history, and evidence for a later discrete cooling episode can only be accepted if this scenario provides a significantly improved fit to the data. Geological evidence and consistency of estimates between a series of samples can also be used to verify evidence for a second episode.

In practise, most typical AFTA datasets are only sufficient to resolve two discrete episodes of heating and cooling. One notable exception to this is when a sample has been totally annealed in an early episode, and has then undergone two (or more) subsequent episodes with progressively lower peak paleotemperatures in each. But in general, complex cooling histories involving a series of episodes of heating and cooling will allow resolution of only two episodes, and the results will depend on which episodes dominate the data. Typically this will be the earliest and latest episodes, but if multiple cooling episodes occur within a narrow time interval the result will represent an approximation to the actual history.

C.6 Qualitative assessment of AFTA parameters

Various aspects of thermal history can often be assessed by qualitative assessment of AFTA parameters. For example, samples which have reached maximum paleotemperatures sufficient to produce total annealing, and which only contain tracks formed after the onset of cooling, can be identified from a number of lines of evidence. In a vertical sequence of samples showing increasing degrees of annealing, the transition from rapidly decreasing fission track age with increasing depth to more or less the same age over a range of depth denotes the transition from partial to total annealing of all tracks formed prior to the thermal maximum. In samples in which all tracks have been totally annealed, the single grain age data should show that none of the individual grain fission track ages are significantly older than the time of cooling, and grains in all compositional groups should give the same fission track age unless the sample has been further disturbed by a later episode. If the sample cooled rapidly to sufficiently low temperatures, little annealing will have taken place since cooling, and all grains will

give ages which are compatible with a single population around the time of cooling, as shown in Figure C.7.

Inspection of the distribution of single grain ages in partially annealed samples can often yield useful information on the time of cooling, as the most easily annealed grains (those richest in fluorine) may have been totally annealed prior to cooling, while more retentive (Cl-rich) compositions were only partially annealed (as in Figure C.7, centre). The form of the track length distribution can also provide information, from the relative proportions of tracks with different lengths. All of these aspects of the data can be used to reach a preliminary thermal history interpretation.

C.7 Allowing for tracks inherited from source areas

The effect of tracks inherited from source areas, and present at the time the apatite is deposited in the host sediment, is often posed as a potential problem for AFTA. However, this can readily be allowed for in analysing both the fission track age and length data.

In assessing fission track age data to determine the degree of annealing, the only criterion used is the comparison of fission track age with the value expected on the basis of the Default Thermal History. From this point of view, inherited tracks do not affect the conclusion: if a grain or a sample gives a fission track age which is significantly less than expected, the grain or sample has clearly undergone a higher degree of annealing than can be accounted for by the Default Thermal History, and therefore must have been hotter in the past, whether the sample contained tracks when it was deposited or not.

The presence of inherited tracks does impose a limit on our ability to detect post-depositional annealing from age data alone, as in samples which contain a fair proportion of inherited tracks, moderate degrees of annealing may reduce the fission track age from the original value, but not to a value which is significantly less than the stratigraphic age. This is particularly noticeable in the case of Tertiary samples containing apatites derived from Paleozoic basement. In such cases, although fission track age data may show no evidence of post-depositional annealing, track length data may well show such evidence quite clearly.

The influence of track lengths inherited from source areas can be allowed for by comparison of the fission track age with the value predicted by the Default Thermal History combined with inspection of the track length distribution. If the mean length is much less than the length predicted by the Default Thermal History, either the sample has been subjected to elevated paleotemperatures, sufficient to produce the observed degree of length reduction, or else the sample contains a large proportion of shorter

tracks inherited from source areas. However, in the latter case, the sample should give a pooled or central fission track age correspondingly older than the stratigraphic age, while the length distribution should contain a component of longer track lengths corresponding to the value predicted by the Default Thermal History. It is important in this regard that the length of a track depends primarily on the maximum temperature to which it has been subjected, whether in the source regions or after deposition in the sedimentary basin. Thus, any tracks retaining a provenance signature will have lengths towards the shorter end of the distribution where track lengths will not have "equilibrated" with the temperatures attained since deposition.

In general, it is only in extreme cases that inherited tracks render track length data insensitive to post-depositional annealing. For example, if practically all the tracks in a particular sample were formed prior to deposition, perhaps in a Pliocene sediment in which apatites were derived from a stable Paleozoic shield with fission track ages of ~300 Ma or more, the track length distribution will, in general, be dominated by inheritance, as only ~2% of tracks would have formed after deposition. Post-depositional heating will not be detectable as long as the maximum paleotemperature is insufficient to cause greater shortening than that which occurred in the source terrain. Even in such extreme cases, once a sample is exposed to temperatures sufficient to produce greater shortening than that inherited from source areas, the inherited tracks and those formed after deposition will all undergo the same degree of shortening, and the effects of post-depositional annealing can be recognised. In such cases, the presence of tracks inherited from source areas is actually very useful, because the number of tracks formed after deposition is so small that little or no information would be available without the inherited tracks.

C.8 Plots of fission track age and mean track length vs depth and temperature

AFTA data from well sequences are usually plotted as shown in Figure C.8. This figure shows AFTA data for two scenarios: one in which deposition has been essentially continuous from the Carboniferous to the present and all samples are presently at their maximum paleotemperature since deposition (Figure C.8a); and, one in which the section was exposed to elevated paleotemperatures prior to cooling in the Early Tertiary (Figure C.8b).

In both figures, fission track age and mean track length are plotted against depth and present temperature. Presentation of AFTA data in this way often provides insight into the thermal history interpretation, following principles outlined earlier in this Appendix.

In Figure C.8a**,** for samples at temperatures below ~70°C, the fission track age is either greater than or close to the stratigraphic age, and little fission track age reduction has affected these samples. Track lengths in these samples are all greater than ~13 µm. In progressively deeper samples, both the fission track age and mean track length are progressively reduced to zero at a present temperature of around 110°C, with the precise value depending on the spread of apatite compositions present in the sample. Track length distributions in the shallowest samples would be a mixture of tracks retaining information on the thermal history of source regions, while in deeper samples, all tracks would be shortened to a length determined by the prevailing temperature. This pattern of AFTA parameters is characteristic of a sequence which is currently at maximum temperatures.

The data in Figure C.8b show a very different pattern. The fission track age data show a rapid decrease in age, with values significantly less than the stratigraphic age at temperatures of ~40 to 50°C, at which such a degree of age reduction could not be produced in any geological timescale. Below this rapid fall, the fission track ages do not change much over ~1 km (30°C). This transition from rapid fall to consistent ages is diagnostic of the transition from partial to total annealing. Samples above the "break-in slope" contain two generations of tracks: those formed prior to the thermal maximum, which have been partially annealed (shortened) to a degree which depends on the maximum paleotemperature; and, those formed after cooling, which will be longer. Samples below the break-in slope contain only one generation of tracks, formed after cooling to lower temperatures at which tracks can be retained. At greater depths, where temperatures increase to ~90°C and above, the effect of present temperatures begins to reduce the fission track ages towards zero, as in the "maximum temperatures now" case.

The track length data also reflect the changes seen in the fission track age data. At shallow depths, the presence of the partially annealed tracks shortened prior to cooling causes the mean track length to decrease progressively as the fission track age decreases. However, at depths below the break in slope in the age profile, the track length increases again as the shorter component is totally annealed and so does not contribute to the measured distribution of track lengths. At greater depths, the mean track lengths decrease progressively to zero once more due to the effects of the present temperature regime.

Examples of such data have been presented, e.g. by Green (1989) and Kamp and Green (1990).

C.9 Determining paleogeothermal gradients and amount of section removed on unconformities

Estimates of maximum paleotemperatures in samples over a range of depths in a vertical sequence provides the capability of determining the paleogeothermal gradient immediately prior to the onset of cooling from those maximum paleotemperatures. The degree to which the paleogeothermal gradient can be constrained depends on a number of factors, particularly the depth range over which samples are analysed. If samples are only analysed over ~1 km, then the paleotemperature difference over that range may be only ~20 to 30°C. Since maximum paleotemperatures can often only be determined within a ~10°C range, this introduces considerable uncertainty into the final estimate of paleogeothermal gradient (see Figure C.9).

Another important factor is the difference between maximum paleotemperatures and present temperatures ("net cooling"). If this is only ~10°C, which is similar to the uncertainty in absolute paleotemperature determination, only broad limits can be established on the paleogeothermal gradient. In general, the control on the paleogeothermal gradient improves as the amount of net cooling increases. However, if the net cooling becomes so great that many samples were totally annealed prior to the onset of cooling - so that only minimum estimates of maximum paleotemperatures are possible - constraints on the paleogeothermal gradient from AFTA come only from that part of the section in which samples were not totally annealed. In this case, integration of AFTA data with VR measurements can be particularly useful in constraining the paleo-gradient.

Having constrained the paleogeothermal gradient at the time cooling from maximum paleotemperatures began, if we assume a value for surface temperature at that time, the amount of section subsequently removed by uplift and erosion can be calculated as shown in Figure C.10. The *net* amount of section removed is obtained by dividing the difference between the paleo-surface temperature (T_s) and the intercept of the paleotemperature profile at the present ground surface (T_i) by the estimated paleogeothermal gradient. The *total* amount of section removed is obtained by adding the thickness of section subsequently redeposited above the unconformity to the *net* amount estimated as in Figure C.10. If the analysis is performed using depths from the appropriate unconformity, then the analysis will directly yield the *total* amount of section removed.

Geotrack have developed a method of deriving estimates of both the paleogeothermal gradient and the net amount of section removed using estimated paleotemperatures

derived from AFTA and VR. Perhaps more importantly, this method also provides rigorous values for upper and lower 95% confidence limits on each parameter. The method is based on maximum likelihood estimation of the paleogeothermal gradient and the surface intercept, from a table of paleotemperature and depth values. The method is able to accept ranges for paleotemperature estimates (e.g. where the maximum paleotemperature can only be constrained to between, for example, 60 and 90°C), as well as upper and lower limits (e.g. <60°C for samples which show no detectable annealing; >110°C in samples which were totally annealed). Estimates of paleotemperature from AFTA and VR may be combined or analysed separately. Some results from this method have been reported by Bray et al. (1992). Full details of the methods employed are presented in a confidential, in-house, Geotrack research report, copies of which are available on request from the Melbourne office.

Results are presented in two forms. Likelihood profiles, plotting the log-likelihood as a function of either gradient or section removed, portray the probability of a given value of gradient or section removed. The best estimate is given by the value of gradient or section removed for which the log-likelihood is maximised. Ideally, the likelihood profiles should show a quadratic form, and values of gradient or section removed at which the log-likelihood has fallen by two from the maximum value define the upper and lower 95% confidence limits on the estimates. An alternative method of portraying this information is a crossplot of gradient against section removed, in which values which fall within 95% confidence limits (in two dimensions) are contoured. Note that the confidence limits defined by this method are rather tighter than those from the likelihood profiles, as the latter only reflect variation in one parameter, whereas the contoured crossplot takes variation of both parameters into account.

It must be emphasised that this method relies on the assumption that the paleotemperature profile was linear both throughout the section analysed and through the overlying section which has been removed. While the second part of this assumption can never be confirmed independently, visual inspection of the paleotemperature estimates as a function of depth should be sufficient to verify or deny the linearity of the paleotemperature profile through the preserved section.

Results of this procedure are shown in this report if the data allow sufficiently well-defined paleotemperature estimates to justify use of the method. Where the AFTA data suggest that the section is currently at maximum temperature since deposition, or that the paleotemperature profile was non-linear, or where data are of insufficient quality to allow rigorous paleotemperature estimation, the method is not used.

References

Carlson, W.D. (1990) Mechanisms and kinetics of apatite fission-track annealing. *American Mineralogist*, 75, 1120 - 1139.

Corrigan, J. (1992) Annealing models under the microscope, *On Track*, 2, 9-11.

Crowley, K.D., Cameron, M. and Schaefer, R.L. (1991) Experimental studies of annealing of etched fission tracks in apatite. *Geochimica et Cosmochimica Acta*, 55, 1449-1465.

Duddy, I.R., Green, P.F. and Laslett G.M. (1988) Thermal annealing of fission tracks in apatite 3. Variable temperature behaviour. *Chem. Geol. (Isot. Geosci. Sect.)* , 73, 25-38.

Gleadow, A.J.W. and Duddy, I.R. (1981) A natural long-term track annealing experiment for apatite. *Nuclear Tracks*, 5, 169-174.

Gleadow, A.J.W., Duddy, I.R. and Lovering, J.F. (1983) Fission track analysis; a new tool for the evaluation of thermal histories and hydrocarbon potential. *APEA J*, 23, 93-102.

Gleadow, A.J.W., Duddy, I.R., Green, P.F. and Lovering, J.F. (1986) Confined fission track lengths in apatite - a diagnostic tool for thermal history analysis. *Contr. Min. Petr.*, 94, 405-415.

Green, P.F. (1988) The relationship between track shortening and fission track age reduction in apatite: Combined influences of inherent instability, annealing anisotropy, length bias and system calibration. *Earth Planet. Sci. Lett.*, 89, 335-352.

Green, P.F., Duddy, I.R., Gleadow, A.J.W., Tingate, P.R. and Laslett, G.M. (1986) Thermal annealing of fission tracks in apatite 1. A qualitative description. *Chem. Geol. (Isot. Geosci. Sect.)* , 59, 237-253.

Green, P.F., Duddy, I.R., Gleadow, A.J.W. and Lovering, J.F. (1989a) Apatite Fission Track Analysis as a paleotemperature indicator for hydrocarbon exploration. *In:* Naeser, N.D. and McCulloh, T. (eds.) *Thermal history of sedimentary basins - methods and case histories*, Springer-Verlag, New York, 181-195.

Green, P.F., Duddy, I.R., Laslett, G.M., Hegarty, K.A., Gleadow, A.J.W. and Lovering, J.F. (1989b) Thermal annealing of fission tracks in apatite 4. Quantitative modelling techniques and extension to geological timescales. *Chem. Geol. (Isot. Geosci. Sect.)*, 79, 155-182

Green, P.F., Laslett, G.M. and Duddy, I.R. (1993) Mechanisms and kinetics of apatite fission track annealing: Discussion. *American Mineralogist*, 78, 441-445.

Laslett, G.M., Kendall, W.S., Gleadow, A.J.W. and Duddy, I.R. (1982) Bias in measurement of fission track length distributions. *Nuclear Tracks*, 6, 79-85.

Laslett, G.M., Green, P.F., Duddy, I.R. and Gleadow, A.J.W. (1987) Thermal annealing of fission tracks in apatite 2. A quantitative analysis. *Chem. Geol. (Isot. Geosci. Sect.)*, 65, 1-13.

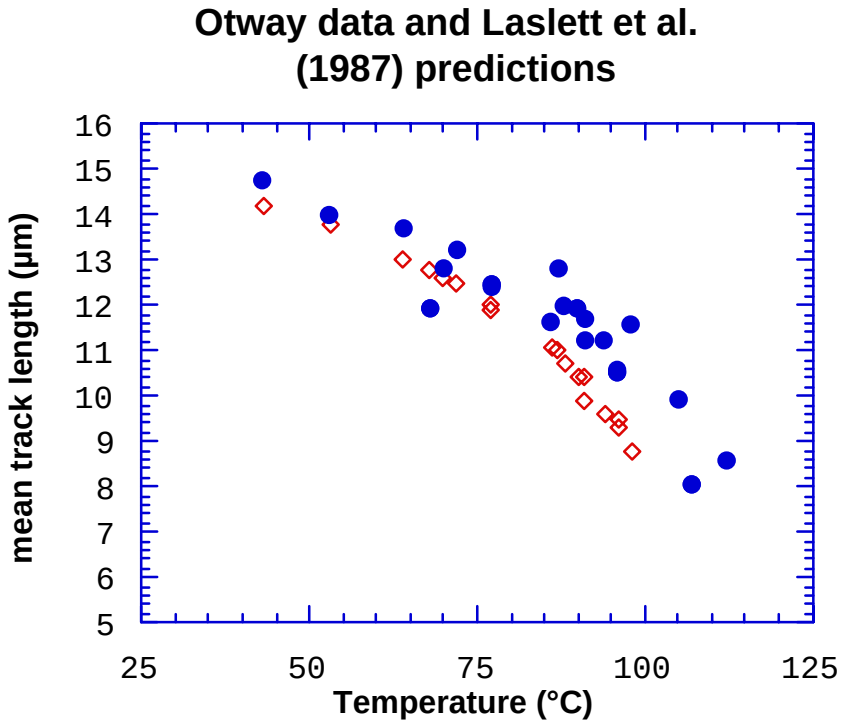

Figure C.1a Comparison of mean track length (solid circles) measured in samples from four Otway Basin reference wells (from Green et al, 1989a) and predicted mean track lengths (open diamonds) from the kinetic model of fission track annealing from Laslett et al. (1987). The predictions underestimate the measured values, but they refer to an apatite composition that is more easily annealed than the majority of apatites in these samples, so this is expected.

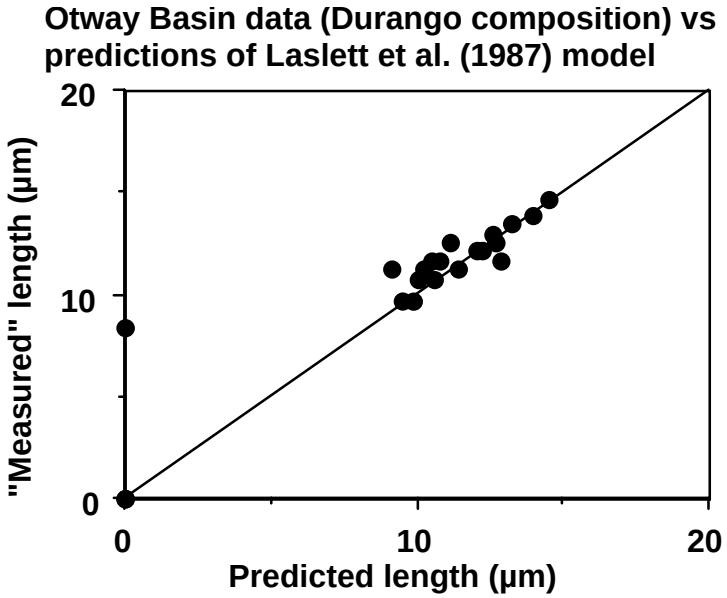

Figure C.1b Comparison of the mean track length in apatites of the same Cl content as Durango apatite from the Otway Group samples illustrated in figure C.1a, with values predicted for apatite of the same composition by the model of Laslett et al. (1987). The agreement is clearly very good except possibly at lengths below ~10 µm.

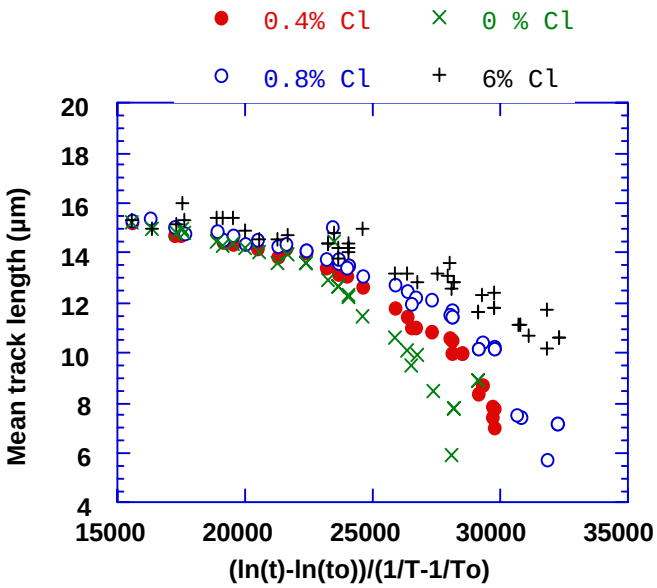

Figure C.2 Mean track length in apatites with four different chlorine contents, as a combined function of temperature and time, to reduce the data to a single scale. Fluorapatites are more easily annealed than chlorapatites, and the annealing kinetics show a progressive change with increasing Cl content.

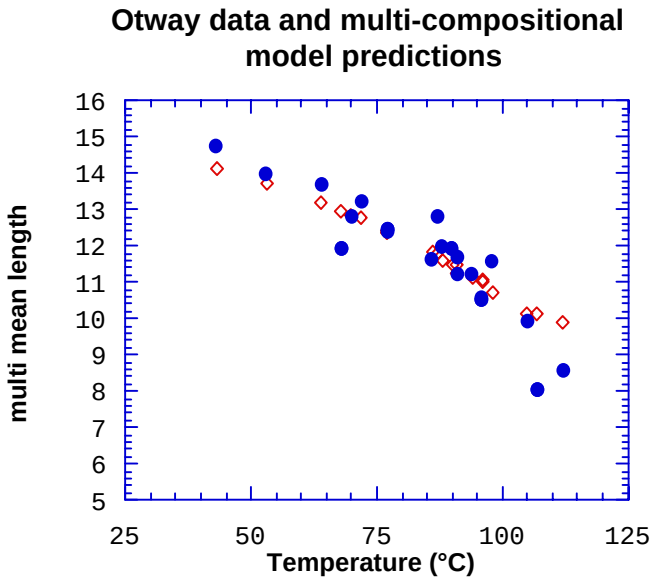

Figure C.3 Comparison of measured mean track length (solid circles) in samples from four Otway Basin reference wells (from Green et al, 1989a) and predicted mean track lengths (open diamonds) from the new multi-compositional kinetic model of fission track annealing described in Section C.3. This model takes into account the spread of Cl contents in apatites from the Otway Group samples and the influence of Cl content on annealing rate. The agreement is clearly very good over the range of the data.

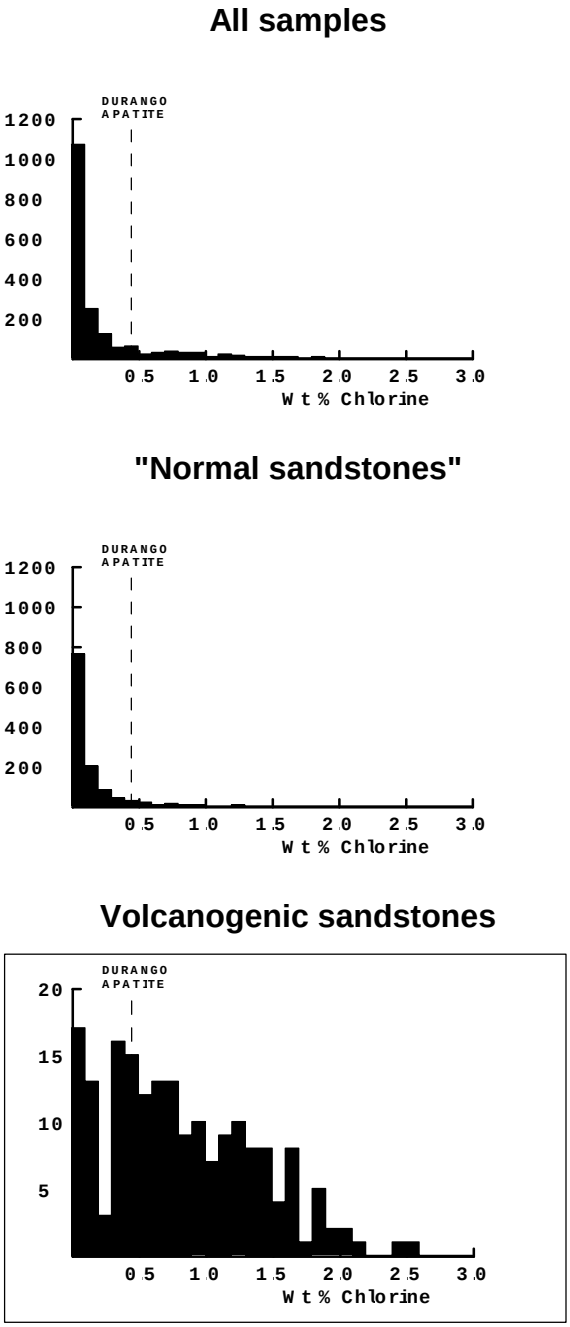

Figure C.4 **a:** Histogram of Cl contents (wt%) in over 1750 apatite grains from over 100 samples of various sedimentary and igneous rocks. Most samples give Cl contents below ~0.5 wt %, while those apatites giving higher Cl contents are characteristic of volcanogenic sandstones and basic igneous sources.

b: Histogram of Cl contents (wt%) in 1168 apatite grains from 61 samples which can loosely be characterised as "normal sandstone". The distribution is similar to that in the upper figure, except for a lower number of grains with Cl contents greater than ~1%.

c: Histogram of Cl contents (wt%) in 188 apatite grains from 15 samples of volcanogenic sandstone. The distribution is much flatter than the other two, with much higher proportion of Cl-rich grains.

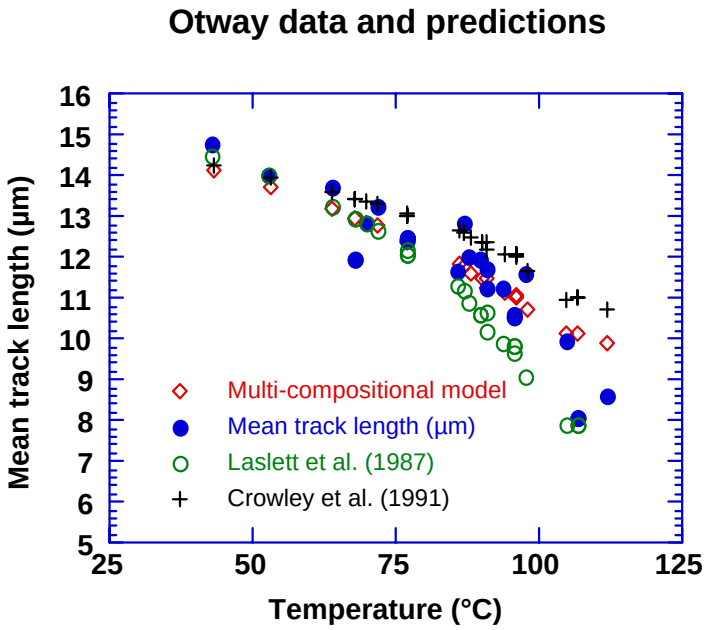

Figure C.5 Comparison of mean track length in samples from four Otway Basin reference wells (from Green et al, 1989a) and predicted mean track lengths from three kinetic models for fission track annealing. The Crowley et al. (1991) model relates to almost pure Fluorapatite (B-5), yet overpredicts mean lengths in the Otway Group samples which are dominated by Cl-rich apatites. The predictions of that model are therefore not reliable.

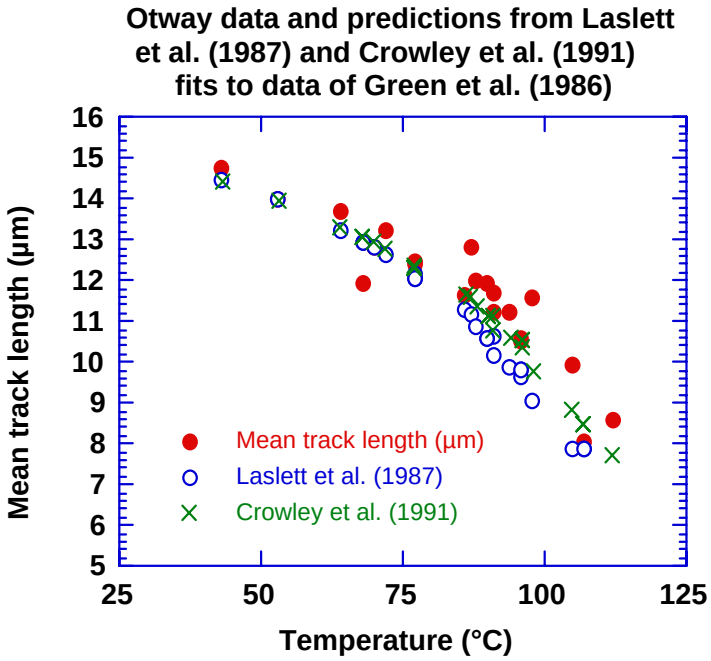

Figure C.6 Comparison of mean track length in samples from four Otway Basin reference wells with values predicted from Laslett et al. (1987) and the model fitted to the annealing data of Green et al. (1986) by Crowley et al. (1991). The predictions of the two models are not very different.

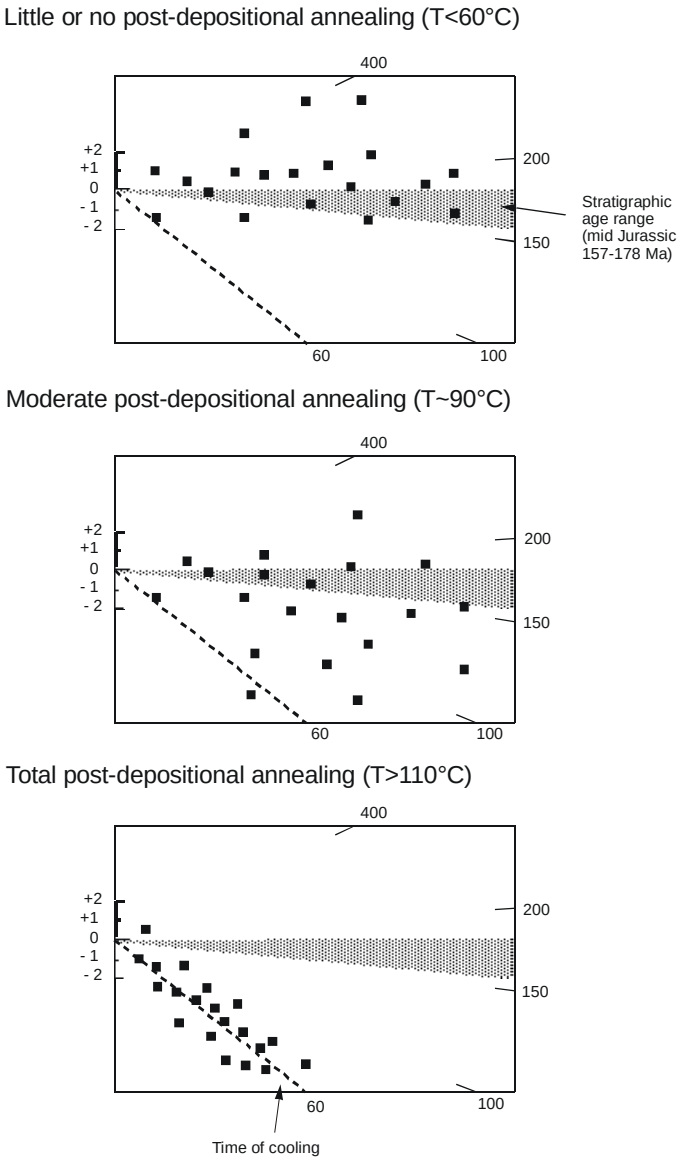

Figure C.7 Radial plots of single grain age data in three samples of mid-Jurassic sandstone that have been subjected to varying degrees of post-depositional annealing prior to cooling at ~60 Ma. The mid-point of the stratigraphic age range has been taken as the reference value (corresponding to the horizontal).

The upper diagram represents a sample which has remained at paleotemperatures less than ~60°C, and has therefore undergone little or no post-depositional annealing. All single grain ages are either compatible with the stratigraphic age (within y = ±2 in the radial plot) or older than the stratigraphic age ($y_i > 2$).

The centre diagram represents a sample which has undergone a moderate degree of post-depositional annealing, having reached a maximum paleotemperature of around ~90°C prior to cooling. While some of the individual grain ages are compatible with the stratigraphic age ($-2 < y_i < +2$) and some may be significantly greater than the stratigraphic age ($y_i > 2$), a number of grains give ages which are significantly less than the stratigraphic age ($y < 2$).

The lower diagram represents a sample in which all apatite grains were totally annealed, at paleotemperatures greater than ~110°C, prior to rapid cooling at ~60 Ma. All grains give fission track ages compatible with a fission track age of ~60 Ma (i.e., all data plot within ±2 of the radial line corresponding to an age of ~60 Ma), and most are significantly younger than the stratigraphic age.

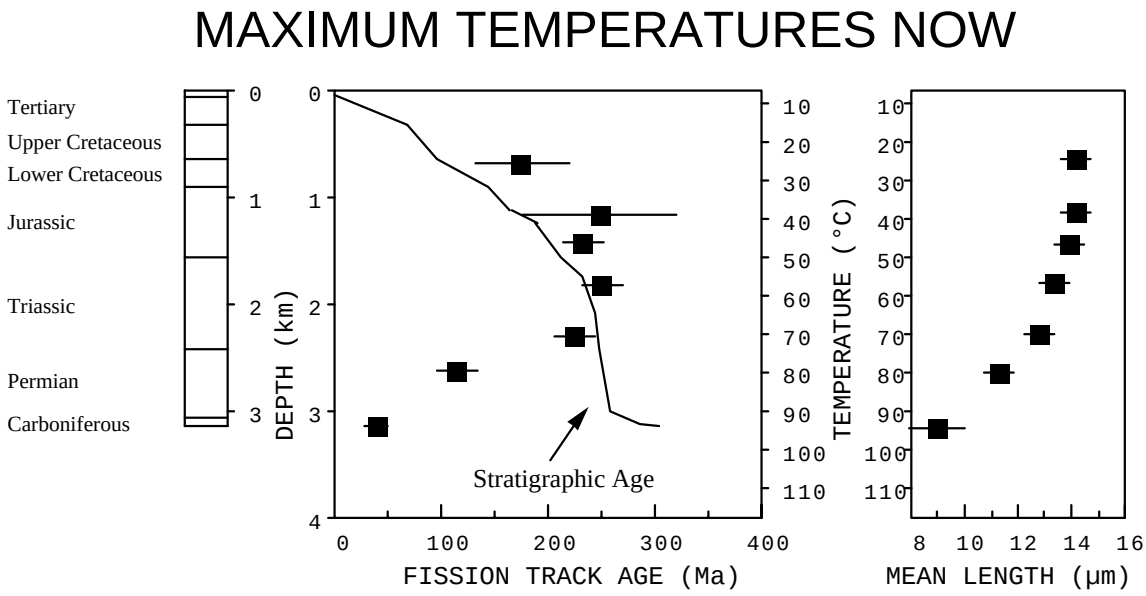

Figure C.8a Typical pattern of AFTA parameters in a well in which samples throughout the entire section are currently at their maximum temperatures since deposition. Both the fission track age and mean track length undergo progressive reduction to zero at temperatures of ~100 - 110°C, the actual value depending on the range of apatite compositions present.

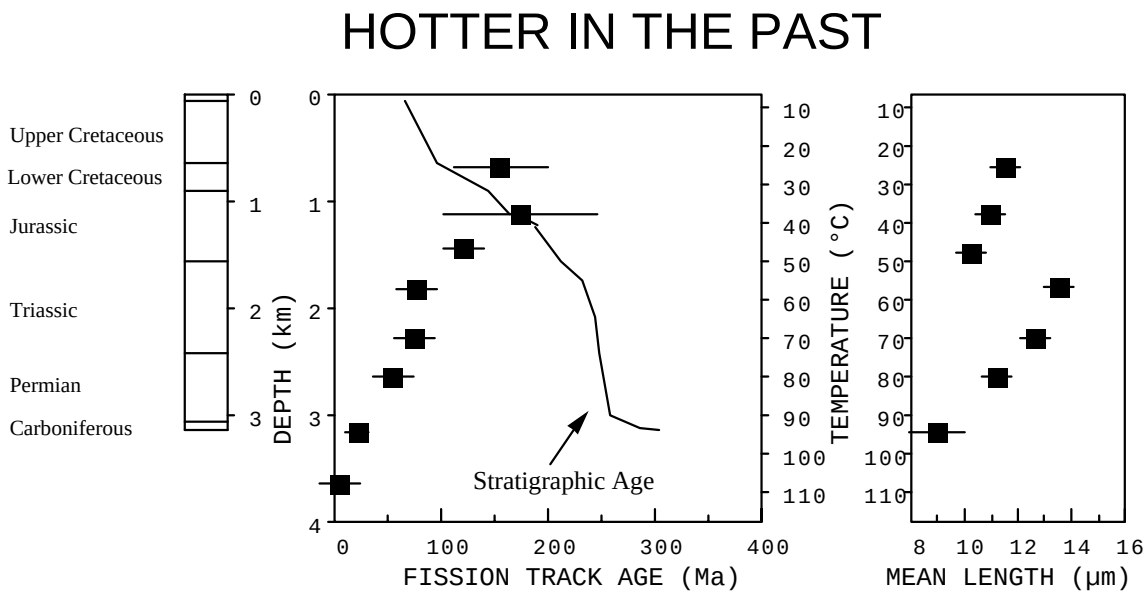

Figure C.8b Typical pattern of AFTA parameters in a well in which samples throughout the section were exposed to elevated paleotemperatures after deposition (prior to cooling in the Early Tertiary, in this case). Both the fission track age and mean track length show more reduction at temperatures of ~40 to 50°C than would be expected at such temperatures. At greater depths (higher temperatures), the constancy of fission track age and the increase in track length are both diagnostic of exposure to elevated paleotemperatures. See Appendix C for further discussion

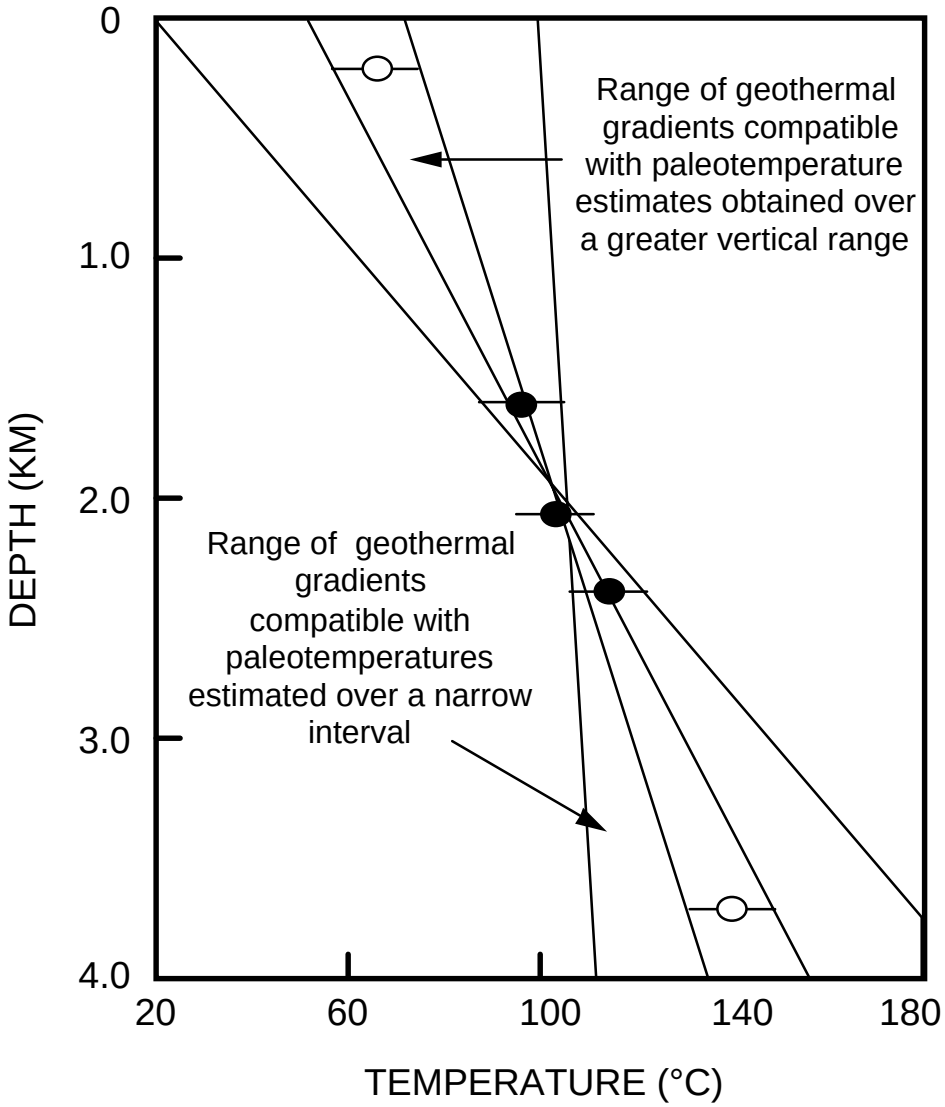

Figure C.9 It is important to obtain paleotemperature constraints over as great a range of depths as possible in order to provide a reliable estimate of paleogeothermal gradient. If paleotemperatures are only available over a narrow depth range, then the paleogeothermal gradient can only be very loosely constrained.

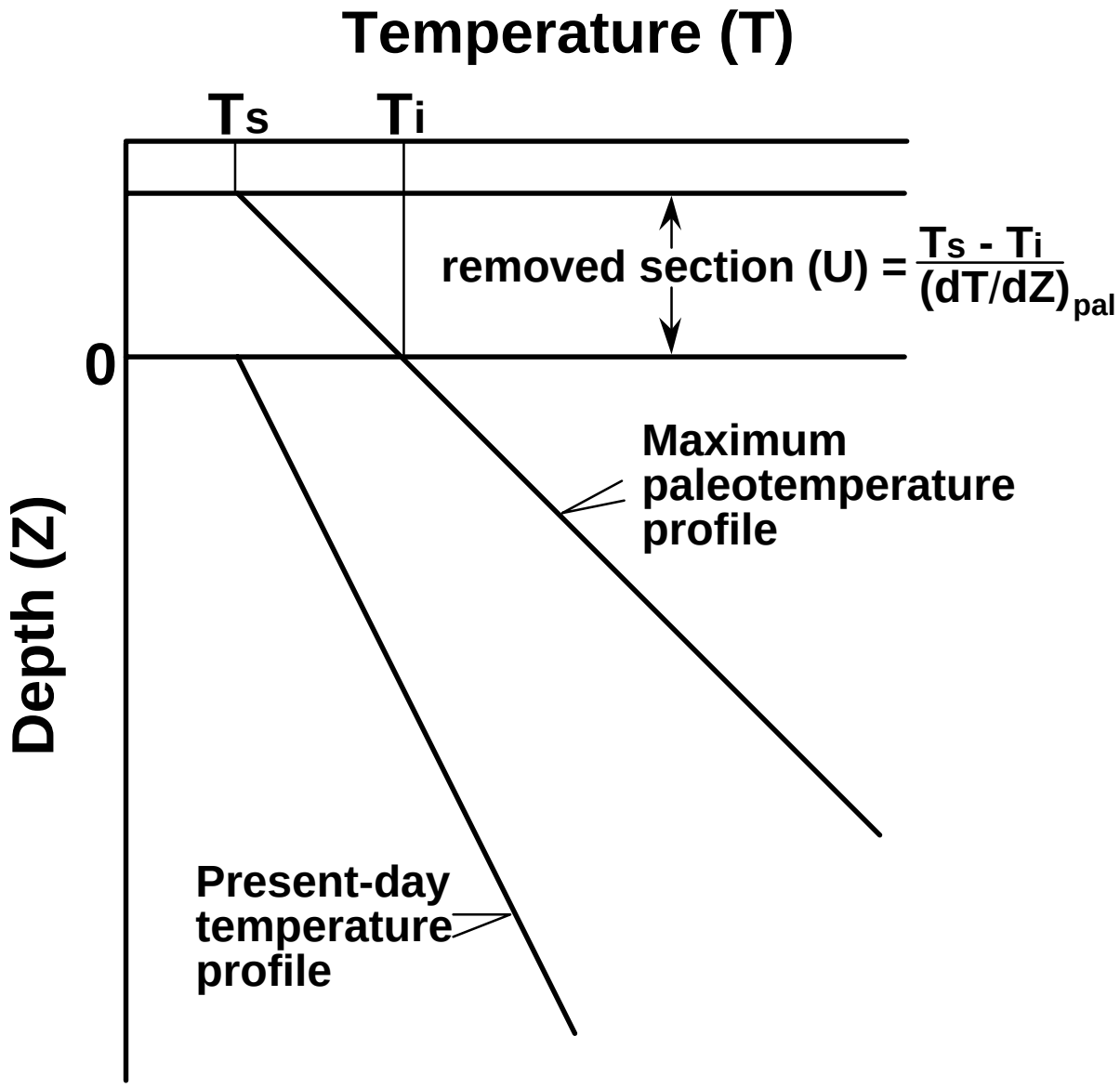

Figure C.10 If the paleogeothermal gradient can be constrained by AFTA and VR, as explained in the text, then for an assumed value of surface temperature, T_S, the amount of section removed can be estimated, as shown.

APPENDIX D

Vitrinite Reflectance Measurements

D.1 Integration of vitrinite reflectance data with AFTA

Vitrinite reflectance is a time-temperature indicator governed by a kinetic response in a similar manner to the annealing of fission tracks in apatite as described in Appendix C. In this study, vitrinite reflectance data are interpreted on the basis of the distributed activation energy model describing the evolution of VR with temperature and time described by Burnham and Sweeney (1989), as implemented in the BasinMod™ software package of Platte River Associates. In a considerable number of wells from around the world, in which AFTA has been used to constrain the thermal history, we have found that the Burnham and Sweeney (1989) model gives good agreement between predicted and observed VR data, in a variety of settings.

As in the case of fission track annealing, it is clear from the chemical kinetic description embodied in equation 2 of Burnham and Sweeney (1989) that temperature is more important than time in controlling the increase of vitrinite reflectance. If the Burnham and Sweeney (1989) distributed activation energy model is expressed in the form of an Arrhenius plot (a plot of the logarithm of time versus inverse absolute temperature), then the slopes of lines defining contours of equal vitrinite reflectance in such a plot are very similar to those describing the kinetic description of annealing of fission tracks in Durango apatite developed by Laslett et al. (1987), which is used to interpret the AFTA data in this report. This feature of the two quite independent approaches to thermal history analysis means that for a particular sample, a given degree of fission track annealing in apatite of Durango composition will be associated with the same value of vitrinite reflectance regardless of the heating rate experienced by a sample. Thus paleotemperature estimates based on either AFTA or VR data sets should be equivalent, regardless of the duration of heating. As a guide, Table D.1 gives paleotemperature estimates for various values of VR for two different heating times.

One practical consequence of this relationship between AFTA and VR is, for example, that a VR value of 0.7% is associated with total annealing of all fission tracks in apatite of Durango composition, and that total annealing of all fission tracks in apatites of more Chlorine-rich composition is accomplished between VR values of 0.7 and ~0.9%.

Furthermore, because vitrinite reflectance continues to increase progressively with increasing temperature, VR data allow direct estimation of maximum paleotemperatures

in the range where fission tracks in apatite are totally annealed (generally above ~110°C) and where therefore AFTA only provides minimum estimates. Maximum paleotemperature estimates based on vitrinite reflectance data from a well in which most AFTA samples were totally annealed will allow constraints on the paleogeothermal gradient that would not be possible from AFTA alone. In such cases the AFTA data should allow tight constraints to be placed on the time of cooling and also the cooling history, since AFTA parameters will be dominated by the effects of tracks formed after cooling from maximum paleotemperatures. Even in situations where AFTA samples were not totally annealed, integration of AFTA and VR can allow paleotemperature control over a greater range of depth, e.g. by combining AFTA from sand-dominated units with VR from other parts of the section, thereby providing tighter constraint on the paleogeothermal gradient.

Equivalent vitrinite reflectance estimation from inertinite reflectance

Inertinite is another common organic maceral with a reflectance higher than that of vitrinite. The relationship between vitrinite and inertinite reflectance can be rather variable from province to province and with stratigraphic age and there is no universal kinetic relationship available. However, comparison of vitrinite and inertinite reflectance from the same samples has allowed Geotrack to develop a reasonable calibration to provide an equivalent vitrinite reflectance level from inertinite reflectance. The correlation table is provided in Table D.1B.

Equivalent vitrinite reflectance estimation from Rock-Eval Tmax

A correlation table between Rock-Eval T_{max} values and equivalent VR levels is provided in Table D.1C. This calibration is taken from data provided by Tissot and Welte (1984) as shown in Figure D.1, and can provide reasonable maturity estimates but must be used with care, as it is known that T_{max} varies with kerogen type at the same level of maturity. In general, we recommend the use of T_{max} as a maturity indicator only when vitrinite reflectance data cannot be obtained, but in some cases, Tmax can provide a useful corroboration of otherwise uncertain VR values.

D.2 Supplied vitrinite reflectance values and other organic maturity indicators

Vitrinite reflectance values supplied by the client are summarised in Table D.2. A summary of the new Rock-Eval T_{max} data are provided in Table D.3. Spore Colour Index (SCI) values provided by the client are summarised in Table D.4.

References

Burnham, A.K. and Sweeney, J.J. (1989). A chemical kinetic model of vitrinite reflectance maturation. *Geochim. et Cosmochim. Acta*, 53, 2649-2657.

Laslett, G.M., Green, P.F., Duddy, I.R. and Gleadow, A.J.W. (1987). Thermal annealing of fission tracks in apatite 2. A quantitative analysis. *Chem. Geol. (Isot. Geosci.Sect.)*, 65, 1-13.

Tissot, B.P. and Welte, D.H. 1984. Petroleum formation and occurrence. Springer Verlag (Berlin).

Table D.1A: Paleotemperature - vitrinite reflectance nomogram based on Equation 2 of Burnham and Sweeney (1989)

Paleotemperature (°C / °*F*)	Vitrinite Reflectance (%) 1 Ma Duration of heating	10 Ma Duration of heating
40 / *104*	0.29	0.32
50 / *122*	0.31	0.35
60 / *140*	0.35	0.40
70 / *158*	0.39	0.45
80 / *176*	0.43	0.52
90 / *194*	0.49	0.58
100 / *212*	0.55	0.64
110 / *230*	0.61	0.70
120 / *248*	0.66	0.78
130 / *266*	0.72	0.89
140 / *284*	0.81	1.04
150 / *302*	0.92	1.20
160 / *320*	1.07	1.35
170 / *338*	1.23	1.55
180 / *356*	1.42	1.80
190 / *374*	1.63	2.05
200 / *392*	1.86	2.33
210 / *410*	2.13	2.65
220 / *428*	2.40	2.94
230 / *446*	2.70	3.23

Table D.1B: Equivalent vitrinite reflectance estimated from inertinite reflectance (Geotrack unpublished correlation).

Measured Inertinite Reflectance (%)	Calculated Vitrinite Reflectance (%)
0.88	0.27
0.95	0.3
1.14	0.4
1.31	0.5
1.45	0.6
1.57	0.7
1.68	0.8
1.78	0.9
1.87	1.0
1.97	1.1
2.07	1.2
2.18	1.3
2.31	1.4
2.46	1.5
2.63	1.6
2.84	1.7
3.08	1.8
3.37	1.9
3.70	2.0
4.20	3.0
6.00	5.0

Table D.1C: Equivalent vitrinite reflectance estimated from Rock-Eval Tmax

Ro(max) (%)	T_{max} (°C)
0.20	390
0.30	410
0.40	420
0.53	430
0.7	440
0.94	450
1.16	460
1.39	470
1.59	480
1.73	490
1.95	510
2.15	530

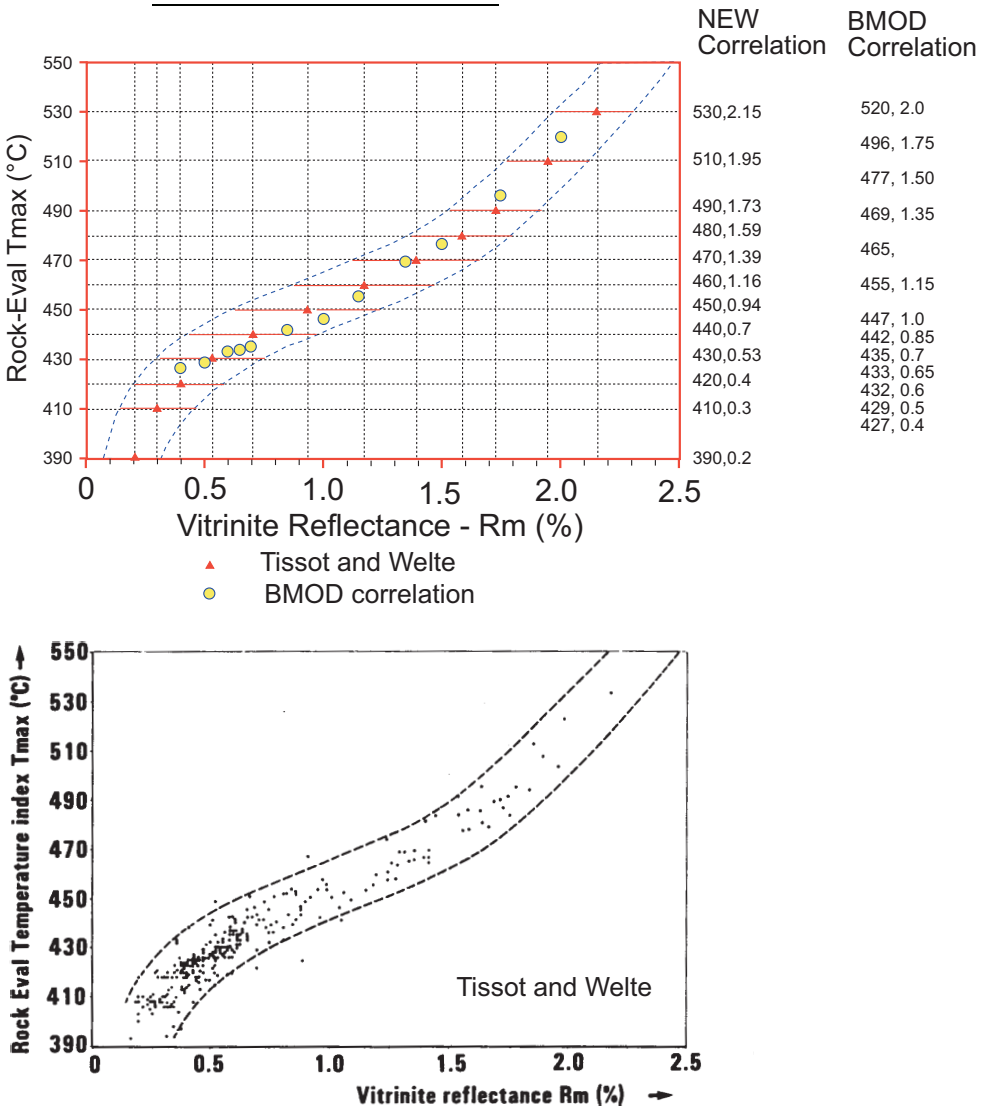

Figure D.1: Conversion from T_{max} to VR_{eq} adopted in this study. Lower plot shows the database from Tissot and Welte (1984) while the upper plot shows the conversion adopted from this data, which is slightly different to that commonly employed e.g. in BasinMod, as indicated.

Table D.2: Vitrinite reflectance and Tmax sample details and results supplied by client - East Greenland (Geotrack Report #1052)

Source	Depth (m)	Stratigraphic Subdivision	Stratigraphic age (Ma)	Present temperature *1 (°C)	VR (Range) %	N	Tmax	VRE %
Blokelv borehole								
16813	0.00	Hareelv Fm	159-146		-		440	0.74
16701	2.67	Hareelv Fm	159-146	5	-		434	0.63
16702	2.96	Hareelv Fm	159-146	5	-		431	0.57
16820	3.51	Hareelv Fm	159-146	5	-		431	0.57
16703	6.44	Hareelv Fm	159-146	5	-		376	-
16704	9.17	Hareelv Fm	159-146	5	-		438	0.70
16705	10.21	Hareelv Fm	159-146	5	-		422	0.43
16706	10.61	Hareelv Fm	159-146	5	-		427	0.51
16821	11.73	Hareelv Fm	159-146	5	-		438	0.70
16707	12.62	Hareelv Fm	159-146	5	-		431	0.57
16708	13.04	Hareelv Fm	159-146	5	-		434	0.63
16709	13.71	Hareelv Fm	159-146	5	-		433	0.61
16710	16.42	Hareelv Fm	159-146	5	-		431	0.57
16711	17.00	Hareelv Fm	159-146	6	-		426	0.49
16712	18.77	Hareelv Fm	159-146	6	-		427	0.51
16713	20.15	Hareelv Fm	159-146	6	-		428	0.52
16714	20.67	Hareelv Fm	159-146	6	-		436	0.66
16715	22.55	Hareelv Fm	159-146	6	-		433	0.61
16716	23.35	Hareelv Fm	159-146	6	-		434	0.63
16822	23.59	Hareelv Fm	159-146	6	0.52	43		
16822	23.59	Hareelv Fm	159-146	6	-		436	0.66
16717	24.26	Hareelv Fm	159-146	6	-		438	0.70
16738	24.68	Hareelv Fm	159-146	6	-		437	0.68
16737	24.92	Hareelv Fm	159-146	6	-		437	0.68
16718	25.15	Hareelv Fm	159-146	6	-		442	0.78
16736	25.24	Hareelv Fm	159-146	6	-		437	0.68
16735	25.59	Hareelv Fm	159-146	6	-		328	-
16719	25.76	Hareelv Fm	159-146	6	-		324	-
16734	25.88	Hareelv Fm	159-146	6	-		329	-
16733	26.00	Hareelv Fm	159-146	6	-		328	-
16720	26.15	Hareelv Fm	159-146	6	-		357	-
16721	26.23	Hareelv Fm	159-146	6	-		420	0.40

Table D.2: Continued

Source	Depth (m)	Stratigraphic Subdivision	Stratigraphic age (Ma)	Present temperature *1 (°C)	VR (Range) %	N	Tmax	VRE %
16722	27.11	Hareelv Fm	159-146	6	-		305	-
16739	27.31	Hareelv Fm	159-146	6	-		462	1.19
16740	27.46	Hareelv Fm	159-146	6	-		397	0.20
16741	28.30	Hareelv Fm	159-146	6	-		318	-
16723	28.33	Hareelv Fm	159-146	6	-		346	-
16742	28.49	Hareelv Fm	159-146	6	-		435	0.64
16743	28.69	Hareelv Fm	159-146	6	-		447	0.88
16724	29.24	Hareelv Fm	159-146	6	-		439	0.72
16725	32.10	Hareelv Fm	159-146	6	-		437	0.68
16823	32.78	Hareelv Fm	159-146	6	0.54	84		
16823	32.78	Hareelv Fm	159-146	6	-		439	0.72
16726	34.33	Hareelv Fm	159-146	6	-		434	0.63
16727	35.05	Hareelv Fm	159-146	6	-		431	0.57
16728	35.87	Hareelv Fm	159-146	6	-		431	0.57
16729	39.43	Hareelv Fm	159-146	6	-		426	0.49
16730	41.53	Hareelv Fm	159-146	6	-		429	0.54
16824	44.80	Hareelv Fm	159-146	6	-		437	0.68
16731	45.87	Hareelv Fm	159-146	6	-		430	0.56
16732	46.53	Hareelv Fm	159-146	6	-		432	0.59
16744	47.08	Hareelv Fm	159-146	6	-		432	0.59
16745	50.27	Hareelv Fm	159-146	7	-		433	0.61
16746	51.99	Hareelv Fm	159-146	7	-		438	0.70
16825	56.66	Hareelv Fm	159-146	7	-		433	0.61
16747	59.39	Hareelv Fm	159-146	7	-		433	0.61
16748	60.64	Hareelv Fm	159-146	7	-		431	0.57
16749	64.91	Hareelv Fm	159-146	7	-		432	0.59
16750	67.17	Hareelv Fm	159-146	7	-		432	0.59
16751	68.02	Hareelv Fm	159-146	7	-		432	0.59
16752	68.73	Hareelv Fm	159-146	7	-		432	0.59
16826	68.77	Hareelv Fm	159-146	7	0.50	39		
16826	68.77	Hareelv Fm	159-146	7	-		432	0.59
16763	68.97	Hareelv Fm	159-146	7	-		430	0.56
16765	74.61	Hareelv Fm	159-146	7	-		433	0.61
16766	79.96	Hareelv Fm	159-146	7	-		434	0.63

Table D.2: Continued

Source	Depth (m)	Stratigraphic Subdivision	Stratigraphic age (Ma)	Present temperature *1 (°C)	VR (Range) %	N	Tmax	VRE %
16827	80.77	Hareelv Fm	159-146	7	0.55	82		
16827	80.77	Hareelv Fm	159-146	7	-		433	0.61
16767	82.14	Hareelv Fm	159-146	7	-		434	0.63
16768	84.03	Hareelv Fm	159-146	8	-		433	0.61
16769	85.41	Hareelv Fm	159-146	8	-		433	0.61
16770	86.56	Hareelv Fm	159-146	8	-		434	0.63
16771	87.28	Hareelv Fm	159-146	8	-		433	0.61
16772	88.19	Hareelv Fm	159-146	8	-		434	0.63
16773	89.22	Hareelv Fm	159-146	8	-		434	0.63
16774	90.12	Hareelv Fm	159-146	8	-		433	0.61
16775	91.25	Hareelv Fm	159-146	8	-		433	0.61
16776	92.21	Hareelv Fm	159-146	8	-		432	0.59
16828	92.74	Hareelv Fm	159-146	8	0.56	97		
16828	92.74	Hareelv Fm	159-146	8	-		432	0.59
16777	93.02	Hareelv Fm	159-146	8	-		433	0.61
16778	97.42	Hareelv Fm	159-146	8	-		447	0.88
16779	98.48	Hareelv Fm	159-146	8	-		473	1.42
16780	103.98	Hareelv Fm	159-146	8	-		331	-
16829	104.79	Hareelv Fm	159-146	8	-		450	0.94
16781	105.72	Hareelv Fm	159-146	8	-		444	0.82
16782	106.59	Hareelv Fm	159-146	8	-		437	0.68
16783	108.47	Hareelv Fm	159-146	8	-		434	0.63
16784	110.86	Hareelv Fm	159-146	8	-		433	0.61
16785	112.79	Hareelv Fm	159-146	8	-		435	0.64
16786	114.60	Hareelv Fm	159-146	8	-		434	0.63
16830	116.82	Hareelv Fm	159-146	9	0.56	101		
16830	116.82	Hareelv Fm	159-146	9	-		438	0.70
16795	117.73	Hareelv Fm	159-146	9	-		433	0.61
16796	120.06	Hareelv Fm	159-146	9	-		436	0.66
16797	121.62	Hareelv Fm	159-146	9	-		437	0.68
16798	123.71	Hareelv Fm	159-146	9	-		438	0.70
16799	125.32	Hareelv Fm	159-146	9	-		436	0.66
16800	127.56	Hareelv Fm	159-146	9	-		435	0.64
16831	128.77	Hareelv Fm	159-146	9	-		443	0.80

Table D.2: Continued

Source	Depth (m)	Stratigraphic Subdivision	Stratigraphic age (Ma)	Present temperature *1 (°C)	VR (Range) %	N	Tmax	VRE %
16801	131.65	Hareelv Fm	159-146	9	-		434	0.63
16802	133.36	Hareelv Fm	159-146	9	-		435	0.64
16803	135.41	Hareelv Fm	159-146	9	-		435	0.64
16832	140.75	Hareelv Fm	159-146	9	-		447	0.88
16804	142.84	Hareelv Fm	159-146	9	-		436	0.66
16805	145.46	Hareelv Fm	159-146	9	-		437	0.68
16806	147.27	Hareelv Fm	159-146	9	-		437	0.68
16807	149.48	Hareelv Fm	159-146	9	-		437	0.68
16833	152.75	Hareelv Fm	159-146	10	0.61	47		
16833	152.75	Hareelv Fm	159-146	10	-		448	0.90
16808	153.29	Hareelv Fm	159-146	10	-		438	0.70
16809	155.20	Hareelv Fm	159-146	10	-		441	0.76
16810	156.89	Hareelv Fm	159-146	10	-		440	0.74
16811	158.83	Hareelv Fm	159-146	10	-		441	0.76
16812	160.80	Hareelv Fm	159-146	10	-		440	0.74
16834	164.82	Hareelv Fm	159-146	10	0.68	150		
16834	164.82	Hareelv Fm	159-146	10	-		435	0.64
16814	167.92	Hareelv Fm	159-146	10	-		438	0.70
16815	170.67	Hareelv Fm	159-146	10	-		440	0.74
16816	172.62	Hareelv Fm	159-146	10	-		443	0.80
16817	174.46	Hareelv Fm	159-146	10	-		442	0.78
16818	176.44	Hareelv Fm	159-146	10	-		441	0.76
16835	176.77	Hareelv Fm	159-146	10	0.62	86		
16835	176.77	Hareelv Fm	159-146	10	-		440	0.74
16819	178.36	Hareelv Fm	159-146	10	-		443	0.80
16841	185.11	Hareelv Fm	159-146	11	-		443	0.80
16842	186.36	Hareelv Fm	159-146	11	-		443	0.80
16836	188.77	Hareelv Fm	159-146	11	0.65	77		
16836	188.77	Hareelv Fm	159-146	11	-		445	0.84
16843	190.61	Hareelv Fm	159-146	11	-		442	0.78
16844	195.26	Hareelv Fm	159-146	11	-		441	0.76
16845	196.42	Hareelv Fm	159-146	11	-		444	0.82
16846	198.25	Hareelv Fm	159-146	11	-		443	0.80
16847	200.22	Hareelv Fm	159-146	11	-		443	0.80

Table D.2: Continued

Source	Depth (m)	Stratigraphic Subdivision	Stratigraphic age (Ma)	Present temperature *1 (°C)	VR (Range) %	N	Tmax	VRE %
16837	200.76	Hareelv Fm	159-146	11	0.66	107		
16837	200.76	Hareelv Fm	159-146	11	-		440	0.74
16848	202.05	Hareelv Fm	159-146	11	-		443	0.80
16849	203.91	Hareelv Fm	159-146	11	-		444	0.82
16850	205.84	Hareelv Fm	159-146	11	-		444	0.82
16851	207.77	Hareelv Fm	159-146	11	-		447	0.88
16852	209.82	Hareelv Fm	159-146	11	-		447	0.88
16853	211.79	Hareelv Fm	159-146	11	-		448	0.90
16838	212.77	Hareelv Fm	159-146	11	0.78	98		
16838	212.77	Hareelv Fm	159-146	11	-		447	0.88
16854	213.81	Hareelv Fm	159-146	11	-		445	0.84
16855	215.83	Hareelv Fm	159-146	11	-		446	0.86
16856	218.50	Hareelv Fm	159-146	12	-		446	0.86
16857	224.00	Hareelv Fm	159-146	12	-		444	0.82
16839	224.74	Hareelv Fm	159-146	12	0.74	48		
16839	224.74	Hareelv Fm	159-146	12	-		445	0.84
16858	232.05	Hareelv Fm	159-146	12	-		446	0.86
16840	233.71	Hareelv Fm	159-146	12	-		452	0.98

Note: Some samples may contain both vitrinite and inertinite. Only vitrinite data is shown.

*1 See Appendix A for discussion of present temperature data.